TECHNICKÁ UNIVERZITA V LIBERCI
Fakulta textilní

Pokročilé vlákenné materiály pro akustický výkon

Disertační práce

Studijní program: P3106 – Textile Engineering
Studijní obor: 3106V015 – Textile Technics and Materials Engineering

Autor práce: **Tao Yang, M.Eng.**
Vedoucí práce: doc. Rajesh Mishra, Ph.D.

Liberec 2018

TECHNICAL UNIVERSITY OF LIBEREC
Faculty of Textile Engineering

Advanced Fibrous Materials for Acoustic Performance

Dissertation

Study programme: P3106 – Textile Engineering
Study branch: 3106V015 – Textile Technics and Materials Engineering

Author: **Tao Yang, M.Eng.**
Supervisor: doc. Rajesh Mishra, Ph.D.

Liberec 2018

Prohlášení

Byl jsem seznámen s tím, že na mou disertační práci se plně vztahuje zákon č. 121/2000 Sb., o právu autorském, zejména § 60 – školní dílo.

Beru na vědomí, že Technická univerzita v Liberci (TUL) nezasahuje do mých autorských práv užitím mé disertační práce pro vnitřní potřebu TUL.

Užiji-li disertační práci nebo poskytnu-li licenci k jejímu využití, jsem si vědom povinnosti informovat o této skutečnosti TUL; v tomto případě má TUL právo ode mne požadovat úhradu nákladů, které vynaložila na vytvoření díla, až do jejich skutečné výše.

Disertační práci jsem vypracoval samostatně s použitím uvedené literatury a na základě konzultací s vedoucím mé disertační práce a konzultantem.

Současně čestně prohlašuji, že tištěná verze práce se shoduje s elektronickou verzí, vloženou do IS STAG.

Datum:

Podpis:

Acknowledgement

This dissertation has been completed with the guidance and mentorship of many people. I would like to gratefully acknowledge their support of this thesis.

Firstly, I would like to express my sincere gratitude to my supervisor, Associate Professor Rajesh Mishra, for the continuous support of my Ph.D. study and related research, for his patience, motivation, and immense knowledge. His guidance helped me in all the time of research and writing of this thesis. I could not have imagined having a better advisor and mentor for my Ph.D study. Besides my supervisor, I would like to give my appreciation to Professor Jiri Militky, who committed his expertise and knowledge to assist in the completion of this work.

I would like to express my special gratitude to Dr. Jan Novak, for his great help on the efficient acoustic measurements throughout the project. I would like to thank Dr. Jiri Chaloupek and Mr. Filip Sanetrnik, for their help on my samples preparation at TUL. My sincere thanks also goes Professor Jakub Wiener, Professor Lubos Hes, doc. Dr. Dana Kremenakova, Dr Veronika Tunakova, Dr. Jana Salacova and Ms. Jana Stranska for their technical support and allowing me to use their instruments. I thank and appreciate all the technical staff of TUL for their accessibility and openness to make this research a wonderful experience. My special thanks to the Dean of Faculty of Textile Engineering, Dr. Jana Drasarova, Vice Dean Dr. Gabriela Krupincova and Vice Dean Dr. Pavla Tesinova for their continuous support. I also thank our HOD Dr. Blanka Tomkova, Secretary Katerina Struplova, Katerina Nohynkova, Hana Musilova, Bohumila Keilova for their seamless coordination and efficiency. My hearty thanks to management of Technical University of Liberec for the sustained support to pursue Ph.D degree in this esteemed institution. I really endear the relationship that we have established over the years and the support and availability to use the research facilities in TUL. In particular, I am grateful to Professor Kirill V Horoshenkov at The University of Sheffield and Dr. Jean-Philippe Groby at Le Mans University, for their altruistic guide and professional suggestions during my internships in the UK and France.

Last but not the least, I would like to thank my family: my parents and my brother for supporting me spiritually throughout writing this thesis and my life in general. My final appreciation goes to my wife, Xiaoman Xiong, the person who supported and companied me the most the last several years through thick and thin. Thank you, my wife, for your support and patience.

I look forward to starting and successfully finishing more new chapters in life.

Tao Yang

Technical University of Liberec

Synopsis

The objective of this thesis was to examine multi-functional properties of high-loft perpendicularly-laid nonwoven fabrics, which can be used to noise reduction application at building and automotive field. It presents an experimental and numerical investigation on acoustic properties of perpendicularly-laid nonwoven fabrics.

Perpendicularly-laid nonwoven samples were made by two different manufacturing techniques: vibration and rotating perpendicular lapper. Heat-pressing method was employed to form samples with varying thickness. This study determines the influence of some structural characteristics and laying techniques on the sound absorption properties of perpendicularly-laid nonwovens.

Normally incident sound absorption coefficient and surface impedance were measured by Brüel and Kjær type 4206 impedance tube. Several airflow resistivity models grouped in theoretical and empirical categories were used to study the suitable model for perpendicularly-laid nonwoven fabrics. The commonly used impedance models such as Delany-Bazley, Miki, Garai-Pompoli and Komatsu models were applied to predict the acoustic properties. The measured and predicted values were compared to figure out the accuracy of the existing models. One simple model was developed to rapidly obtain the airflow resistivity of perpendicularly-laid nonwovens.

The compression energy and compression load of perpendicularly-laid nonwovens were carried out by using a universal testing machine (TIRATEST 2300). The potential compression mechanism of the nonwoven fabric was identified with support of the compression stress-strain curve at different compression stages.

Perpendicularly-laid nonwoven fabrics have special thermal and air permeability behavior compared with traditional cross-laid nonwovens due to their through-plane fiber orientation. Hence this research work also investigates the influence of different structural parameters of perpendicularly-laid nonwoven fabrics, such as areal density, porosity, thickness, on thermal properties and air permeability. The potential relationships between thermal resistivity, air permeability and acoustic properties were also investigated.

Aerogel have high porosity (>90%), a high specific surface area, lightweight, and low sound velocity. Due to these characteristics, aerogels can be used in sound absorption and thermal insulation fields. Thus, this thesis also investigated sound absorption performance of aerogel

based nonwoven fabrics. Polyester/polyethylene nonwovens embedded with hydrophobic amorphous silica aerogel were chosen for sound absorption measurements. The sound absorption coefficient (SAC) of single and multilayered of aerogel nonwovens blankets was tested by Brüel and Kjær impedance tube.

Statistical analysis software, Originlab 8.5 and Matlab_R2017a were used to conduct all the statistical results in this study. The findings are significant and can be used for further study in the areas of sound absorption behavior of fibrous materials, the application of perpendicularly-laid nonwoven fabrics for the noise treatment application in building and automotive fields.

Keywords: perpendicularly-laid nonwoven; acoustic properties; thermal resistivity; airflow resistivity; compressibility; impedance models

Abstrakt

Cílem této práce bylo prozkoumat multifunkční vlastnosti vysoko-loftových kolmo kladených netkaných textilií, které mohou být aplikovány ke snížení hluku v oblasti stavebnictví a automobilového průmyslu. Představuje experimentální a numerické vyšetřování akustických vlastností kolmo kladených netkaných textilií.

Kolmo kladené vzorky z netkané textilie byly vyrobeny dvěma různými výrobními postupy: vibracemi a rotujícími kolmými lamelami. Metoda tepelného lisování byla použita pro tvorbu vzorků s různou tloušťkou. Tato studie určuje vliv některých konstrukčních charakteristik a technik kladení na vlastnosti absorpce zvuku kolmo kladených netkaných textilií.

Obvykle koeficient absorpce hluku a povrchová impedance byly měřeny impedanční trubkou typu Brüel a Kjær 4206. Několik modelů odporového proudu vzduchu seskupených v teoretických a empirických kategoriích bylo použito ke studiu vhodného modelu pro kolmo kladené netkané materiály. Pro předpovědi akustických vlastností byly použity běžně používané impedanční modely jako modely Delany-Bazley, Miki, Garai-Pompoli a Komatsu. Naměřené a předpovězené hodnoty byly porovnány s výpočtem přesnosti stávajících modelů. Jeden jednoduchý model byl vyvinut pro rychlé získání odporu proudění vzduchu kolmo kladených netkaných textilií.

Kompresní energie a zatížení stlačením kolmo kladených netkaných textilií byly provedeny univerzálním zkušebním strojem (TIRATEST 2300). Potenciální kompresní mechanismus netkané textilie byl identifikován s podporou kompresní křivky napětí-deformace, práce a účinnosti v různých kompresních stupních.

Kolmo kladené netkané textilie mají zvláštní tepelnou a vzduchovou propustnost ve srovnání s tradičními netkanými vrstvami z důvodu jejich orientace přes uvnitř vlákenné vrstvy. Proto tato výzkumná práce také zkoumá vliv různých strukturálních parametrů kolmo kladených netkaných textilií, jako je plošná hustota, pórovitost, tloušťka, na tepelné vlastnosti a propustnost vzduchu. Rovněž byly zkoumány potenciální vztahy mezi tepelným odporem, propustností pro vzduch a akustickými vlastnostmi.

Airgel má vysokou pórovitost (> 90%), vysokou specifickou plochu, nízkou hmotnost a nízkou rychlost zvuku. Vzhledem k těmto vlastnostem mohou být aerogely použity v oblastech pohlcování hluku a tepelné izolace. Tato práce také zkoumala výkon absorpce zvuku z netkaných textilií na bázi aerogelu. Pro měření zvukové pohltivosti byly vybrány

polyesterové / polyethylenové netkané textilie opatřené hydrofobním amorfním oxidem křemičitým. Koeficient absorpce zvuku (SAC) jednoplášťových a vícevrstvých pokrývek z netkaného vzduchu byl testován impedanční trubkou Brüel a Kjær.

Statistický analytický software, Originlab 8.5 a Matlab_R2017a, byl použit k provádění všech statistických výsledků v této studii. Zjištění jsou významná a mohou být použity pro další studium v oblastech chování pohlcování zvuku vláknitých materiálů, aplikací kolmo kladených netkaných textilií pohlcování hluku v budovách a automobilech.

Klíčová slova: kolmo kladené netkané textilie; akustické vlastnosti; tepelný odpor; proudění vzduchu; stlačitelnost; impedanční modely

摘要

该论文的目的是研究可应用于建筑和汽车领域的吸声降噪的高孔隙率纤维垂直排列非织造材料的多种性能。纤维垂直排列非织造材料通过两种不同的生产工艺制造：振动和旋转垂直铺网。并采用热压法获得不同厚度的样品。该论文分析了不同结构参数和制造技术对纤维垂直排列非织造材料的吸声性能的影响。

该论文对纤维垂直排列非织造材料的声学特性进行了模型分析和实验研究。AFD300 AcoustiFlow 流阻测试仪被用来表征非织造材料的流阻，理论和经验模型也被用于研究该材料的流阻，并开发了一种能快速获该材料流阻的模型。非织造材料的垂直入射吸声系数和表面阻抗通过 Brüel & Kjær 型 4206 阻抗管测得。一些广泛应用的阻抗模型如 Delany-Bazley、Miki、Garai-Pompoli 和 Komatsu 模型被用来预测该材料的声学特性。通过对比测试数据和预测值获得模型的准确性。

该种材料的抗压性和压缩载荷性能通过 TIRATEST 2300 试验机进行了表征。通过压缩应力应变曲线的分析，得出不同压缩阶段的效率来表征非织造织物的压缩机理。

与传统的水平铺设非织造布相比，纤维垂直排列非织造材料具有特殊的导热和透气性能。因此，该论文还研究了纤维垂直排列非织造材料的不同结构参数的影响，例如面密度、孔隙率、厚度，对热性能和透气性的影响。还研究了隔热性、透气性和吸声性之间的潜在关系。

气凝胶具有很高的孔隙率（> 90%），高比表面积，重量轻和低声音传播速度（低至 90m/s）。由于这些特性，气凝胶可用于吸音和隔热领域。因此，本论文还研究了气凝胶/聚合物非织造材料的吸声性能。嵌有疏水性无定形二氧化硅气凝胶的聚酯/聚乙烯无纺布被用于吸声性能研究。气凝胶非织造布材料的单层和多层的吸声系数同样由 Brüel & Kjær 阻抗管测得。

数据统计分析软件 Originlab 8.5 和 Matlab_R2017a 用于进行本研究中的所有统计分析。该研究结果具有重要意义，可用于纤维材料吸声性能领域的进一步研究及纤维垂直分布无纺布在建筑和汽车领域的噪声处理应用中的应用。

关键词：-纤维垂直排列非织造材料、声学性能、热学性能、流阻、压缩性能、阻抗模型

Table of Contents

List of Figures

List of Tables

List of Symbols and Abbreviations

Symbols		Description
ε		Porosity
ρ	[kg/m^3]	Fabric bulk density
ρ_f	[kg/m^3]	Fiber density
ρ_s	[g/m^2]	Areal/surface density
q	[mm/s]	Air permeability
k_p	[m^2]	Permeability coefficient
k		Kozeny constant
t_f		Tortuosity
ΔP	[Pa]	Pressure gradient
η	[Pa·s]	Viscosity of airflow
l	[mm]	Material/sample thickness
l_e	[mm]	Effective channel length
k_0		Shape factor
s	$[(\mathrm{Pa}\cdot\mathrm{s})^{-1/2}]$	Channel wetted surface
u	[m/s]	Airflow velocity
Z_s		Surface characteristic impedance
Z_c		Characteristic impedance
k		Complex wavenumber
α		Sound absorption coefficient
R		Pressure reflection coefficient
ρ_0	[kg/m^3]	Air density at room temperature
c_0	[m/s]	Sound speed in air media at room temperature
σ	[Pa•s/m2]	Airflow resistivity
σ_m	[Pa•s/m2]	Measured airflow resistivity
σ_p	[Pa•s/m2]	Predicted airflow resistivity
d	[m]	Fiber diameter
n		Fiber count
λ	$[\mathrm{W}\cdot\mathrm{m}^{-1}\cdot\mathrm{K}^{-1}]$	Thermal conductivity
Q	[W·s]	Amount of conducted heat
F	[m^2]	The area through which heat is conducted

τ	[s]	The time of heat conduction
ΔT	[°C]	Difference of the temperatures
R	$[\mathrm{m}^2 \cdot \mathrm{K} \cdot \mathrm{W}^{-1}]$	Thermal resistance
W_i	[J]	Incident sound energy
W_q	[J]	The sound energy transformed into heat
W_r	[J]	Reflected sound energy
W_t	[J]	Transmitted sound energy
$\bar{\alpha}$		Average value of sound absorption coefficient
α_{250Hz}		Sound absorption coefficient at 250 Hz
α_{500Hz}		Sound absorption coefficient at 500 Hz
α_{1000Hz}		Sound absorption coefficient at 1000 Hz
α_{2000Hz}		Sound absorption coefficient at 2000 Hz
α_{meas}		Measured absorption coefficient
α_{pred}		Predicted absorption coefficient
F_1		Lower bound of sound frequency in testing (=100 Hz)
F_2		Upper bound of sound frequency in measurement (=6400 Hz)
R^2		Coefficients of determination
Adj. R^2		Adjusted coefficients of determination

Abbreviations	Description
MAVRE	Mean absolute values of relative error
STRUTO	Vibrating perpendicular lapper
WAVEMAKER	Rotating perpendicular lapper
ISO	International Organization for Standardization
ASTM	American Society for Testing and Materials
GSM	Areal density/surface density
micro-CT	Micro Computed Tomography
PET	Polyethylene terephthalate
SEM	Scanning electron microscope
B&K	Brüel and Kjær
SAC	Sound absorption coefficient
NRC	Noise reduction coefficient
SD	Standard deviation

Chapter 1 Introduction

Noise, produced by household gadgets, big trucks, vehicles and motorbikes on the road, jet planes and helicopters hovering over cities and loud speakers, is considered as environmental pollution and becoming an increasing public health concern because it could cause a lot of problems such as stress related illnesses, speech interference, hearing loss, sleep disruption and so on. Most importantly, the immediate and acute effect of noise pollution to a person will impair the hearing if it lasts for a period of time. Prolonged exposure to impulsive noise to a person will damage their eardrum, which may result in a permanent hearing impairment. Moreover, health effects of noise like anxiety and stress reaction may bring physiological manifestations, such as headaches, feeling of fatigue, irritability and nervousness.[1]

In order to minimize the adverse effect caused by noise pollution, a variety of ways are available to reduce noise. The most efficient and classical solution to the problem has been the elimination of noise at source, but this may not always be possible.[2] Therefore, the reduction of noise emission is usually accomplished by noise isolation and absorption methods. The most common one is to use porous sound absorber to disseminate energy and turn it into heat.[3] A porous sound-absorbing material is a solid that contains cavities, channels or interstices so that sound waves are able to enter through them. As porous material, fibrous textile is widely used in automotive and building industries for noise control. It has been considered to be ideal sound absorber material because of its high porosity, high specific surface area, low-cost, light-weight, no pollution and high-efficient absorbing ability.[2, 4] Nonwoven is one kind of the most common porous sound-absorbing material. Perpendicularly-laid nonwoven, a typical high-loft nonwoven structure, is widely used for thermal and acoustic comfort in automobile industry.[5-10] Due to the majority of fibers orientated in the vertical plane, perpendicularly-laid nonwovens exhibit high resistance to compression and excellent elastic recovery after repeated loading. Moreover, because of their thermal bonded structure and high initial thickness, perpendicularly-laid nonwovens with varying thicknesses can be obtained through thermal treatment. Based on these characteristics, perpendicularly-laid nonwovens can be used in many places of automotive for sound and thermal insulation, such as under bonnet, door panels, headliners, A-B-C pillars and luggage compartment.

Hence, the current study relies entirely on objective measures of perpendicularly-laid

nonwoven fabrics for evaluating the acoustic and non-acoustic properties like sound absorption coefficient, characteristic impedance, airflow resistivity, compression, thermal resistivity and air permeability. This research aims to provide an advanced high-loft structure nonwoven material for noise reduction to replace the tradition sound-absorbing materials such as glass fiber and mineral wool mat. A thorough study of the properties of the processed materials was performed.

This chapter outlines the objectives and foundation of the work described in the thesis. The first section describes the motivation for performing the experimental and analytical work, followed by the sub-objectives of the study. Finally, an overall outline is given that summarizes the contents of the thesis.

1.1 Research objectives

In this work, two types of manufacturing technologies, STRUTO and WAVEMAKER, were used to prepare nonwoven samples. The purpose of this study is to understand the acoustic, compression and thermal performance of perpendicularly-laid nonwoven. The major objectives of this research are as follows:

1.1.1 Studies on acoustic performance of perpendicularly-laid nonwovens with respect to their structural parameters

The Brüel and Kjær impedance and Materiacustica tubes were employed for sound absorption and impedance measurements to study the acoustic properties of nonwoven fabrics. Nonwoven fabrics with varying thickness and density were prepared to investigate the effect of manufacturing technologies, fabric porosity, thickness and areal density on the sound absorption ability of nonwoven samples.

1.1.2 Investigation of compression and resiliency in 3D corrugated nonwovens

Researchers have studied the compression properties of perpendicularly-laid nonwovens, but there is no exiting paper focusing on the influence of fiber orientation on compression performance. In this research, nonwoven samples with different fiber orientation have been chosen to investigate the effect of fiber orientation on compression property of perpendicularly-laid nonwoven fabric. The perpendicularly-laid nonwoven samples were heat treated to change the fiber orientation angle. Besides, the effect of manufacturing technology and fabric density on compression property has been studied. The compression energy and compression load of perpendicularly-laid were measured by using TIRATEST 2300. It was

found that the fiber orientation angle sharply decreases with the increase of load during heat treatment. Perpendicularly-laid nonwovens with higher fiber orientation angle exhibit higher compression resistance. Shearing deformation occurs during compression process of perpendicularly-laid nonwovens. Fiber orientation angle decreases with the increase of thickness reduction.

1.1.3 Study of sound absorption property in relation to thermal properties

Thermal and acoustic properties are very important for the materials applied in automotives and buildings for heat and sound insulation applications. The Alambeta device was used to measure the thermal properties of perpendicularly-laid nonwovens. Based on the results of acoustic and thermal properties, the relationship between these two properties has been studied. In this research, the main purpose is to explore their inter-relation and further understand both acoustic performance and thermal properties of nonwoven fabrics. Most importantly, the result may provide a new approach to evaluate acoustic performance by simple measurement of thermal properties.

1.1.4. Investigation of acoustic behavior and air permeability of perpendicularly-laid nonwovens

This work also deals with the study of acoustic performance of perpendicularly-laid nonwovens and their relation to fabric air permeability. Air permeability of perpendicularly-laid nonwovens was examined by using FX3300 Textech Air Permeability Tester. It was observed that the sound absorption capacity was inversely proportional to air permeability. It was concluded that air permeability can be used as a criterion of sound absorption behavior of perpendicularly-laid nonwovens, a lower air permeability suggested a better sound absorption performance for perpendicularly-laid nonwoven fabric.

1.1.5. Investigation on sound absorption properties of aerogel based nonwovens

This work presents an investigation on sound absorption performance of aerogel based nonwoven fabrics. Polyester/polyethylene nonwovens embedded with hydrophobic amorphous silica aerogel were chosen for sound absorption measurements. The sound absorption coefficient (SAC) of single and multilayered of aerogel based nonwovens blankets was tested by Brüel and Kjær impedance tube, the noise reduction coefficient (NRC) was used for numerical analysis.

1.1.6. Study on some theoretical models of airflow resistivity for multi-component polyester perpendicularly-laid nonwovens

The airflow resistivity is a key parameter to predict accurately the acoustical properties of fibrous media. There is a large number of theoretical and empirical models which can be used to predict the airflow resistivity of this type of porous media. However, there is a lack of experimental data on the accuracy of these models in the case of multi-component fibrous media. This study presents a detailed analysis of the accuracy of several existing models to predict airflow resistivity which make use of the bulk density and mean fiber diameter information. Three types of perpendicularly-laid polyester (PET) nonwoven materials prepared by using regular PET, hollow PET and bi-component PET with a range of densities are chosen for this study. It is shown that some existing models largely under- or over-estimate the airflow resistivity when compared with the measured values. A novel feature of this work is that it studies the relative performance of airflow resistivity prediction models that are based on the capillary channel theory and drag force theory. These two groups of models are then compared to purely empirical models. It is found that the fit by some models is unacceptably high (e.g. error >20-30%). The results suggest that there are existing models which can predict the airflow resistivity of multi-component fibrous media with 12-20% error.

1.1.7. Analysis of acoustic properties of perpendicularly-laid nonwovens

This research presents a numerical investigation for acoustical properties of perpendicularly-laid nonwovens. The widely used impedance models such as Delany-Bazley, Miki, Garai-Pompoli and Komatsu models were used to predict acoustical properties. Comparison between measured and predicted values has been performed to get the most acceptable model for perpendicularly-laid nonwovens. It is shown that Delany-Bazley and Miki models can accurately predict surface impedance of perpendicularly-laid nonwovens, but Komatsu model has inaccuracy in prediction especially at low-frequency band. The results indicate that Miki model is the most acceptable method to predict the sound absorption coefficient with mean absolute error 8.39% from all the samples. The values are 8.92%, 12.58% and 69.67% for Delany-Bazley, Garai-Pompoli and Komatsu models, respectively.

1.2 Dissertation outline

The dissertation is divided into five chapters:

Chapter 1 Introduction: General introduction about the topic of research. It contains details

of the purpose and objectives of this research**.**

Chapter 2 Literature review: A detailed study of previous literature and understanding of studies conducted and identify the limitations in past research.

Chapter 3 Experimental Materials and Methods: An overview about sample materials, production methods, scientific concepts, experimental and prediction models used in this research. This chapter also has elaborate explanation about methods and techniques used for characterization of acoustic, compression, thermal and permeability experiments conducted. Besides, introduction of models for predicting airflow resistivity and sound absorption coefficient was included.

Chapter 4 Results and Discussion: A detailed analysis of the results derived from various experiments. The results were tabulated, suitable graphical representations made and detailed statistical analysis was performed. Various interpretations were drawn from the analysis.

Chapter 5 Conclusion: This chapter contains the broad conclusions drawn from the result and analysis of the research. An additional section discussing future research and recommendation has been included. The outputs are in the form of scientific papers, book chapters and conference proceedings.

Chapter 2 State of the Art in Literature

2.1 Purpose

The purpose of this chapter is to provide a background for the research conducted in this thesis. The first part of this chapter introduces the sound absorption mechanisms of porous materials. The second part of this literature review details the different types of sound-absorbing materials. The following part contains the applications of fibrous sound-absorbing materials. The third part contain details of fibrous materials and its properties such as thermal resistivity, air permeability and resistivity, compressibility and sound absorption. The later part introduces some existing models which used to predict airflow resistivity, impedance and sound absorption coefficient. Finally, the existing literature and the highlighted research gaps relevant to the various objectives of this research work have been summarized.

2.2 Sound absorption mechanism

The energy lost happens when sound propagates in small spaces, such as the interconnected pores of a porous absorber. This is primarily due to viscous boundary layer effects. Air is a typical viscous fluid, and consequently sound energy is dissipated via friction with the pore walls. There is also a loss in momentum due to changes in flow as the sound moves through the irregular pores. The boundary layer in air at audible frequencies is sub-millimeter in size, and consequently viscous losses occur in a small air layer adjacent to the pore walls. As well as viscous effects, there will be losses due to thermal conduction from the air to the absorber material; this is more significant at low frequency. For the absorption to be effective there must be interconnected air paths through the material; so an open pore structure is needed. Losses due to vibrations of the material are usually less important than the absorption as sound moves through the pores.[3]

2.3 Sound-absorbing materials

2.3.1 Main groups of sound-absorbing materials

Sound-absorbing materials can absorb most of the sound energy (e.g. > 80%). Sound-absorbing materials contain a wide range of different materials; their absorption properties depend on frequency, porosity, density, thickness, airflow resistivity, composition, surface finish, and method of mounting. However, materials that have a high value of sound absorption coefficient are usually porous.[11-12]

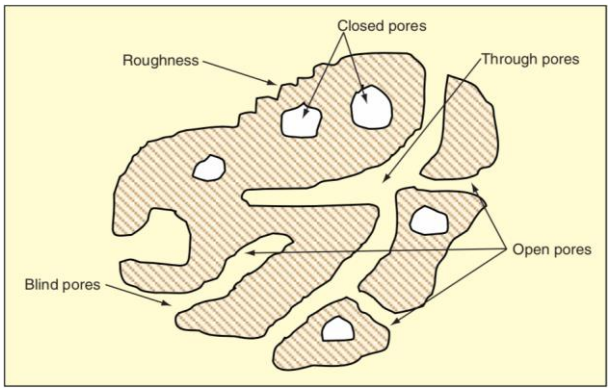

Figure 2.1 Schematic cross-section of a porous solid material[13]

A porous absorbing material is a solid that contains cavities, channels or interstices so that sound waves are able to enter through them. It is possible to classify porous materials according to their availability to an external fluid such as air. Figure 2.1 presents a schematic cross-section of a porous solid material.[13] Those pores that are totally isolated from their neighbors are called “closed” pores. They have an effect on some macroscopic properties of the material such as its bulk density, mechanical strength and thermal resistivity. However, closed pores are substantially less efficient than open pores in absorbing sound energy. On the other hand, “open” pores have a continuous channel of communication with the external surface of the body, and they have great influence on the absorption of sound. Open pores can also be classified into “blind” (open only at one end) or “through” (open at two ends).[13]

Figure 2.2 shows the three main types of porous sound-absorbing materials, their typical microscopic arrangements and the physical models used to describe their airflow and absorbing mechanisms. Porous sound-absorbing materials can be grouped in cellular, fibrous, or granular according to their microscopic configurations. Porous materials are characterized by the fact that their surfaces allow sound waves to enter the materials through a multitude of small holes or openings. Materials made from open-celled polyurethane and foams are examples of cellular materials. Fibrous materials consist of a series of tunnel-like openings that are formed by interstices in material fibers. Fibrous materials include those made from natural, synthetic or mineral fibers.[14] In addition, a porous absorbing material can also be granular. Consolidated granular materials consist of relatively rigid, macroscopic bodies whose dimensions exceed those of the internal voids by many orders of magnitude (agglomerates). Unconsolidated materials consist of loosely packed assemblages of individual particles (aggregates). Granular absorbing materials include some kinds of asphalt, porous concrete, granular clays, sands, gravel, and soils.[15-16] So the acoustical properties of

granular materials are an important factor in controlling outdoor sound propagation.[17]

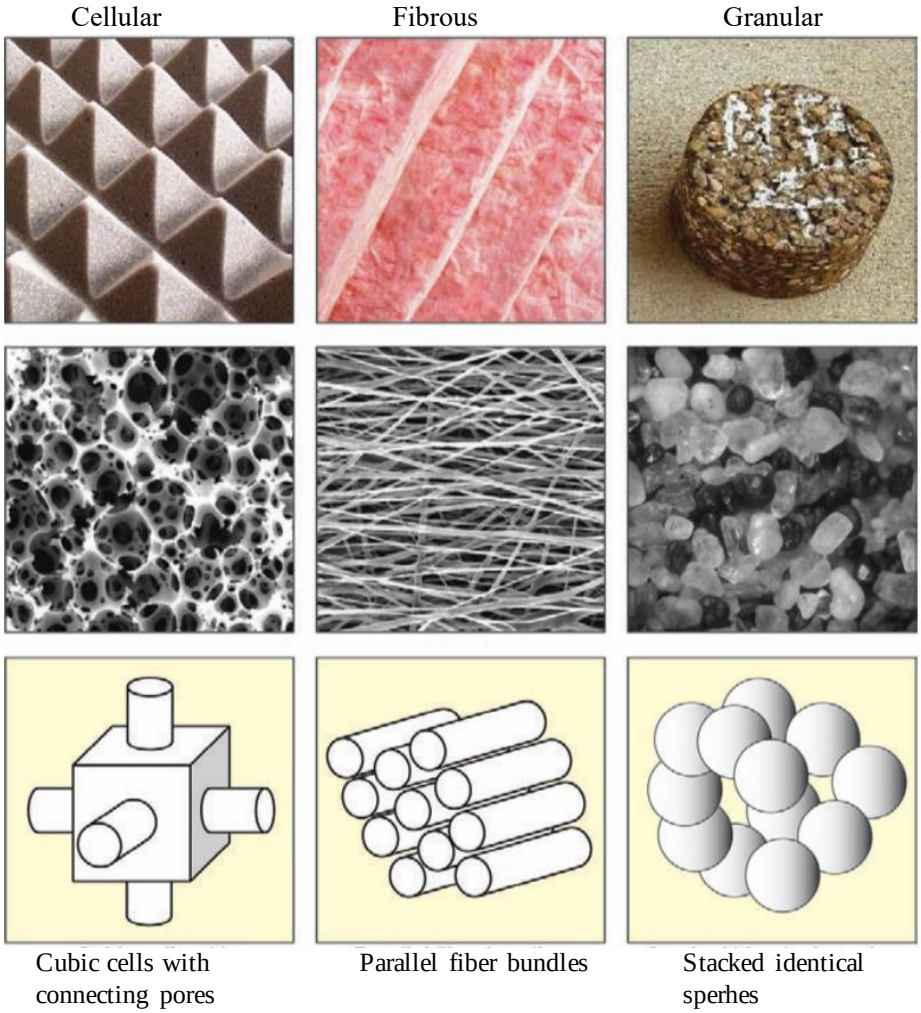

Figure 2.2 The main types of absorbing materials[12]

When a porous material is exposed to incident sound waves, the air molecules at the surface of the material and within the pores of the material are forced to vibrate and, in doing so, lose some of their original energy. This is because part of the energy of the air molecules is converted into heat due to thermal and viscous losses at the walls of the interior pores and tunnels within the material. At low frequencies, these changes are isothermal, while at high frequencies, they are adiabatic. In fibrous materials, much of the energy can also be absorbed by scattering from the fibers and by the vibration caused in the individual fibers. The fibers of the material rub together under the influence of the sound waves.[11, 18]

The sound absorption mechanism in bulk granular materials is quite similar to that in rigid porous materials where the solid structure can be regarded as ideally rigid and stationary. Then the sound absorption is produced by the viscosity of the air contained inside the

interconnecting voids that separate the granules. At low and mid frequencies, the solid structure interacts with the bulk of the gas through an isothermal heat transfer process. In addition, scattering from the granules also influences the absorption of sound energy inside the material.

2.3.2 Fibrous sound-absorbing materials

Most of the porous sound-absorbing materials commercially available are fibrous. Fibrous materials are composed of a set of fibers which can trap air between them. They are produced in rolls or in slabs with different thermal, acoustical, and mechanical properties. Fibers can be classified as natural and synthetic (artificial). Natural fibers can be vegetable (cotton, kenaf, hemp, flax, wood, etc.), animal (wool, fur felt) or mineral (asbestos etc.). Artificial fibers can be based on cellulose (regenerated bamboo fiber, for example), or polymer (polyester, polypropylene, polyamide etc.). Fibrous materials made from polymers are used mostly for sound absorption and thermal isolation. Synthetic fibers are made through high-temperature extrusion and are based on nonrecoverable chemicals, often from petrochemical sources, their carbon footprints are quite significant.

Recently, the use of natural fibers in manufacturing sound-absorbing materials has received much attention.[19-21] Natural fibers are not essentially completely biodegradable and modern technical developments have made natural fiber processing more economical and environmentally friendly. These new methods may result in increased use of high-quality fiber at competitive prices for industrial purposes. Their properties can be modified by pre-treatments or finishing. In addition, natural fibers are also safer for human health compared with most synthetic fibers.

An important geometrical parameter of a fiber is its diameter. The fiber diameter is directly related to the sound-absorbing characteristics of the material. In general, the diameter of natural fibers is unchangeable and diameter of synthetic fibers is tuned as per requirement. Figure 2.3 shows some scanning electron microscope (SEM) images of samples of hemp, glass, PLA and PP fibers. Natural fibers have more irregular shapes and variable diameters compared to synthetic fibers.[22-23]

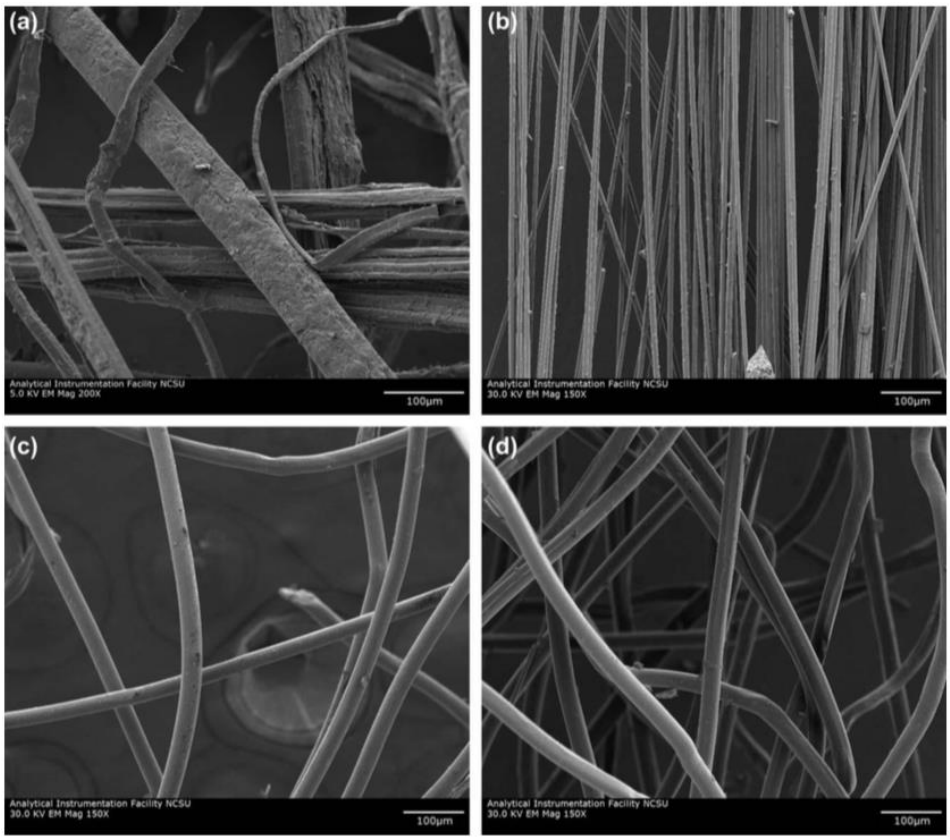

Figure 2.3 SEM images of fibers (a) hemp, (b) glass fiber, (c) PLA, and (d) PP at 30.0 kV. The magnification of hemp fiber (×200) is different from the other fibers (×150) [23]

2.4 Applications of fibrous sound-absorbing materials in automotive

Generally, fibrous sound-absorbing materials are used in the automotive industry to reduce interior noise and vibration and improve the sensation of ride comfort for the passengers. Interior noise is currently a competitive quality characteristic of every mode of transport facility in particular automobiles. Although interior noise lowers the comfort feeling inside a vehicle, it also induces fatigue and may reduce driving safety.[24] Therefore, the use and development of fibrous sound-absorbing materials have been more important in the automobile industry. A variety of sources contribute to the interior noise of a vehicle which can be structure-borne or airborne sound. Fibrous sound-absorbing materials used to control noise in vehicles must provide airborne transmission reduction as well as damping and sound absorption. However, the use of fibrous sound-absorbing materials in vehicles is not only dependent on their acoustic properties but also on additional characteristics. Fibrous sound-absorbing materials applied to reduce noise and vibrations are used either individually or as components of complex composite materials which are an interesting area of research. Figure 2.4 shows the location of major sources of interior noise on an automobile.

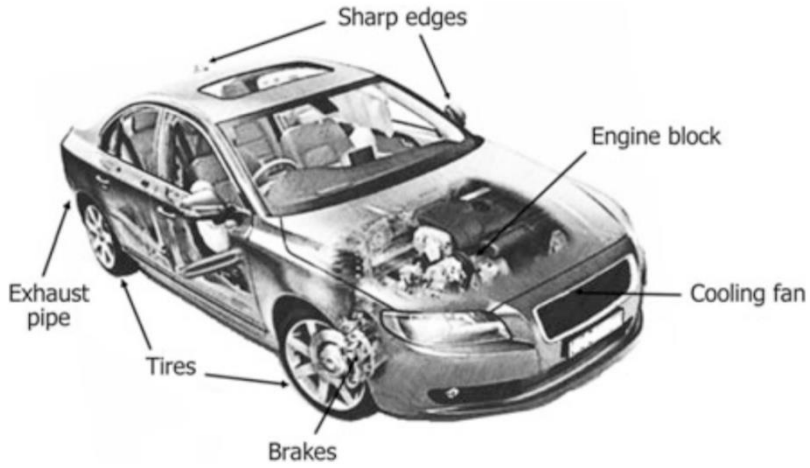

Figure 2.4 Location of some of the sources of power system, tire, and aerodynamic noise on an automobile[24]

Vehicle interior sound pressure levels can be controlled by reducing the noise generated by the sources, by reducing the noise during transmission through air-borne, and structure-borne paths, and by reducing the noise transmitted within the vehicle. Materials used to enclose noise sources are termed barrier materials in the automotive industry.[25] The noise isolation performance of these materials is mostly dominated by their areal density. This is a design challenge since car weight reduction is also a requirement of the transportation industry for fuel and cost reduction. Generally, barrier materials are characterized by transmission loss (TL). For single layers, TL increases theoretically by 6 dB for each doubling of frequency or by 6 dB at a given frequency if their mass/unit area is doubled. Much better performance can be achieved using multilayer panels, and the TL for such panels can be more like 12 dB/octave rather than 6 dB/octave of a single layer.[25]

Noise reduction is also achieved by providing mechanical damping to the structural vibrating panels of the car body, particularly at resonance frequencies. Constrained and unconstrained viscoelastic layers are typically used for this purpose. Damping layer materials add mass, which can also reduce airborne sound transmission through areas such as floor panels.[25] Sound absorption also can reduce interior noise once airborne and structure-borne sound has penetrated into the passenger cabin. TL is combined with the vehicle interior average sound absorption to obtain the total noise reduction. The increase of noise isolation is mathematically estimated by 10 × log of the sound absorption, that is, noise reduction increases by 3 dB for each doubling of total sound absorption.

Sound absorption can be provided on the interior surfaces of the vehicle (sidewalls, rooftop and floor) or within the volume by the seats.[26-28] In buses, the surface below overhead compartments can be used to add extra sound absorption. Although the materials are usually selected for factors other than sound absorption, such as resistance to mechanical damage, ease of cleaning, appearance and acoustic performance, there are several surface areas that can be designed with sound absorption. These include headliners, door casings, carpets, and other interior trims. Figure 2.5 shows locations where barrier and sound-absorbing materials are often applied in an automobile.

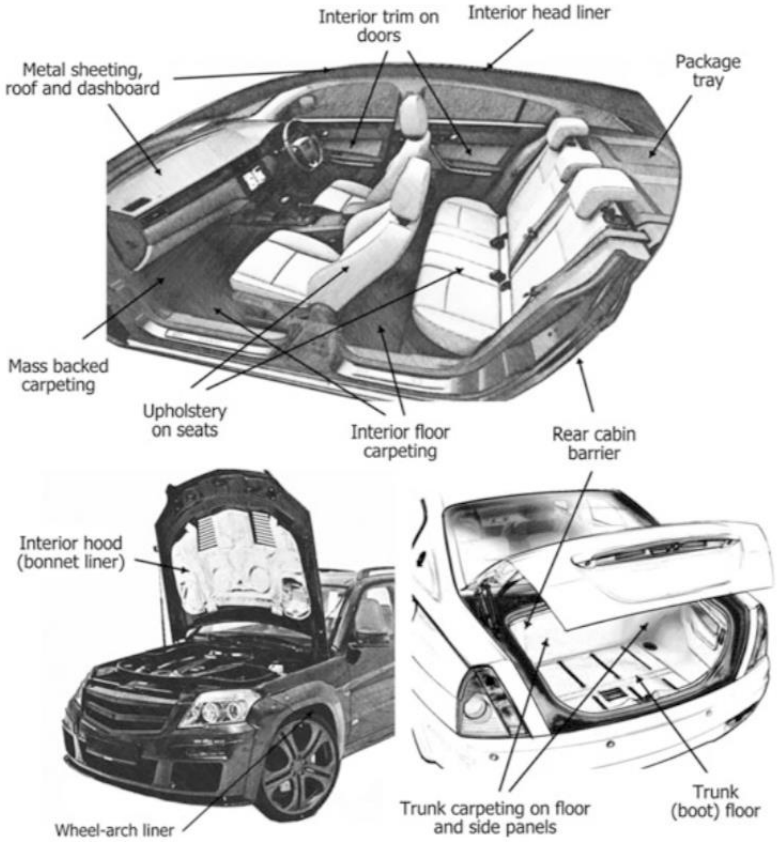

Figure 2.5 Typical locations in an automobile where barrier and sound-absorbing materials are utilized[24]

2.5 Characteristics of fibrous sound-absorbing materials

As previous description, the use of fibrous sound-absorbing materials in vehicles dependent on their acoustic properties and additional characteristics. This section literately presents acoustic properties of fibrous sound-absorbing materials as well as thermal properties, compressibility and air permeability. Later, the airflow resistivity which can be simply used to predict acoustic properties of fibrous material will be detailed introduced.

2.5.1 Acoustic properties of fibrous materials

Physical properties of fibrous materials such as fiber type, fiber size, material thickness, density, airflow resistance and porosity can affect the acoustic properties. This part groups the acoustic properties of fibrous materials into several determining factors such as fiber type, fiber size, structure parameters and so on.

2.5.1.1 Fiber type

The noise reduction application of inorganic fibrous materials, such as glass fiber and mineral wool, attracted a lot of attention due to their large specific surface area and high acoustical performance. The characteristic impedance and sound absorption of glass fiber and mineral wool have been investigated using impedance tube and Johnson-Champoux-Allard (JCA) model in Wang and Torng's study.[29] They stated that the difference in sound absorption ability is not obvious for materials with different bulk densities.

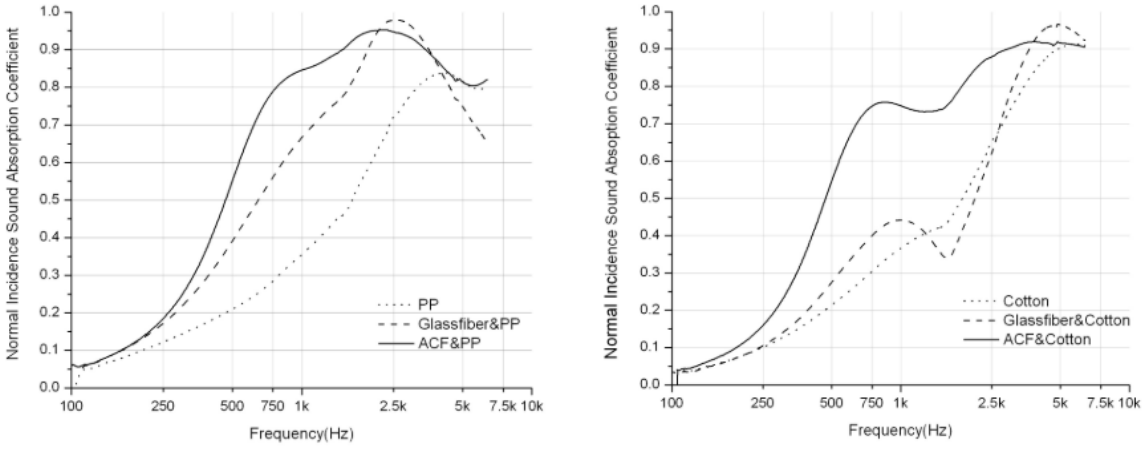

Figure 2.6 Absorption coefficient of PP-based composites and cotton-based composites[30]

Chen and Jiang[30] compared the sound absorption of activated carbon fiber and glass fiber separately laminated with pure cotton, pure ramie and pure polypropylene (PP) nonwovens. Their results indicated that nonwovens with activated carbon fiber as surface layer have better sound absorption than nonwovens with surface layer of glass fiber. Figure 2.6 presents the improvement on sound absorption capacity of PP-based and cotton-based composites by adding one activated carbon fiber layer.

Although inorganic fibrous materials have significant advantages, there are potential human health problems as a result of inhaling fibers or due to skin irritation and lay-down in the lung alveoli.[31] Thus, some researchers investigate the usage of natural fibers instead of inorganic

fibers. Compared to glass fiber and mineral wool, natural fibers as sound-absorbing materials have relatively high thermal and acoustic performances and are more environmentally friendly. Reviews of acoustic properties of natural fibers can be found in literature.[32-33] The sound absorption and physical properties of nonwovens produced via needle-punching through combining banana, bamboo and jute fibers with PP staple fibers have been reported in the ratio of 50 : 50.[34] The SEM photographs of banana/PP, jute/PP, and bamboo/PP needle-punched nonwoven are presented in Figure 2.7. The results showed that bamboo/PP nonwoven exhibits higher stiffness, better sound absorption, higher tensile strength, lower elongation, lower thermal conductivity and lower air permeability. It is known to be more suitable for interior automotive noise control than other fiber composites. Figure 2.8 shows the absorption coefficient of different combinations of nonwovens.

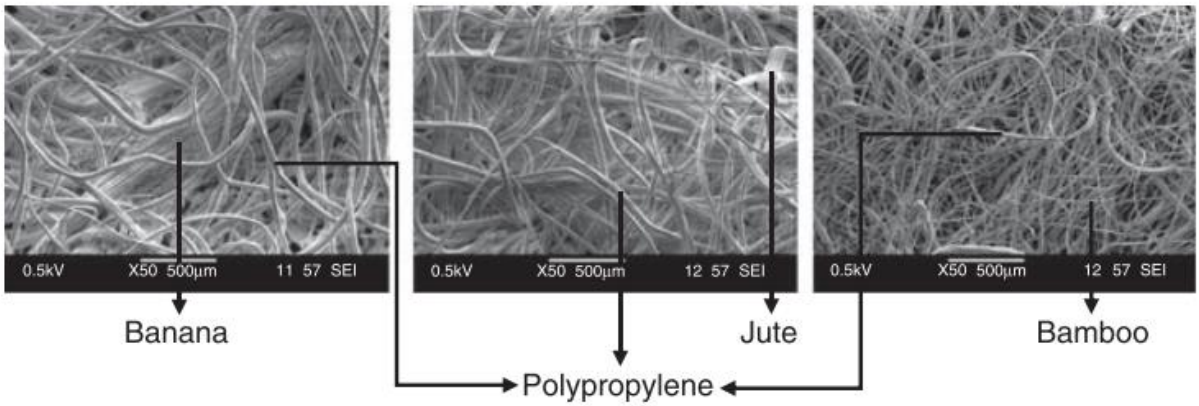

Figure 2.7 SEM photographs of banana/PP, jute/PP, and bamboo/PP needle-punched nonwoven[34]

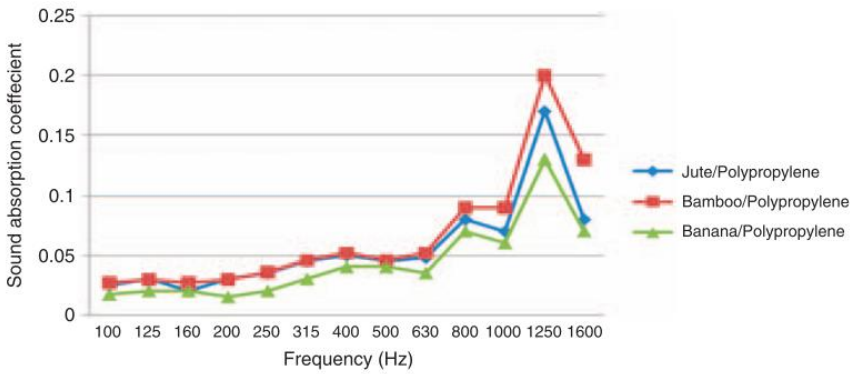

Figure 2.8 Absorption coefficient of different combinations of nonwovens[34]

Oldham et al.[35] carried out experiments for sound absorption on cotton, wool, ramie, flax, jute and sisal fiber through impedance tube and reverberation chamber measurements. Table

2.1 presents the sound absorption coefficient of different fibrous materials at 500 Hz from their results. They studied the effectiveness of both Delany-Bazely and Garai-Pompoli models for the prediction of the absorptive properties of natural fibers. They stated that the two prediction models agree with measured data for natural fibers with less than 60 μm diameter. However, these models have less than satisfactory applicability in the case of most natural fibers where fiber diameters are relatively large.

Table 2.1 List of sound absorption coefficients of different fibrous material at 500 Hz[35]

Materials	Fiber diameter (μm)	Standard deviation of fiber diameter	SAC at 500 Hz
Cotton	13.5	0.9	0.50
Flax	21.8	5.4	0.40
Ramie	24.4	12.1	0.40
Wool	37.1 (coarse wool)	9.1	0.20
Jute	81.2 (bundle)	37	0.20
Sisal	213 (bundle)	16.4	0.10

Beside inorganic and natural fibers, synthetic fibers presently play an important role on the application for noise reduction. Unlike natural fibers, synthetic fibrous materials can be more widely used in various applications for noise reduction due to their possible diversity. Pelegrinis et al.[36] applied an alternative model based on the Kozeny-Carman equation, to theoretically predict the airflow resistivity of polyester materials with uniform fiber diameter. The airflow resistivity retrieved using Miki model from absorption coefficient data has been compared with the predicted airflow resistivity. The results indicated that the flow resistivity retrieved from the acoustical absorption data agreed well with that predicted by the Kozeny-Carman model, giving mean absolute values of relative error (MAVRE) within 10%.

2.5.1.2 Fiber size

Koizumi et al.[37] reported an increase in sound absorption coefficient with a decrease in fiber diameter. This is because, thin fibers can move more easily than thick fibers on sound waves. Moreover, with fine denier fibers more fibers are required to reach equal more fibers for same volume density which results in a more tortuous path and higher airflow resistance was reported by Sun, Banks-Lee and Peng.[38] A study by Youn Eung Lee et al.[39] concluded that the fine fiber content increases sound absorption coefficient values due to an increase in airflow

resistance by means of friction of viscosity through the vibration of the air. A study by Koizumi et al.[37] also showed that fine denier fibers ranging from 1.5 to 6 denier (dpf) perform better acoustically than coarse denier fibers. Moreover, it has been reported by Koizumi[37] that, micro denier fibers (less than 1 denier) provide a dramatic increase in acoustical performance. Na et al.[40] investigated the sound absorption coefficients of five micro-fiber fabrics and one regular fiber fabric by the reverberation room method, and found that the micro-fiber fabrics' sound absorption is superior to that of conventional fabric with the same thickness or weight.

Insulation and absorption properties of nonwoven fabrics depend on fiber geometry and fiber arrangement within the fabric structure. Because of their complex structure, it is very difficult to define the microstructure of nonwovens. The structure of nonwovens only has fibers and voids that are filled by air. The different structures and size of the fibers result in different total surface areas of nonwoven fabrics. Consequently, the sound absorption coefficient can be affected.

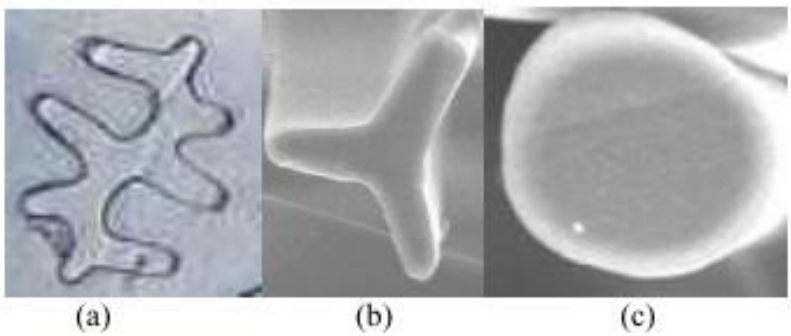

Figure 2.9 (a) 4DG, (b) trilobal, and (c) round fiber cross- sections[22]

Tascan and Vaughn[22] investigated the acoustical insulation of nonwoven fabrics with different polyester fiber (see in Figure 2.9), and stated that fabrics made from 3 denier fibers were better sound insulators than those made from 15 denier fibers. Their results also indicated that the nonwoven fabrics made from 4DG and trilobal fibers have better sound insulation results than nonwoven fabrics made from round fibers. The transmitted sound results of nonwoven fabrics made by different size and shape were shown in Figure 2.10 and Figure 2.11.

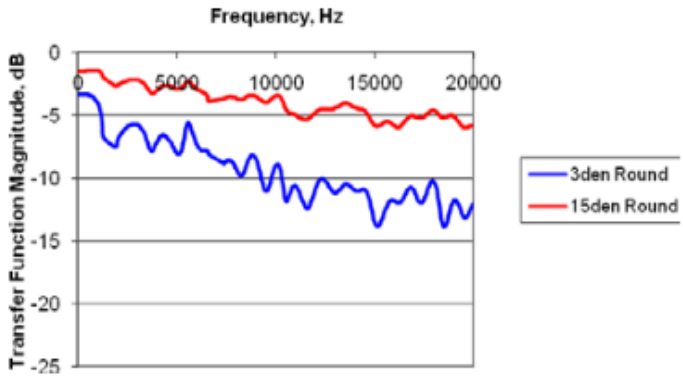

Figure 2.10 Transmitted sound results for vertically lapped nonwoven fabrics made from 3 and 15 denier fibers with 0.07g/cm^3 fabric density[22]

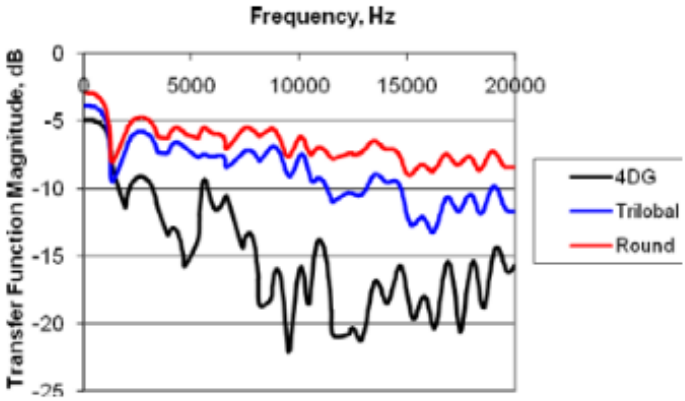

Figure 2.11 Transmitted sound results for vertically lapped fabrics made from 15 denier 4DG, trilobal, and round fibers with 0.43g/cm^3 density[22]

2.5.1.3 Structure parameters

The structure parameters including porosity, areal density (GSM) and thickness. The porosity is a ratio of the pore volume involved in sound propagation to the total volume; this is the open porosity. Porosity of textile structures can be investigated based on the geometrical arrangement of fibers in the textile structure. For evaluation of fibrous materials porosity ε it is simple to use experimentally evaluated fiber density ρ_f [kg/m^3] and density of corresponding fibrous materials ρ [kg/m^3],

$$\varepsilon = 1 - \rho/\rho_f \ . \tag{2.1}$$

The areal density (GSM) ρ_s can be calculate according to the following equation:

$$\rho_s = \rho_f \cdot L \ , \tag{2.2}$$

where L is the fibrous materials thickness.

Density of a material is often considered to be the important factor that governs the sound absorption behavior of the material. At the same time, cost of an acoustical material is directly related to its density. A study by Koizumi et al.[37] showed the increase of sound absorption value in the middle and higher frequency as the density of the sample increased. The number of fibers increases per unit area when the apparent density is large. Energy loss increases as the surface friction increases, thus the sound absorption coefficient increases.

For specialist absorbers, such as mineral wool, the porosity is close to one, and so the value is often assumed rather than measured. Good sound-absorbing materials tend to have high porosity, for example most mineral wools have a porosity of about 0.98, but in designing an absorber, it is possible to trade off porosity against flow resistivity (and to a lesser degree the structural factors outlined later). When determining the porosity, closed pores should not be included in the total pore volume as these are relatively inaccessible to sound waves (closed pores are most commonly found in foams, even ones designed to be open celled). The porosity is a key parameter, but for commonly used bulk absorbing materials, the value of porosity does not vary greatly and is close to unity.[3] Since most of the models used to predict airflow resistivity involves porosity, researchers normally discussed the effect of porosity on airflow resistivity to investigate the influence of porosity on sound absorption properties.[41]

Fibrous material thickness is a very important factor determining the sound absorption ability. Effectiveness of absorption is directly related to the thickness of the material; sound-absorbing materials are most effective when their thickness is between one-fourth and one-half the wavelength of the sound, with the maximum performance where the thickness is one-fourth the wavelength. This means that sound absorbers do a very good job at high frequencies, which have short wavelengths. However, at lower frequencies, very thick materials would be required to yield high sound absorption, which would be impractical on the interior of a car.[41] Generally, the increase of thickness results in an increase of sound absorption coefficient at low-frequency range. Moreover, the sound absorption of fibrous material involves viscous losses, which convert acoustic energy into heat as sound wave travels through the interconnected pores of fibers of the material. Thus, for high areal density samples there are more fibers involved in the viscous losses and more acoustic energy is dissipated in the form of heat energy.[42] From Figure 2.12, it can be seen that the sound absorption coefficient generally increases with increasing of thickness at same frequency.

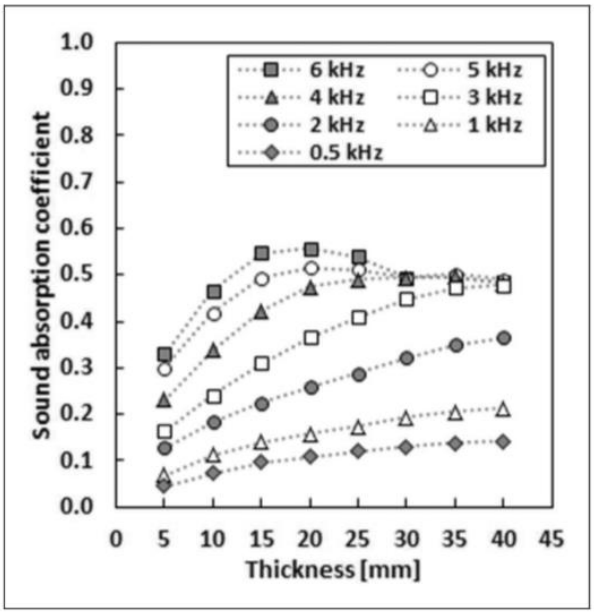

Figure 2.12 Sound absorption of 350 g/m^2 high-loft nonwovens at different thicknesses[42]

2.5.1.4 Airflow resistivity

The airflow resistivity is one of the most critical parameters determining the sound absorption properties of a porous absorber. It is a measure of how easily air can enter a porous absorber and the resistance that airflow meets through a structure. Once the airflow resistivity is known, a series of theoretical or empirical models can be applied to predict the impedance and absorption coefficient of fibrous media.[43] The values of airflow resistivity vary largely between various type of common fibrous absorbent materials. It therefore gives some sense of how much sound energy may be enter the material pores to be lost due to viscous and inertia effects within the material.

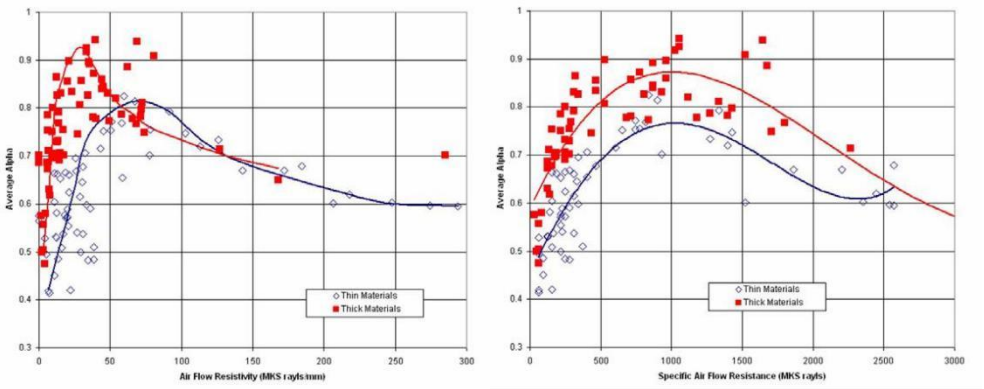

Figure 2.13 The relationship between airflow resistivity (left), airflow resistance (right) and mean value of sound absorption coefficient[41]

Zent and Long[42] studied 128 types of porous absorbers with varying airflow resistivity and

material types (cotton blends, microfibers, etc.). They grouped materials into two groups according to samples thickness. They concluded that a specific air flow resistance of around 1000 MKS rayls can yield good overall absorption regardless of the thickness of the material. Figure 2.13 presents the relationship between airflow resistivity, resistance and sound absorption.

2.5.1.5 Combinations

Besides the material made from different types of fiber, cellular and granular materials also can combine with fibers to form a new sound-absorbing materials. Aerogel is a typical granular material. Aerogel was discovered more than 80 years ago. Aerogels have high porosity (>90%), a high specific surface area, light weight, and low sound velocity (down to 90m/s).[45-46] Due to these characteristics, aerogels can be used in sound absorption and thermal insulation fields. Acoustic properties of aerogels were studied and summarized by researchers.[47-51] Forest et al. measured the reflection coefficient, the attenuation and the sound velocity of the granular aerogels and glass wool sample, and found that the acoustic transmission losses in the aerogel absorber are at least 10 dB higher than in the glass wool sample of the same thickness for the frequency range 300-1700 Hz. Gibiat et al.[52] presented that acoustic properties of cylindrical silica aerogels in ultrasonic and audible range; and reported that the low-density aerogels can exhibit unexpected attenuation for well-defined frequency bands. Their results also showed that an unexpected high attenuation is related to the aerogel density.

Since nonwovens and aerogels have impressive acoustic properties and aerogel based nonwoven can be widely used in various environments because of its flexible structure. It is essential to understand the sound absorption behavior of aerogel based nonwoven fabric. However, the acoustic properties of aerogel based nonwoven fabrics were seldom investigated. Oh et al.[53] prepared PET/Aerogel blankets and measured the acoustic and thermal insulation properties of PET/Aerogel blankets. They reported that the existence of a great amount of silica aerogel of more homogeneous and smaller size in the cell wall material has a positive effect on the sound absorption and thermal insulation.

2.5.2 Thermal properties of fibrous materials

Thermal properties of nonwoven fabrics are extensively studied by researchers. Generally, the thermal insulation properties of nonwoven fabrics have a strong correlation with fabric dimensional and structural parameters.[54] Arambakam et al.[55] numerically investigated the

thermal performance of fibrous insulation materials and concluded that heat conduction through fibrous structures increases by increasing the solid volume fraction, fiber diameter, and fibers' through-plane orientations. In their study, simulations were conducted in 3-D fibrous geometries resembling the microstructure of a fibrous material. They assumed that the heat transfer through the interstitial fluid is independent of the geometrical parameters of the solid phase (for when the porosity is held constant), the energy equation was solved only for the solid structures, and the resulting values were used to predict the effective thermal conductivity of the whole media. The novel feature of their study is that they studied the effect of fiber in- and through-plane orientation on thermal resistivity, the simulations of fiber orientation are presented in Figure 2.14.

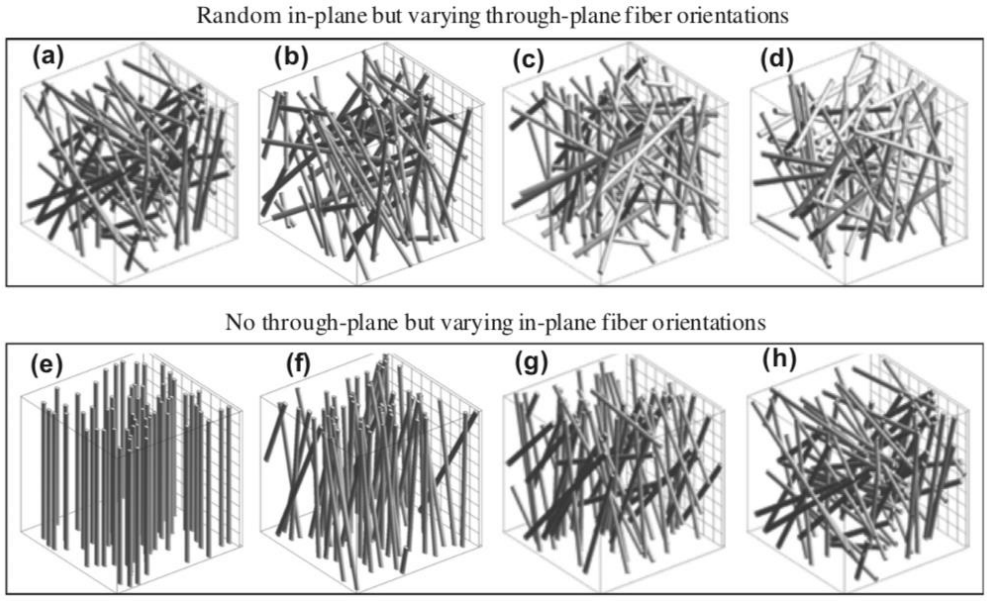

Figure 2.14 (a–d) Show fibrous media with random in-plane but different through-plane fiber orientations. (e–h) Show fibrous media with no through-plane but different in-plane fiber orientations[55]

Researchers[56] summarized that for a fixed weight, thermal insulation increases with thickness. Vallabh[57] confirmed that fabric volume density is a significant factor influencing the radiation component of effective thermal conductivity and the radiative thermal conductivity decreased with increase in the fabric volume density as shown in Figure 2.15. They explained this phenomenon by the fact that, as the density of the nonwoven fabric increases, the packing density increases making the fibrous structure more packed. This causes the mean free path, which is defined as the distance traveled by a photon before hitting the surface of the surrounding fibers, to decrease thus causing a decrease in the heat transfer due to

radiation mode.

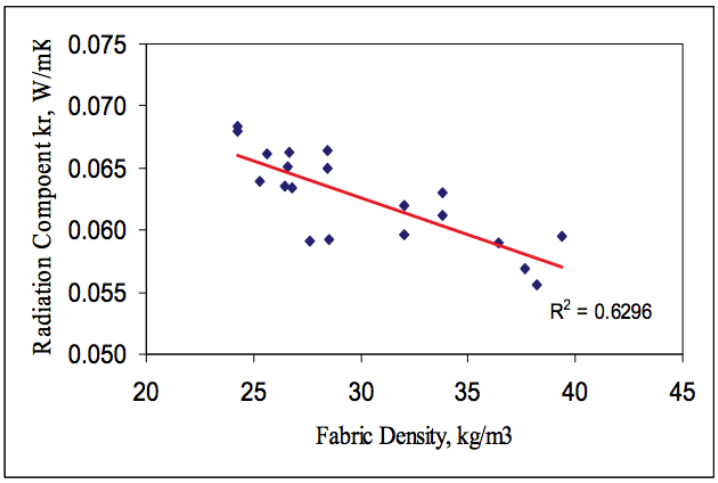

Figure 2.15 Effect of Fabric Density on the Radiative Thermal Conductivity[57]

2.5.3 Compressibility of high-loft fibrous materials

Kang et al.[58] investigated the relationship between the fiber orientation distribution and mechanical properties of perpendicularly-laid nonwovens prepared by air and mechanical folding systems, they stated that with the increase of web density the compressional resistance of air folding nonwoven increases as well while that of mechanical folding material decreases. Their results also showed that air folding nonwoven has lower strain at maximum stress than the mechanical folding nonwoven, as shown in Figure 2.16.

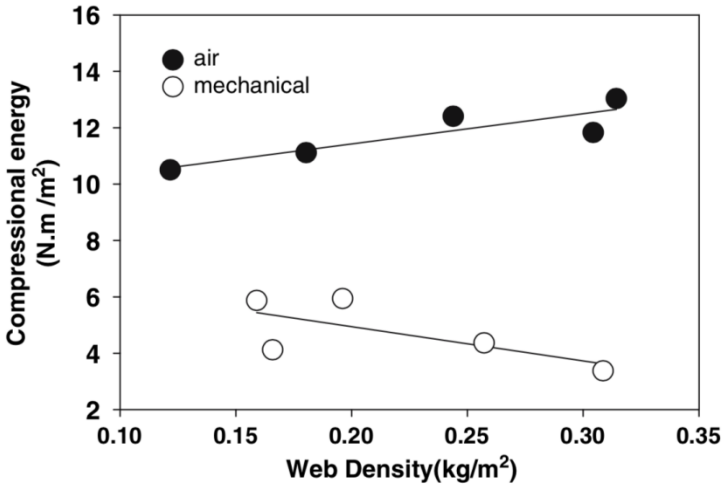

Figure 2.16 Effect of web density on compressional energy of high-loft nonwoven made by air and mechanical folding method[58]

The compressional behavior of perpendicularly-laid nonwovens was introduced by Parikh et al..[59-60] They compared the compressional resistance of perpendicularly-laid and cross-laid

nonwovens, they concluded that perpendicularly-laid nonwovens have higher compressional resistance and their recovery properties are better to cross-laid nonwovens. Figure 2.17 presents the comparison of compression recovery ability between perpendicularly-laid and cross-laid nonwovens, it can be seen that the perpendicularly-laid nonwoven without cotton content has much better compression resistance.

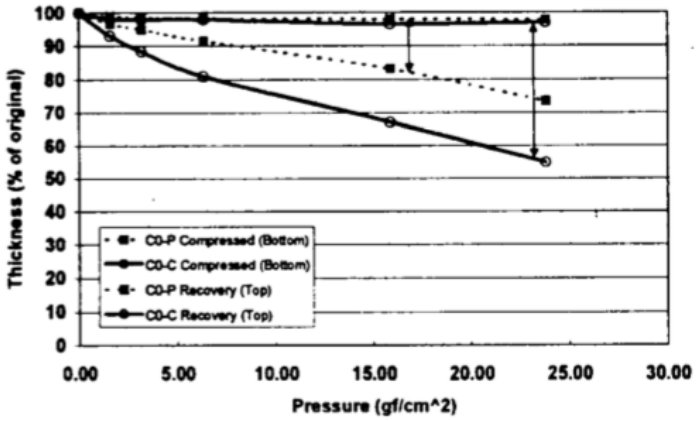

Figure 2.17 Compression curves of perpendicularly-laid and cross-laid nonwovens[51]

2.5.4 Air permeability and airflow resistivity of fibrous materials

Air permeability has been theoretically studied for almost one and a half centuries. Base on Darcy's law and Kozeny Equation, air permeability, q, is directly proportional to the pressure gradient between the two sides of a measuring fabric.[61-62]

$$q = \frac{k_p \cdot \Delta P}{\eta \cdot L}, \tag{2.3}$$

Where k_p, the flow permeability coefficient (1), is

$$k_p = \frac{\varepsilon^3}{\eta \cdot s^2 \cdot k}, \tag{2.4}$$

where k, the Kozeny constant (1), is

$$k = k_0 t_f^2, \tag{2.5}$$

where t_f, the tortuosity (1), is

$$t_f = \frac{l_e}{l}, \tag{2.6}$$

where ΔP is the pressure gradient (Pa), η is the viscosity of the flow (Pa·s), s is channel

wetted surface ($(\mathrm{Pa}\cdot\mathrm{s})^{-1/2}$), l is the thickness of sample (m), l_e is the effective channel length (m), L is the material thickness (m), ε (1) is the porosity of sample and k_0 is the shape factor (1).

Soltani and Zarrebini[63] reported that the acoustic characteristics of woven fabrics are related to fabric structural parameters such as weave type, yarn linear density, yarn twist, and fabric thickness of woven fabric. They concluded that air permeability of woven fabrics, which is strongly dependent on fabric cover factor, can be used as a criterion of sound absorption behavior, as shown in Figure 2.18. In addition, the investigated the effect of weft yarn twist on noise reduction coefficient (NRC) and air permeability. They stated that fabric NRC decreases as weft yarn twist is increased. It must be pointed out that, up to a certain level of twist, fabric air permeability is generally increased. However, fabric air permeability beyond the certain level of twist tends to decrease slightly. Figure 2.19 shows the effect of weft yarn twist on NRC and air permeability.

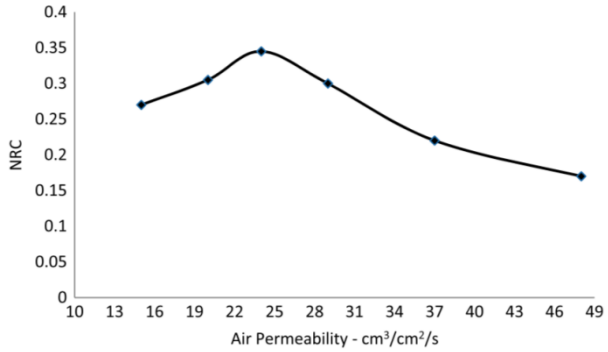

Figure 2.18 Effect of air permeability on NRC[63]

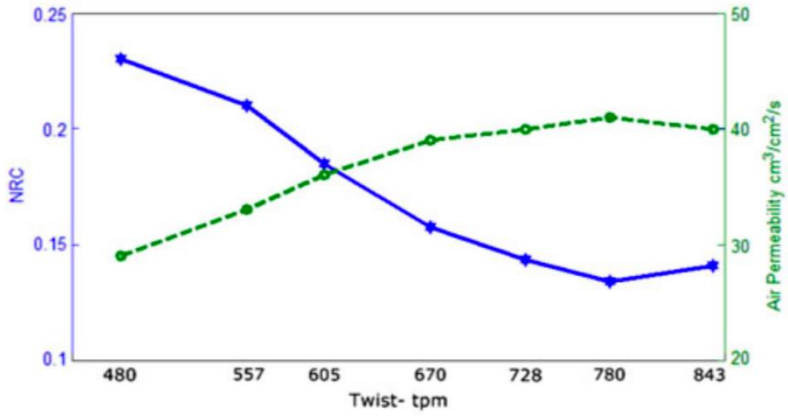

Figure 2.19 Effect of weft yarn twist on NRC and air permeability[63]

Yang and Yu[64] conducted experimental study and found that nonwoven fabrics with highest value of air permeability exhibit inferior acoustic absorbency. They stated that the

permeability is not just linear to porosity, but also relates to many other complex and difficult-to-measured parameters such as tortuosity, shape factor etc. Kucuk and Korkmaz[2] measured sound absorption properties of eight different nonwoven composites including different fiber types mixed with different ratios, they stated that the increase in thickness and the decrease in air permeability results in an increase in sound absorption properties of the material.

According to the direct airflow method detailed in the standard ISO 9053-1991[65], the airflow resistivity is determined by an experiment where a sample of a porous material is placed in a tube, and a steady airflow is passed through the sample. The airflow velocity u, the pressure drop between two sides of the sample Δp, and the thickness of the sample l, are measured.[65] The airflow resistivity, σ (Pa.s/m^2) of the material is defined:

$$\sigma = \frac{\Delta p}{u \cdot l}. \tag{2.7}$$

Xue et al.[66] proposed a modification based on the existing models for two-component fibrous materials with varying fiber diameter. In their paper, the micro-CT measurement was applied to obtain the fiber radii distribution. By applying the fiber radii distribution in one of the Tarnow model, they accurately predicted the airflow resistivity of materials having two fiber components. Hurrell et al.[67] compared the performance of several theoretical and empirical models applied to a representative range of nonwoven fibrous media composed of blends of different fiber sizes and types. Their results indicated that the value of the flow resistivity inverted with either Padé approximation or Miki model is more accurate than that predicted using Bies-Hansen, Garai- Pompoli or Kozeny-Carman equations. The comparison between measured and predicted airflow resistivity from Hurrell et al.[67] is presented in Figure 2.20.

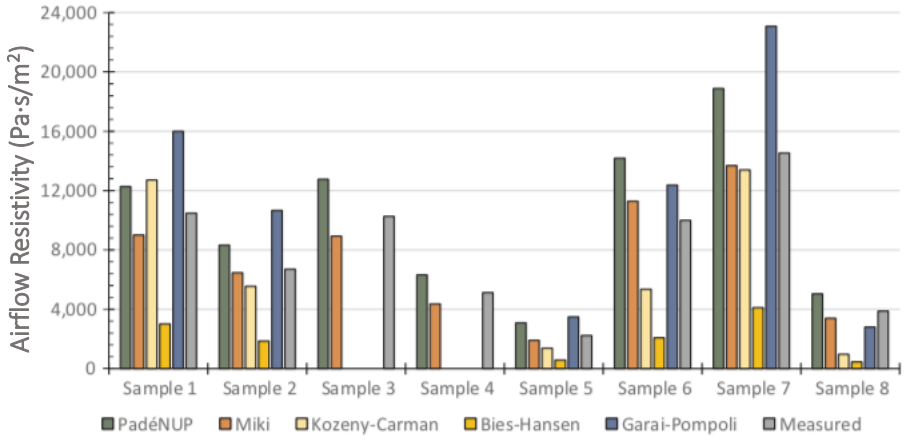

Figure 2.20 The measured, inverted and predicted flow resistivity values[67]

2.6 Models for predicting airflow resistivity, impedance and sound absorption

The presently widely used sound absorption prediction methods are based on the theory proposed by Zwikker and Kosten.[68] In their theory, the surface characteristic impedance of rigidly-backed layer of porous material with finite thickness can be calculated from the following equation:

$$Z_s = Z_c \coth(kl) \,, \tag{2.8}$$

where Z_s is the surface characteristic impedance, Z_c is the characteristic impedance, k is the complex wavenumber, and l is the material thickness. Then, the normal-incidence sound absorption coefficient can be derived from the surface characteristic impedance as

$$\alpha = 1 - |R|^2 = 1 - \left| \frac{\frac{Z_s}{\rho_0 c_0} - 1}{\frac{Z_s}{\rho_0 c_0} + 1} \right|^2 , \tag{2.9}$$

where α is the sound absorption coefficient, R is the pressure reflection coefficient, ρ_0 is the air density at room temperature, and c_0 is the sound speed in air media at room temperature.

2.6.1 Review of previous works on airflow resistivity models

There are a large number of theoretical and empirical models to predict the airflow resistivity for fibrous and granular media. Good reviews of some of these models can be found in Refs. 69-70. These models can be grouped into two main categories: theoretical models and empirical models. In this section, the previous works on airflow resistivity models will be introduced and we will present mathematical expressions from some existing models for the airflow resistivity for completeness. In Chapter 4 we will use these models to predict the measured flow resistivity of multi-component polyester fiber.

2.6.1.1 Theoretical models

There are two main theories in airflow resistivity theoretical models: capillary channel theory and drag force theory. The airflow resistivity models established using capillary channel theory are based on the works of Hagen-Poiseuille, Kozeny and Carman, where the flow through the porous material is treated as a conduit flow between parallel cylindrical capillary tubes.[71-72] Davies presented a model to fit his own transverse permeability data for the flow through porous fibrous materials having a high fabric porosity (as high as 0.7) .[73] The airflow resistivity of fiber orientation along the flow direction was in the same form as the Kozeny-Carman equation, and the airflow resistivity of fiber orientation perpendicular to the flow

direction was obtained using the lubrication approximation, assuming that the narrow gaps between adjacent cylinders dominate the flow resistance.[74-75] Pelegrinis et al.[36] modified the Kozeny-Carmen model to obtain more accurate prediction for the airflow resistivity of uniform fiber diameter polyester material. Lind-Nordgren and Göransson presented a scaling law applied to the airflow resistivity of porous materials having a porosity and tortuosity close to 1.[76] However, it has been argued that those models based on capillary channel theory are unsuitable for high porosity media in which the porosity is greater than 0.8.[72] Airflow resistivity models based on capillary channel theory are summarized in Table 2.2.

Table 2.2 Airflow resistivity models established using capillary channel theory

Method	Airflow resistivity
Davies CN[73]	$\sigma = \frac{64\eta(1-\varepsilon)^{1.5}[1+56(1-\varepsilon)^3]}{d^2}$
Kozeny-Carman[72]	$\sigma = \frac{180\eta(1-\varepsilon)^2}{d^2\varepsilon^3}$
Lind-Nordgren[76]	$\sigma = \frac{128\eta(1-\varepsilon)^2}{d^2\varepsilon}$
Doutres *et al.*[77]	$\sigma = \frac{128\eta(1-\varepsilon)^2}{d^2}$
Pelegrinis *et al.*[36]	$\sigma = \frac{180\eta(1-\varepsilon)^2}{d^2}$

η is the air dynamic viscosity (Pa·s), ε is the material porosity and d is the fiber diameter (m).

There are a number of airflow resistivity models which are based on drag force theory. In these models the fibers in the porous material that form the walls of the pores in the structure, are treated as obstacles to an otherwise straight flow of the fluid and the fibers cannot be displaced.[78] The sum of all the 'drags' is assumed to be equal to the total resistance to flow in the porous material. Unlike capillary flow theory, drag force theory and unit cell models demonstrate the relationship between permeability and the internal structural architecture of the porous material. In drag force models, the fibers are assumed to be aligned unidirectionally in a periodic pattern such as a square, triangular or hexagonal array. The airflow resistivity of unidirectional fibrous materials can then be solved using the Navier-Stokes equation in the unit cell with appropriate boundary conditions.[33] One of the earliest equivalent dimensionless permeability for flow parallel to an array of fibers was developed by Langmuir.[79] Tarnow presented a new way to calculate the airflow resistivity of randomly placed parallel fibers based on Voronoi polygons.[80] In his study, Tarnow discussed a two-

dimensional model consisting of parallel fibers randomly spaced for flow parallel and perpendicular to the fibers. A number of other theoretical, drag force models have been developed to predict the flow resistivity of fibers. A summary of these models is given in Table 2.3.

Table 2.3 Airflow resistivity models established using drag force theory

Method	Airflow resistivity
Langmuir[79]	$\sigma = \frac{16\eta(1-\varepsilon)}{d^2[-\ln(1-\varepsilon) - 1.5 + 2(1-\varepsilon) - \frac{(1-\varepsilon)^2}{2}]}$
Hasimoto[81]	$\sigma = \frac{32\eta(1-\varepsilon)}{d^2(-\ln(1-\varepsilon) - 1.476)}$
Kuwabara[82]	$\sigma = \frac{32\eta(1-\varepsilon)}{d^2[-\ln(1-\varepsilon) - 1.5 + 2(1-\varepsilon) - \frac{(1-\varepsilon)^2}{2}]}$
Happel[83]	
	A. Flow parallel to fibers
	$\sigma = \frac{72\eta(1-\varepsilon)}{d^2[-\ln(1-\varepsilon) - 3 + 4(1-\varepsilon) - (1-\varepsilon)^2]}$
	B. Flow perpendicular to fibers
	$\sigma = \frac{72\eta(1-\varepsilon)}{d^2[-\ln(1-\varepsilon) - \frac{1-(1-\varepsilon)^2}{1+(1-\varepsilon)^2}]}$
Tarnow[80]	Flow parallel to fibers
	A. Square lattice
	$\sigma = \frac{16\eta(1-\varepsilon)}{d^2[-\ln(1-\varepsilon) + 0.5 - 2\varepsilon]}$
	B. Random lattice
	$\sigma = \frac{16\eta(1-\varepsilon)}{d^2[-1.280\ln(1-\varepsilon) + 0.526 - 2\varepsilon]}$
	Flow perpendicular to fibers
	C. Square lattice
	$\sigma = \frac{16\eta(1-\varepsilon)}{d^2\{\ln[(1-\varepsilon)^{-1/2}] - 0.5\varepsilon - 0.25\varepsilon^2\}}$
	D. Random lattice
	$\sigma = \frac{16\eta(1-\varepsilon)}{d^2[-0.640\ln(1-\varepsilon) + 0.263 - \varepsilon]}$

2.6.1.2 Empirical models

The empirical model of airflow resistivity was first introduced by Nichols, who suggested that the airflow resistance, $\sigma \sim \frac{h*\rho^{1+x}}{d^2}$, where the adjustable parameter, h, is $0.3 \leq x \leq 1$. This parameter value depends on the distribution of the fibers in material.[84] Based on the work by Nichols, Bies and Hansen presented a simple model which allows the calculation of the airflow resistivity of fiber glass starting from the values of its bulk density and fiber diameter.[85] Garai and Pompoli investigated the airflow resistivity of double fiber component polyester materials and extended the Bies and Hansen model to predict the flow resistivity of polyester fibers.[86] Manning and Panneton analyzed the acoustic behavior of shoddy fiber materials manufactured by three different methods: mechanical bonding, thermal bonding, and resin bonding. They established three simple airflow resistivity models based on weight-of-evidence approach.[87] A summary of the equations for these empirical models is given in Table 2.4.

Table 2.4 Airflow resistivity models established using empirical method

Method	Airflow resistivity	
Bies & Hansen[85]		$\sigma = \frac{3.18 \times 10^{-9} \rho^{1.53}}{d^2}$
Garai & Pompoli[86]		$\sigma = \frac{2.83 \times 10^{-8} \rho^{1.404}}{d^2}$
Manning & Panneton[87]	Mechanically bonded	$\sigma = \frac{2.03 \times 10^{-8} \rho^{1.485}}{d^2}$
	Resin bonded	$\sigma = \frac{3.61 \times 10^{-9} \rho^{1.804}}{d^2}$
	Thermally bonded	$\sigma = \frac{1.94 \times 10^{-8} \rho^{1.516}}{d^2}$

Note: These models are dimensionally nonhomogeneous since they are based on empirical formula. ρ is the material density (kg/m^3), d is the fiber diameter (m).

2.6.2 Some impedance models

When modelling the acoustical behavior of porous materials, non-acoustic parameters such as porosity, airflow resistivity, tortuosity, thermal permeability and viscous and thermal characteristic lengths are tiring and time consuming to determine. Therefore, usage of empirical models that are developed by regression method is more common, in which such parameters are not necessary. As described in Eqs. (2.6) and (2.7), it is essential to obtain the characteristic impedance and complex wavenumber to predict the surface characteristic

impedance and sound absorption coefficient. Several impedance models are introduced in this section.

2.6.2.1 Delany-Bazley model

Delany and Bazley[88] carried out several impedance tube measurements in the 1960s with which they could derive empirical relationships between impedance and wavenumber to the airflow resistivity. These relationships are widely used across quite a wide frequency range due to the reasonable estimations. It is necessary to note that several empirical models have been developed based on Delany-Bazley model. In Delany-Bazley model,[24] only a non-acoustical parameter of airflow resistivity is required to predict acoustical characteristics.

$$Z_c = \rho_0 c_0 \left(1 + 0.0571 \left(\frac{\rho_0 f}{\sigma}\right)^{-0.754} - j0.087 \left(\frac{\rho_0 f}{\sigma}\right)^{-0.732}\right) \tag{2.10}$$

$$k = \frac{\omega}{c_0}\left(0.189 \left(\frac{\rho_0 f}{\sigma}\right)^{-0.595} + j\left(1 + 0.0978 \left(\frac{\rho_0 f}{\sigma}\right)^{-0.7}\right)\right), \tag{2.11}$$

where σ is the airflow resistivity, f is the frequency, $j = \sqrt{-1}$ is the complex number and $\omega = 2\pi f$ is the angular frequency.

2.6.2.2 Miki model

Miki[89] developed a new regression model based on experimental data from Delany and Bazley's study in 1989. Miki's proposed modifications to the Delany-Bazley model were in order to generate a more accurate model, valid for a broader frequency range. The characteristic impedance and wavenumber in Miki's model[89] is given by:

$$Z_c = \rho_0 c_0 \left(1 + 0.0699 \left(\frac{f}{\sigma}\right)^{-0.632} - j0.107 \left(\frac{f}{\sigma}\right)^{-0.632}\right) \tag{2.12}$$

$$k = \frac{\omega}{c_0}\left(0.160 \left(\frac{f}{\sigma}\right)^{-0.618} + j\left(1 + 0.109 \left(\frac{f}{\sigma}\right)^{-0.618}\right)\right). \tag{2.13}$$

2.6.2.3 Garai-Pompoli model

Besides a new simple model for airflow resistivity prediction which has been developed by Garai and Pompoli, they also presented a modified impedance model based on Delany-Bazley method.[86] The accuracies of Delany-Bazley, Dunn-Davern and Garai-Pompoli prediction models were investigated by comparing the measured sound absorption of polyester materials with diameter ranging from18 to 48 μm[22], suggesting a suitable method

of prediction for the acoustical characteristics of polyester materials. They performed a similar set of measurements on polyester materials to those of Delany-Bazely's to obtain the following expressions for predicting the characteristic impedance and wavenumber:

$$Z_c = \rho_0 c_0 \left(1 + 0.078 \left(\frac{\rho_0 f}{\sigma}\right)^{-0.623} - j0.074 \left(\frac{\rho_0 f}{\sigma}\right)^{-0.660}\right) \tag{2.14}$$

$$k = \frac{\omega}{c_0}\left(0.159 \left(\frac{\rho_0 f}{\sigma}\right)^{-0.571} + j\left(1 + 0.121 \left(\frac{\rho_0 f}{\sigma}\right)^{-0.530}\right)\right). \tag{2.15}$$

2.6.2.4 Komatsu model

Komatsu[90] proposed a new prediction model based on the impedance tube measurements from 15 types of glass fiber and 9 types of mineral wool samples in 2008. The airflow resistivity of the samples ranges from 6000 to 72900 Pa·s/m^2. He stated that the Komatsu model is more accurate to predict the acoustical properties of a fibrous material compared with the Delany-Bazley and Miki models,

$$Z_c = \rho_0 c_0 \left(1 + 0.00027 \left(2 - \log\frac{f}{\sigma}\right)^{6.2} - j0.0047 \left(2 - \log\frac{f}{\sigma}\right)^{4.1}\right) \tag{2.16}$$

$$k = \frac{\omega}{c_0}\left(0.0069 \left(2 - \log\frac{f}{\sigma}\right)^{4.1} + j\left(1 + 0.0004 \left(2 - \log\frac{f}{\sigma}\right)^{6.2}\right)\right). \tag{2.17}$$

Chapter 3 Experimental part

3.1 Materials

3.1.1 Perpendicularly-laid nonwoven fabrics

Five perpendicularly-laid nonwoven fabrics prepared by vibrating perpendicular lapper at the Technical University of Liberec, Czech Republic, as well as two types of commercial available nonwoven fabrics which separately made by vibrating perpendicular lapper and rotating perpendicular lapper were selected to carry out this study.

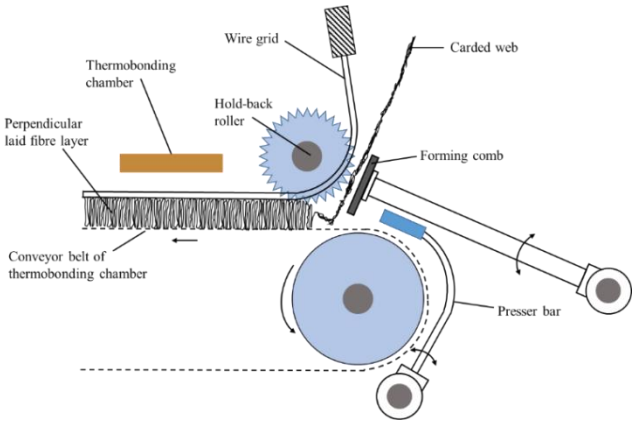

Figure 3.1 Vibrating perpendicular lapper

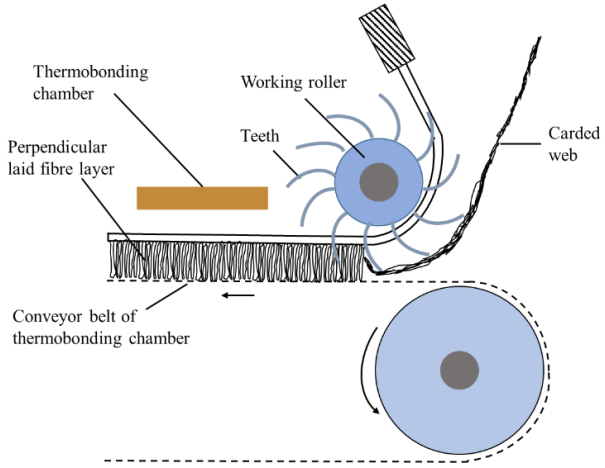

Figure 3.2 Rotating perpendicular lapper

The vibrating perpendicular lapper (STRUTO) is illustrated in Figure 3.1. The carded web is fed onto conveyor belt and a reciprocating forming comb pulls the carded web towards the hold back roller to form a fold. The fold is pulled off the comb by a system of needles placed on a reciprocating compressing bar and pushed to the fiber layer which is created and moved between the conveyor belt and a wire grid. The fiber layer is bonded by melt-bonding fibers

present in the fiber blend when it passes through thermobonding chamber. The rotating perpendicular lapper (WAVEMAKER) is shown in Figure 3.2. Carded web is brought to the working roller. The teeth of the working roller form the carded web into folds creating a fiber layer between the conveyor belt and wire grid. Again, the fiber layer is bonded in the thermobonding chamber.[91]

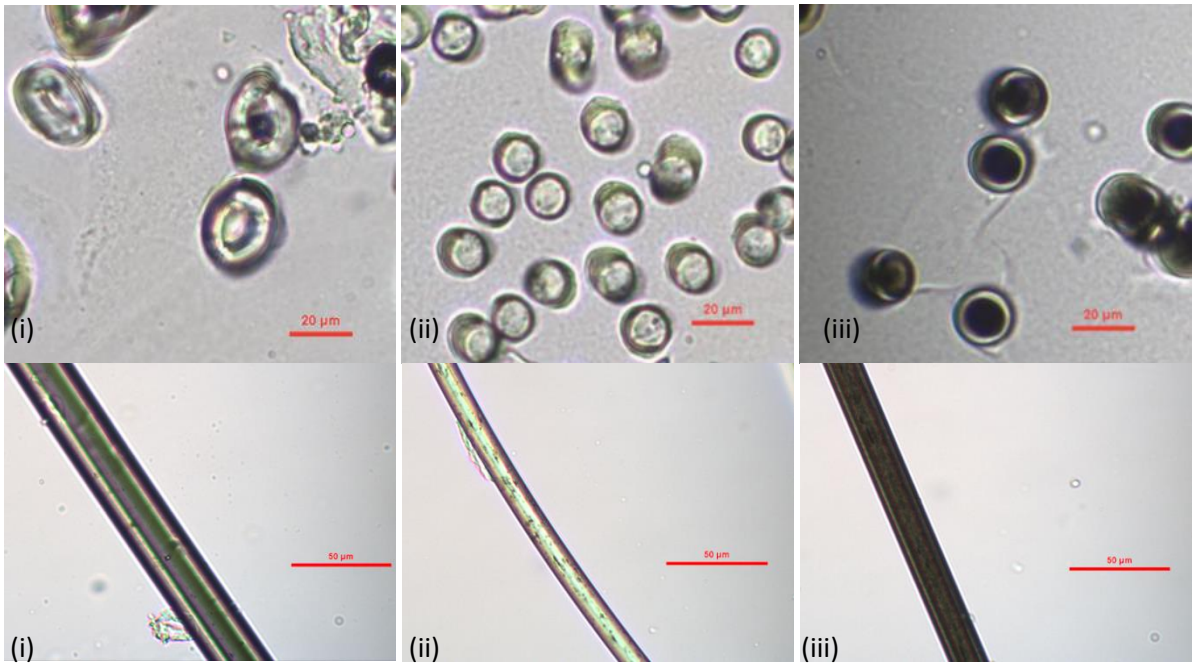

Figure 3.3 Cross-sectional and longitudinal microscopic images of polyester fibers: (i) hollow PET; (ii) PET; (iii) bi-component PET

Table 3.1 Fiber specifications[92]

Fiber Code	Types of PET	Diameter (µm)	95% confidence interval for diameter	Staple Length (mm)	Ratio of Core and Sheath
i	Hollow PET	24.45	24.45 ± 0.709	70.00	----
ii	PET	13.18	13.18 ± 0.158	50.00	----
iii	Bicomponent PET	17.93	17.93 ± 0.229	50.00	3:1
iv	PET	26.91	26.91 ± 0.439	57.00	----
v	Bicomponent PET	14.58	14.58 ± 0.198	38.00	3:1

PET: polyethylene terephthalate.

Table 3.2 Characteristics of perpendicularly-laid nonwovens

Samples type	Samples code	Fiber content	Mean diameter (μm)	Manufacturing techniques	Thickness (mm)	Areal density ($g \cdot m^{-2}$)	Porosity (%)	Bulk density ($kg \cdot m^{-3}$)	Airflow resistivity ($Pa \cdot s/m^2$)
Original	A	30%-i 45%-ii 25%-iii	15.94	WAVEMAKER	24.09	507.5	98.15	21.07	5757.05
	A1			WAVEMAKER	20.71	506.3	97.86	24.45	7319.58
	A2			WAVEMAKER	18.80	502.2	97.66	26.71	7530.23
Heat compressed	A3			WAVEMAKER	18.51	509.8	97.59	27.54	9829.76
	A4			WAVEMAKER	14.29	508.2	96.89	35.56	14989.14
	A5			WAVEMAKER	14.02	503.1	96.86	35.87	15414.89
	A6			WAVEMAKER	11.05	503.5	96.01	45.56	19733.06
Original	B			STRUTO	28.36	478.3	98.52	16.87	4828.55
	B1			STRUTO	20.37	479.5	97.94	23.54	7498.51
Heat compressed	B2			STRUTO	19.14	469.6	97.85	24.54	7412.32
	B3			STRUTO	15.52	480.2	97.29	30.94	13397.13
	B4			STRUTO	12.81	472.5	96.59	36.88	16750.24
Original	C			STRUTO	27.48	465.2	98.15	16.93	4108.94
	C1			STRUTO	23.76	463.1	97.86	19.49	5337.58
Heat compressed	C2			STRUTO	20.96	471.4	97.66	22.49	7029.82
	C3			STRUTO	16.61	458.6	97.59	27.61	10181.53
	C4			STRUTO	13.51	472.3	96.89	34.95	12868.69
	C5			STRUTO	10.50	468.5	96.86	44.60	20474.6
Original	D	70%-iv 30%-v	20.83	STRUTO	20.82	335.7	98.68	16.12	2208.3
Original	E			STRUTO	19.85	317.5	98.69	15.99	2031.52
Original	F			STRUTO	20.12	198.6	99.19	9.87	1024.4
Original	G			STRUTO	20.66	259.3	98.97	12.55	1727.8

Note: WAVEMAKER is rotating perpendicular lapper; STRUTO is vibrating perpendicular lapper.

The perpendicularly-laid nonwoven samples were made by different types of polyester fibers. Samples A, B and C have same fiber content, while samples D, E, F and G have another fiber content. The details of five types of fiber i, ii, iii, iv and v are illustrated in Table 3.1. The sheath part of fibers iii and v are low-melting polyethylene terephthalate (PET). In order to get the cross-sectional slice of fibers, the resin embedding technology was utilized. Cross sectional and longitudinal microscopic images were also captured (see in Figure 3.3) at the Technical University of Liberec using JENAPOL microscope and NIS-elements software. Since fiber i, ii and iii are the contents of samples A, B and C which will be mainly investigated their properties, the microscopic images of fibers iv and v are not necessary to take.

In this study, sample A was prepared by rotating perpendicular, samples B, C, D, E, F and G were produced by vibrating perpendicular lapper. In order to produce nonwoven samples with different thicknesses, the heat-pressing method was applied. Samples A, B and C were compressed under 600 Pa pressure at 130 ℃ for 5 minutes, thickness gauges were applied to obtain sample at certain thicknesses. The schematic of heat-pressing method was shown in Figure 3.4.

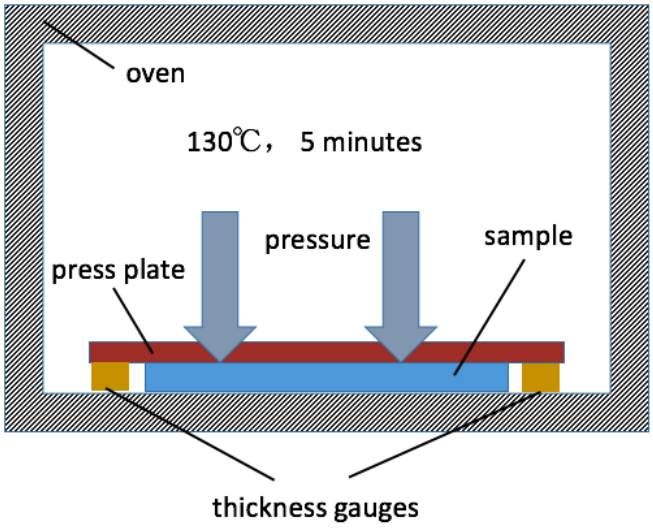

Figure 3.4 Schematic of heat-pressing method

The characteristics of the nonwoven specimens are listed in Table 3.2. According to ASTM C830-00, sample porosities were determined.[93] The content percentage of samples is based on weight. The fiber diameter has been determined using the ImageJ software based on the scanning electron microscope (SEM) images (see Figure 3.5), so that the fiber diameter distribution for polyester nonwovens A, B and C were obtained. 2358 fiber diameters from

150 SEM images were measured in total to ensure reproducible statistics.

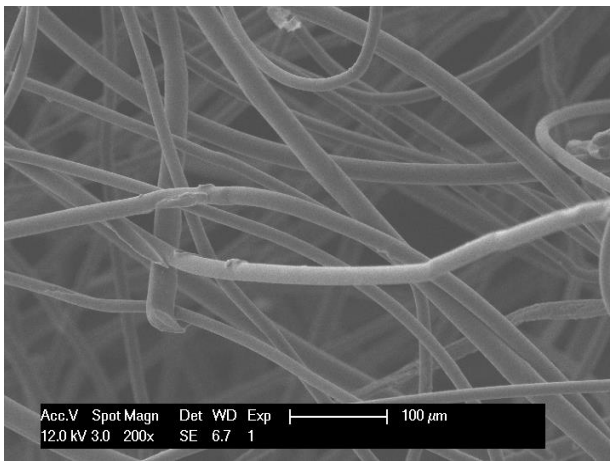

Figure 3.5 Scanning electron microscope (SEM) image of sample A

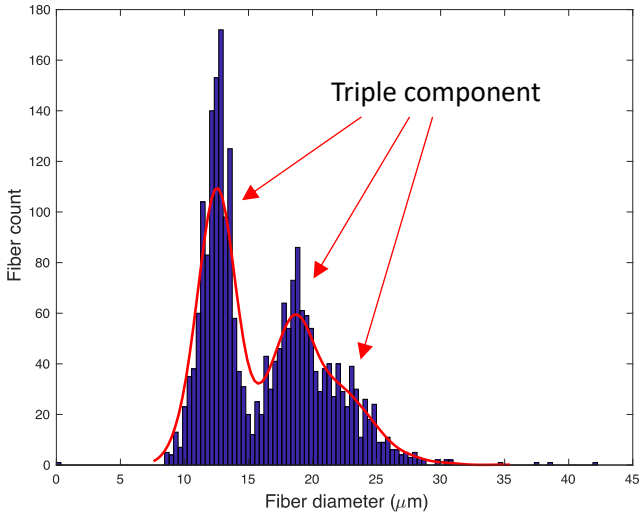

Figure 3.6 Fiber diameter distribution of polyester nonwovens A, B and C obtained for 2358 fiber diameter data

The fiber diameter distribution is shown in Figure 3.6. The kernel density estimation was applied to get the distribution line in the image analysis. Obviously, some of the features are that it has at least two peaks and one tail at the large diameter end. A symmetric fiber diameter distribution on either side of the highest peak implies that the finest fiber is the key component which is 45% in polyester materials. An asymmetric fiber diameter distribution can be found at the second peak from the left and the slope of distribution line has a slight decrease after the peak. It indicates that there is another type of polyester fiber besides the two types of fiber which can be easily distinguished from the first and second peaks from the left. Thus, samples A, B and C have triple fiber components with rough diameter of 13, 19

and 22 μm. The mean fiber diameter of multi-component polyester materials was determined according to the following equation:

$$d = \frac{\sum_{i=1}^{n} d_i}{n} \quad , \tag{3.1}$$

where n is the total fiber count, d_i is the diameter for each fiber. The mean diameter of polyester fibers was presented in Table 3.2. The same method was applied to obtain fiber diameter of samples D, E, F and G.

The densities of the fiber types i, ii, iii, iv and v were measured by liquid pycnometry method, the values are 947.97 kg/m^3, 1228.93 kg/m^3, 1217.64 kg/m^3, 1177.52 kg/m^3 and 1318.61 kg/m^3 for fiber i, ii, iii, iv and v, respectively. Since the closed pores have little or no effect on the airflow resistivity and sound absorption, voids in hollow fibers were not included in this analysis.[94] By means of an Alambeta device (SENSORA), fabric thicknesses were measured and fabric areal density was determined according to ISO 9073-1:1989.[95] Figure 3.7 illustrates that the majority of fibers in an uncompressed sample are vertically orientated and parallel arranged. The orientation angle of fibrous layer in this study (Figure 3.7, areas highlighted in red) was defined as the angle between the surface of sample and the dominant fibrous layer axis. Such an angle is dependent on material density or compression degree of the fibrous specimen. During the process of heat press, the angle of fibrous layer orientation decreased and consequently, thickness of specimen reduced and material density increased.

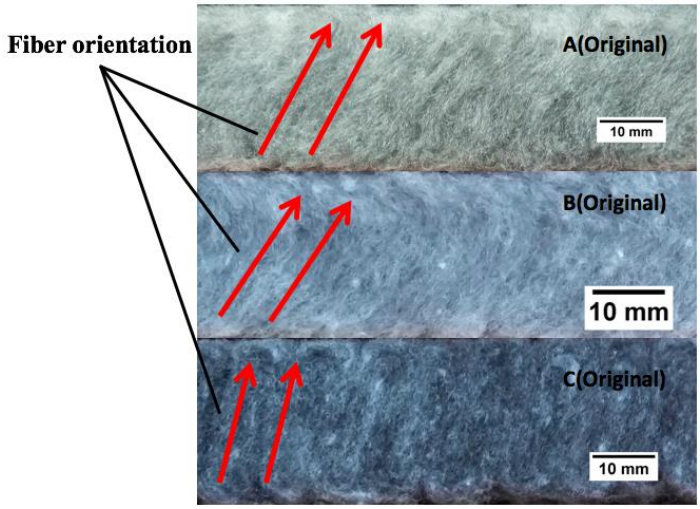

Figure 3.7 Cross-sectional macroscopic images of original samples A, B and C

Circular specimens with 100 mm diameter were cut with an ELEKTRONISCHE

STANZMASCHINE TYPE 208. Measurements were carried out in a standard setup for air flow resistivity. In current study, the airflow resistivity was measured directly with an AFD300 AcoustiFlow device (Gesellschaft für Akustikforschung Dresden mbH, Dresden, Germany) according to ISO 9053:1991.[65] The AcoustiFlow device determines the airflow resistivity based on direct-airflow method on open porosity porous materials. For each perpendicularly-laid nonwoven fabric, ten samples were measured to ensure the reproducibility of the airflow resistivity experiment, results summarized in Table 3.2.

3.1.2 Aerogel based nonwoven fabrics

Aerogel was discovered more than 80 years ago. Aerogels have high porosity (>90%), a high specific surface area, low weight, and low sound velocity.[96-97] Due to these characteristics, aerogels can be used in sound absorption and thermal insulation fields. The specifications of amorphous silica aerogel involved in this work are shown in Table 3.3.

Table 3.3 Amorphous silica aerogel specification

Properties	Value range
Particle size range	0.1–0.7 mm
Pore diameter	~20 nm
Density	135±15 kg/m^3

Table 3.4 Characteristics of aerogel based nonwoven fabrics

Sample No.	Fabric density kg/m^3	95% confidence interval	Areal density g/m^2	95% confidence interval	Thickness mm	95% confidence interval	% of aerogel
AP-A	79.6	79.6 ± 0.512	278.6	278.6 ± 1.021	3.5	3.5 ± 0.02	1.5
AP-B	80.4	80.4 ± 0.623	498.5	498.5 ± 1.102	6.2	6.2 ± 0.01	2.5
AP-C	66.7	66.7 ± 0.324	440.2	440.2 ± 1.045	6.6	6.6 ± 0.07	2.0

50:50 ratio compositions of polyester/polyethylene thermal-bounded nonwoven fabrics embedded with aerogel were selected. The type of aerogel used was hydrophobic amorphous silica aerogel, which is excellent for ambient and sub-ambient insulating applications.[98] The aerogel particles were added during thermal bonding of the nonwoven web. High resolution images for the aerogel based nonwoven fabrics are shown in Figure 3.8. It can be seen that

the aerogel is uniformly dispersed between the fibers in the structure. The physical properties are shown in Table 3.4.

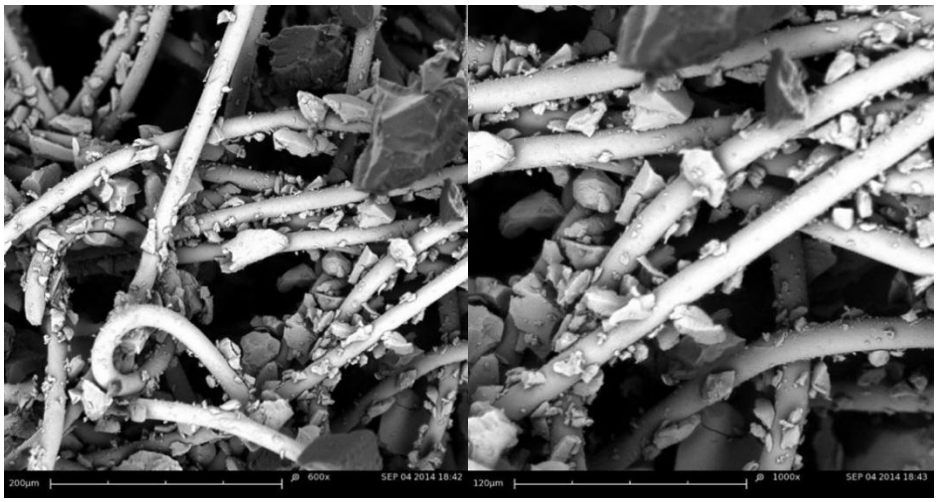

Figure 3.8 Scanning electron microscope (SEM) images of aerogel based nonwovens[98]

3.2 Evaluation of sound absorption

3.2.1 Impedance tube measurement

Acoustic properties of materials can be evaluated by steady-state methods, reverberant chamber methods, impedance tube methods, etc. In this study, the impedance tube was used to obtain normal incidence impedance. The surface impedance of perpendicularly-laid nonwovens was determined according to ISO 10534-2.[99] The 45 mm impedance tube manufactured by Materiacustica (as shown in Figure 3.9) was applied to carry out the impedance measurements. The measurement frequency range starts from 200 and goes up to 4200 Hz. The measurements of airflow resistivity and impedance were carried in the Jonas Lab at the University of Sheffield. For each nonwoven fabric, ten samples were measured.

Figure 3.9 Materiacustica 45 mm impedance tube

Besides, a Brüel and Kjær measuring instrument (as shown in Figure 3.10) containing Type

4206 Impedance Tube, PULSE Analyzer Type 3560, and Type 7758 Material Test Software was used for sound absorption testing within the frequency range 50Hz–6.4 kHz. A large tube (100 mm in diameter) and a small tube (29 mm in diameter) were set up for measuring the sound absorption in low-frequency range from 50-1600Hz and high-frequency range 500-6400Hz respectively. The curves from both measurements were merged. The sound absorption values of lower common frequencies (start from 50 to 1600 Hz) were mainly from the large tube and the higher common frequencies (up to 1600 Hz) were mainly from the small tube.[8] The lower boundary was chosen higher than the tube limit in order to avoid inaccuracies caused by structural vibrations or phase mismatch.[67] The sound absorption coefficient measurements were carried out by using Brüel and Kjær measuring instrument at Technical University of Liberec.

Figure 3.10 Brüel and Kjær measuring instrument

Although two different impedance tube measurement systems were applied, the measurement principles are same. A sound source is mounted at one end of the impedance tube and the material sample is placed at the other end. The loudspeaker generates broadband, stationary random sound waves. These incident sound signals propagate as plane waves in the tube and hit the sample surface. The reflected wave signals are picked up and compared to the incident sound wave.[100]

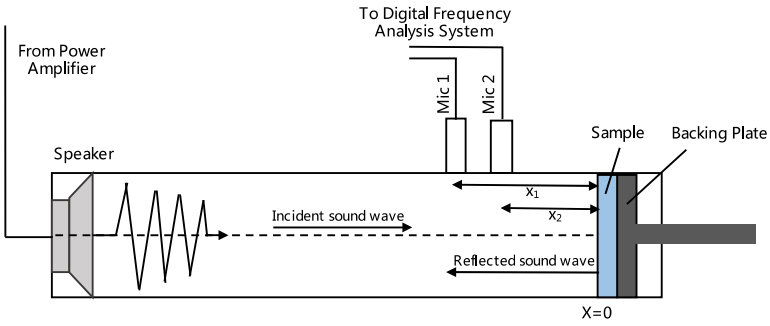

Figure 3. 11 Two-microphone impedance tube schematic

.A schematic of the two microphone impedance tube setup used in this work is depicted in Figure 3.11. Steady state pressure in the impedance tube is given by:

$$p = A\left(e^{jkx} + Re^{-jkx}\right), \tag{3.2}$$

where A is a complex constant, R is the pressure reflection coefficient, k is the wavenumber, $j = \sqrt{-1}$ is the complex number, and x is the position of sample surface.

There are two standard methods for sampling the pressure within the tube: standing wave ratio method and transfer function technique.[3] The second method was applied for determination of impedance in this work. The transfer function between two microphone positions in the impedance tube is measured as shown in Figure 3.8. The transfer function is the ratio of pressure between two microphone positions:

$$H_{12} = \frac{p_{x2}}{p_{x1}}, \tag{3.3}$$

and then using Eq. (3.3), the transfer function is given by:

$$H_{12} = \frac{e^{jkx_2} + Re^{-jkx_2}}{e^{jkx_1} + Re^{-jkx_1}}, \tag{3.4}$$

where $x_1$and x_2 are the positions of the microphones as shown in Figure 3. From Eq. (3.5), the complex pressure reflection coefficient can be obtained by:

$$R = \frac{H_{12}e^{jkx_1} - e^{jkx_2}}{e^{-jkx_2} - H_{12}e^{-jkx_1}}. \tag{3.5}$$

Appling Eq. (3.6) to Eq. (2.7), the surface impedance and sound absorption coefficient are consequently attained.

3.2.2 Measurement of thermal properties

Alambeta instrument was used to measure thermal conductivity and thermal resistance, according to EN 31092 standard. The measuring head of the Alambeta contains a copper block which is electrically heated to approximately 32℃ to simulate human skin temperature, which is maintained by a thermometer connected to the regulator. The lower part of the heated block is equipped with a direct heat flow sensor which measures the thermal drop between the surfaces of a very thin, non-metallic plate using a multiple differential micro-thermocouple.[101] Each specimen was tested five times and the results were averaged.

3.2.2.1 Thermal conductivity

Thermal conductivity, λ , measures the rate at which heat is transferred through unit area of the fabric across unit thickness under a specified temperature gradient and thus is defined by the relation[102]

$$\lambda(W \cdot m^{-1} \cdot K^{-1}) = \frac{Q}{F\tau\frac{\Delta T}{l}}, \tag{3.6}$$

where Q is the amount of conducted heat, F is the area through which heat is conducted, τ is the time of heat conduction, ΔT is the difference of the temperatures and l is the fabric thickness.

3.2.2.2 Thermal resistance

Thermal resistance expresses the ability of material to prevent heat flow through the thickness over unit surface area. Fabric thickness and thermal conductivity are important factors governing thermal insulation of textiles. Usually, the higher the thermal resistance, the lower the heat loss. The thermal resistance, R, is connected with the thermal conductivity, λ, and the fabric thickness, l, as follows

$$R(m^2 \cdot K \cdot W^{-1}) = \frac{l}{\lambda}. \tag{3.7}$$

3.2.3 Measurement of compression properties

The compression energy and compression load of perpendicularly-laid nonwovens were carried out by using a universal testing machine (TIRATEST 2300). Circular perpendicularly-laid nonwoven samples of diameter 10 cm were prepared. The compression tests were conducted at the velocity of 10 mm/min according to the ASTM D575-91 (Standard Test Methods for Rubber Properties in Compression). All the nonwoven specimens were compressed up to a deformation 90% of the initial thickness in an atmospheric condition of 20 ℃ and 65% relative humidity. Five tests were carried out for each sample. The fiber orientation angle at different compression stages was analyzed.

3.2.4 Measurement of air permeability

Air permeability measures the ability of a porous medium to transmit fluids. It depends on the porous geometrical structure.[103] The air permeability of perpendicularly-laid nonwovens were measured using FX3300 Textech Air Permeability Tester (Figure 3.12). The fabric sample is fixed as an obstacle in a flow of air by the clamping holder. A pressure difference

Δp between both sides of the fabric sample develops as a consequence of hydraulic losses. The pressure difference is recorded by using of the manometer. The measured value is a speed of air in meter per second or a volume rate of the flow in liter per hour.

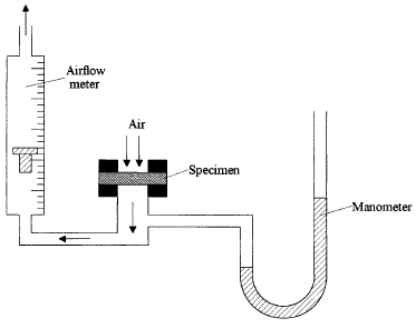

Figure 3.12 Set-up for measuring air permeability

3.2.5 Measurement of airflow resistivity

100 mm diameter circular shape samples were cut with an ELEKTRONISCHE STANZMASCHINE TYPE 208 machine to measure the airflow resistivity using a standard setup. In the present study, the airflow resistivity was measured with an AFD300 AcoustiFlow device (The Gesellschaft für Akustikforschung Dresden mbH, Dresden, Germany) according to ISO 9053:1991.[65] The measurement device is presented in Figure 3.13. Ten samples were measured for each perpendicularly-laid nonwoven fabric to study the reproducibility of the airflow resistivity experiment and scattering in the obtained data.

Figure 3.13 AFD300 AcousticFlow device

In the measurement process, the device generates different rate of airflow. Then, the pressure drop between two sides will be measured. The airflow resistance ($= \frac{\Delta P}{u}$) can be calculated from pressure drop and rate of airflow. Various pressure drop under different rate of airflow will be determined used to get the airflow resistance at 0.5 mm/s using linear regression

method. The airflow resistivity will be obtained by dividing material thickness to the airflow resistance at 0.5 mm/s.

3.3 Statistical analysis

Statistical analysis software, Origin 8.5 and Matlab_R2017a were used to conduct all the statistical tests mentioned in this work. All of the statistical analysis work related to airflow resistivity and surface impedance models were well done in Matlab_R2017a. Power-model was used to get the most suitable empirical model for airflow resistivity of perpendicularly-laid nonwoven fabrics in the Matlab_R2017a software.

Chapter 4 Results and Discussion

This chapter outlines the results of the work described in this thesis. The first section describes the sound absorption properties of perpendicularly-laid nonwovens. The second section describes the acoustic properties of aerogel based nonwovens. The prediction and accuracy of airflow resistivity and impedance prediction models are presented in third and fourth sections. The later sections discuss compressibility, thermal and permeability of perpendicularly-laid nonwoven.

4.1 Sound absorption properties of perpendicularly-laid nonwovens

The sound absorption coefficient SAC (α) indicates how much of the sound is absorbed in the material. When sound wave propagate into a media part of input sound energy W_i [J] is transform into heat (W_q [J]), part is reflected back (W_r [J]) and part is transmitted through insulation layer (W_t [J]). The sound absorption coefficient SAC (α) can be defined as:

$$\alpha = 1 - \frac{W_r}{W_i} = \frac{W_q + W_t}{W_i}. \tag{4.1}$$

The normal incidence sound absorption coefficient of perpendicularly-laid nonwovens was determined as a function of the sound frequency. The normal incidence SAC of part of the perpendicularly-laid nonwoven samples was measured by using Brüel and Kjær impedance tube (as shown in Figure 3.10). The characteristics of fourteen samples, A, A1, B, B1, C, C1, C2, C3, C4, C5, D, E, F and G, are presented in Table 3.2.

The Brüel and Kjær impedance tube contains a large tube (100 mm in diameter) and a small tube (29 mm in diameter) which used to obtain the sound absorption coefficient in low-frequency range from 50-1600Hz and high-frequency range 500-6400Hz respectively. Later the measurement data from large and small tube were combined to form the curves for the frequency range between 50-6400 Hz. The normal incidence sound absorption coefficient of original perpendicularly-laid nonwovens is shown in Figure 4.1.

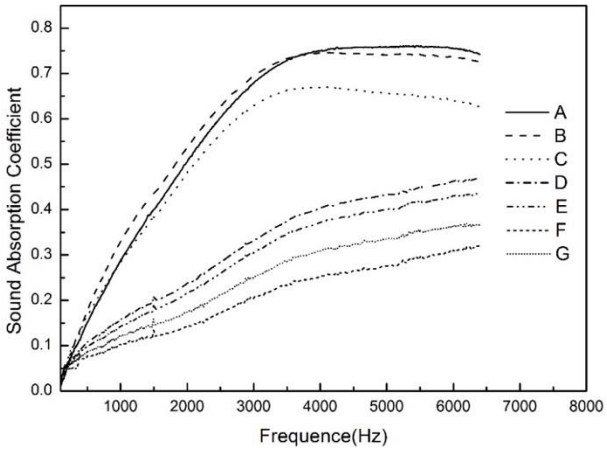

Figure 4.1 Sound absorption coefficient of original perpendicularly-laid nonwovens

It is observed that sound absorption coefficient of the test samples lies in the range of 0.017-0.76. Apparently, the value of absorption coefficient for samples A, B and C sharply increases at frequency bands 50 Hz-3500 Hz and the maximum value of absorption coefficient occurs at frequency bands 4000 Hz-5400 Hz. However, samples D, E, F and G show lower absorption coefficient value in comparison to samples A, B and C, and the value of absorption coefficient increases with the increasing of frequency at the whole measurable frequency bands (50Hz-6400 Hz). Results indicate that perpendicularly-laid nonwoven exhibits much better sound absorption ability at frequency bands 3000 Hz-6400 Hz.

Samples produced by different manufacturing techniques were measured for sound absorption performance and the results are shown in Figure 4.2. Sample A was produced by rotating perpendicular lapper (WAVEMAKER), and samples B and C were prepared by vibrating perpendicular lapper (PERPENDICULARLY-LAID). The manufacturing techniques, thicknesses and areal densities of samples are listed following sample codes. WAVEMAKER is rotating perpendicular lapper, STRUTO is vibrating perpendicular lapper, SAC is sound absorption coefficient. Samples A1, B1 and C2 were obtained from samples A, B and C through heat-pressing method. It is obviously found that all the samples SAC sharply rise with the increasing frequency, but the curves turn to be flat after around 3500 Hz. From Figure 4.2(a), it can be seen that sample B exhibits the highest SAC at low-frequency band, but after 3500 Hz sample A shows better sound absorption ability. Meanwhile, sample C shows the lowest SAC after 1000 Hz compared to samples B and C. In Figure 4.2(b), sample A exhibits the best sound absorption ability while sample C shows the lowest SAC. It is found that samples with higher areal density have better sound absorption performance, and samples with lower areal density are weaker absorbers. The reason for this phenomenon

can be samples thickness and areal density differences.[41-42] Nonwoven thickness is a very important factor determining the sound absorption ability. Generally, the increase of thickness results in an increase of sound absorption coefficient at low-frequency range. Moreover, the sound absorption of fibrous material involves viscous losses, which convert acoustic energy into heat as sound wave travels through the interconnected pores of fibers of the material. Thus, for high areal density samples there are more fibers involved in the viscous losses and more acoustic energy is dissipated in the form of heat energy.[42] In the case of similar thickness, the increase of fabric areal density leads to an increase in sound absorption performance. Based on above analysis, by comparing SAC of samples A, B, C, A1, B1 and C2, it is hard to conclude that samples produced by rotating perpendicular lapper have better sound absorption performance.

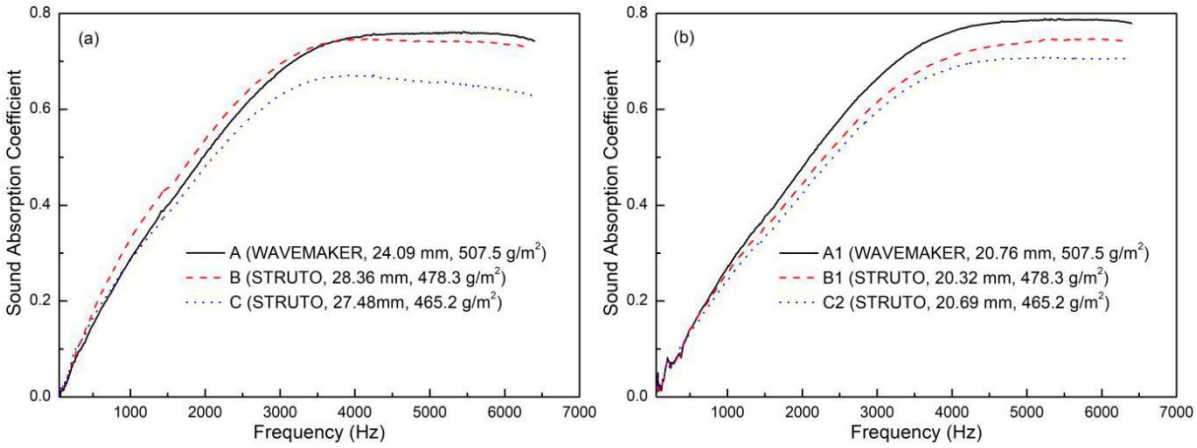

Figure 4.2 SAC of samples produced by different manufacturing techniques: (a) SAC of original samples; (b) SAC of samples prepared by the heat-pressing method from original samples

The sound absorption results obtained by impedance tube are plotted against frequency between 50 and 6400 Hz. In order to numerically investigate the effect of perpendicularly-laid nonwoven fabric structure properties on the sound absorption ability, the noise reduction coefficient (NRC) and average value of SAC ($\bar{\alpha}$) of all the nonwovens were calculated. The NRC has been calculated as the average value of measured values for 250, 500, 1000 and 2000 Hz, which provides a decent and simple quantification of how well the porous material will absorb the noise. The $\bar{\alpha}$ is the average of the SAC for the whole sound absorption coefficient measurement range. The NRC of perpendicular nonwovens were calculated using the following equations:

$$NRC = \frac{\alpha_{250Hz}+\alpha_{500Hz}+\alpha_{1000Hz}+\alpha_{2000Hz}}{4} \quad (4.2)$$

During the impedance tube measurement process, the sound absorption coefficient was measured at even number of frequency in the range of 2 to 6400 Hz. The values of sound absorption coefficient are not accurate under 50 Hz, so the $\bar{\alpha}$ was calculated from 50 to 6400 Hz. The equation for calculating $\bar{\alpha}$ is as follows:

$$\bar{\alpha} = \frac{\int_{F_1}^{F_2} \alpha \ f \ df}{F_2 - F_1} \tag{4.3}$$

where F_1 (50 Hz) is lower bound of sound frequency in testing and F_2 (6400 Hz) is upper bound of sound frequency in measurement.[92] The NRC and computed $\bar{\alpha}$ values for the perpendicularly-laid nonwovens are listed in Table 4.1.

Table 4.1 $\bar{\alpha}$ and NRC of perpendicularly-laid nonwovens

Sample codes	$\bar{\alpha}$		NRC	
	Mean value	95% confidence interval	Mean value	95% confidence interval
A	0.580	0.58 ± 0.00789	0.254	0.254 ± 0.00263
A1	0.581	0.581 ± 0.00614	0.239	0.239 ± 0.00351
B	0.588	0.588 ± 0.00614	0.281	0.281 ± 0.00263
B1	0.545	0.545 ± 0.0105	0.228	0.228 ± 0.00438
C	0.523	0.523 ± 0.00526	0.255	0.255 ± 0.00438
C1	0.544	0.544 ± 0.00526	0.242	0.242 ± 0.00175
C2	0.521	0.521 ± 0.00438	0.216	0.216 ± 0.00263
C3	0.528	0.528 ± 0.00701	0.191	0.191 ± 0.00263
C4	0.433	0.433 ± 0.0131	0.147	0.147 ± 0.00438
C5	0.444	0.444 ± 0.0245	0.136	0.136 ± 0.00526
D	0.315	0.315 ± 0.0245	0.142	0.142 ± 0.00877
E	0.290	0.29 ± 0.0149	0.129	0.129 ± 0.00526
F	0.201	0.201 ± 0.00614	0.092	0.092 ± 0.00351
G	0.242	0.242 ± 0.0123	0.110	0.11 ± 0.00438

$\bar{\alpha}$: average value of sound absorption coefficient; NRC: noise reduction coefficient.

In order to investigate the effect of areal density on sound absorption performance of perpendicularly-laid nonwovens, seven types of nonwoven samples with similar thickness were compared in Figure 4.3 and Figure 4.4. It is found that SAC of samples D, E, F and G sharply increase with the increase of frequency at whole measured band, while the curves of samples A1, B1 and C1 no longer sharply increase after 3500 Hz. Also, the sound absorption

performance shows similar trend as samples areal density. It means that the sound absorption ability of similar thickness perpendicularly-laid nonwovens increase with an increase of samples areal density or bulk density. As analyzed earlier, in the case of similar thickness, the increase of fabric areal density leads to an increase in sound absorption performance. This phenomenon can be seen in Figure 4.4, both NRC and average value of SAC increase with the increase of areal density. It is also observed that the NRC and average value of SAC have a strong quadratic correlation with areal density: the adjusted coefficients of determination (R^2) are 0.99676 and 0.99685, respectively. It can be concluded that higher areal density gives better sound absorption ability for perpendicularly-laid nonwovens when materials have similar thickness.

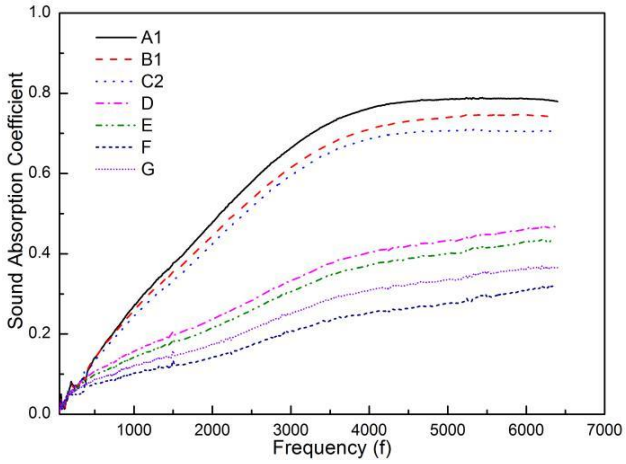

Figure 4.3 SAC of nonwovens with different areal densities

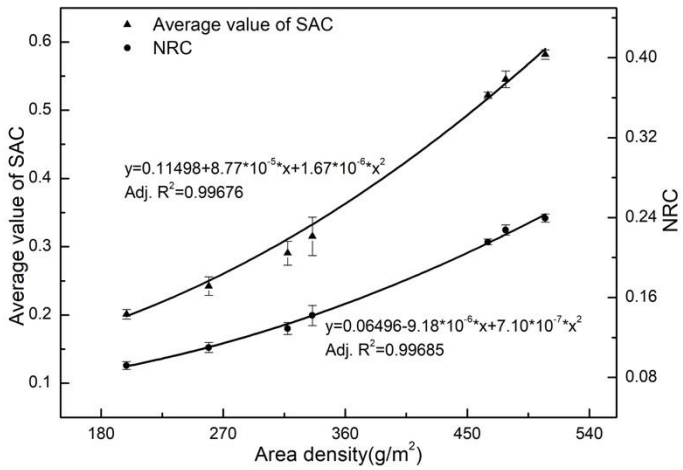

Figure 4.4 Effect of areal density on sound absorption performance

Table statistical characteristics of regression

Equation $y = y0 + b1*x+b2*x^2$	Value	t-test Significance "Yes" or "No"	Adj. R-Square	F-test Significance "Yes" or "No"

Average value of SAC	y0	0.11498	Yes		
	b1	$8.77*10^{-5}$	Yes	0.99676	Yes
	b2	$1.67*10^{-6}$	Yes		
NRC	y0	0.06496	Yes		
	b1	$-9.18*10^{-6}$	Yes	0.99685	Yes
	b2	$7.10*10^{-7}$	Yes		

The coefficient of determination, R^2, is the proportion of the variance in the dependent variable that is predictable from the independent variable(s). The use of an adjusted R^2 is an attempt to take account of the phenomenon of the R^2 automatically and spuriously increasing when extra explanatory variables are added to the model. It is a modification that adjusts for the number of explanatory terms in a model relative to the number of data points.

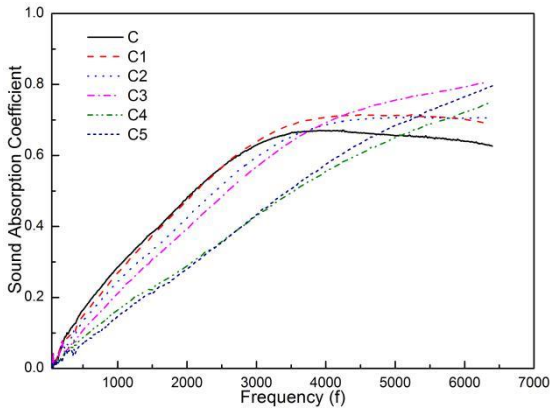

Figure 4.5 SAC of samples with a different thickness

Samples C1, C2, C3, C4 and C5 were made from sample C through heat-pressing method. As the material gets thicker, the sound absorption at low-frequency range increases as well.[92, 104-105] Sound absorption performance of samples with same areal density but different thicknesses are shown in Figure 4.5. It can be seen that samples sound absorption ability at low-frequency bands decreased with the decrease of samples thickness. Meanwhile, the SAC increases at high-frequency bands with the decrease of thickness. This can be explained by the resonance, the resonance phenomena occur towards the low-frequency band for thicker samples.[98] It is also found that the peak values of SAC increase and shift towards the higher frequencies side with decrease of sample thickness. But the effect of decreasing thickness on SAC peak values is limited, since the peak values no longer increase after the thickness reaches a critical value. In addition, samples (C4, C5) with thickness less than 16.85 mm show a significant decrease of SAC at 50-4500 Hz range.

The effect of thickness on the sound absorption performance is presented in Figure 4.6. The adjusted coefficients of determination between the NRC and thickness is 0.96966, and this value is 0.07321 for average value of SAC and thickness, indicating that the NRC of perpendicularly-laid nonwovens has a very strong correlation with thickness while an insignificant relationship between average value of SAC and thickness. As described above, the increase of thickness results in SAC increases at low-frequency bands while SAC decrease at high-frequency bands. Meanwhile, NRC was defined as material's sound absorption ability at low frequency and average value of SAC was described as sound absorption ability for whole measurement frequency. This can be the reason of this phenomenon.

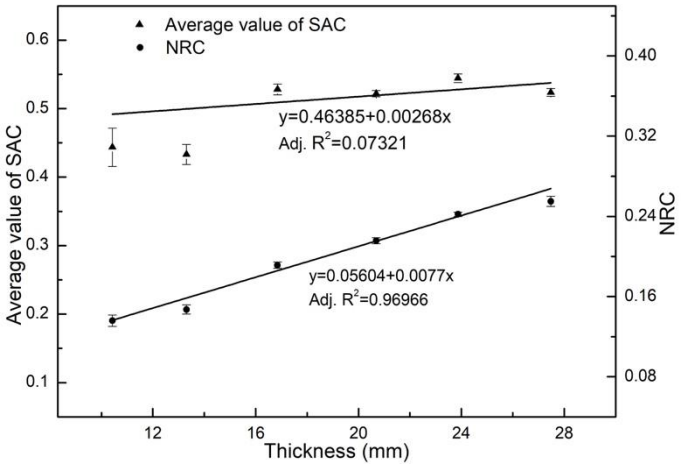

Figure 4.6 Effect of thickness on sound absorption performance

Table Statistical characteristics of regression

	Equation y = y0 + b*x	**Value**	**t-test Significance "Yes" or "No"**	**Adj. R-Square**	**F-test Significance "Yes" or "No"**
Average value of SAC	y0	0.46385	Yes	0.07321	Yes
	b	0.00286	Yes		
NRC	y0	0.05604	Yes	0.96966	Yes
	b	0.0077	Yes		

Porosity has a strong influence on sound absorption performance of fibrous materials. Figure 4.7 illustrates the effect of porosity on sound absorption performance of perpendicularly-laid nonwovens. It can be seen that the average value of SAC increases with the increase of porosity, the average value of SAC reached peak values between 97% and 98% of porosity, but average value of SAC sharply decreases after 98% of porosity. The porosity is inversely proportional to perpendicularly-laid nonwoven specific air flow resistance.[92] Lower porosity

means higher specific air flow resistance, which means fiber movement rarely occurs when sound wave passes through the materials.[107] High porosity results in fewer number of fibers involved in the viscous losses, which will decrease the sound absorption performance of the materials. The quadratic correlation between porosity and average value of SAC was calculated and mentioned in Figure 4.7. It can be found that porosity has a quadratic relation with average value of sound absorption coefficient with adjusted coefficient of determination 0.87779.

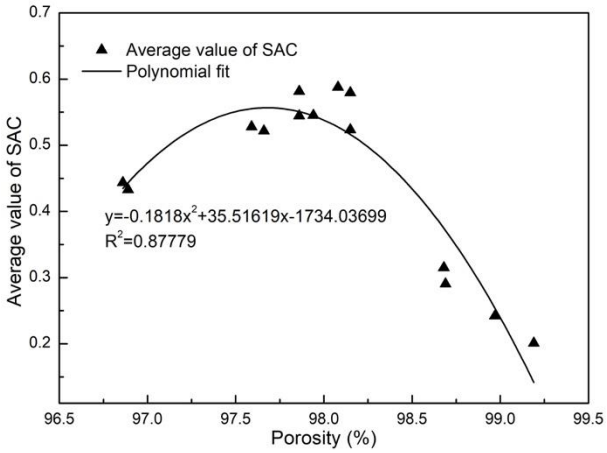

Figure 4.7 Effect of porosity on sound absorption performance

Table Statistical characteristics of regression

	Equation $y = y0 + b1*x+b2*x^2$	**Value**	**t-test Significance "Yes" or "No"**	**Adj. R-Square**	**F-test Significance "Yes" or "No"**
Average value of SAC	y0	-1734.037	Yes	0.87779	Yes
	b1	35.51619	Yes		
	b2	-0.1818	Yes		

Airflow resistivity is a measure of how easily air can enter a porous material and the resistance that airflow goes through a structure. The airflow resistivity of a porous material is one of the most important defining characteristics. Once the airflow resistivity is known, a series of empirical models can be used to find the characteristic impedance and wavenumber, and thus to obtain the surface impedance and sound absorption coefficient. But the modelling process of determination of impedance and sound absorption coefficient through airflow resistivity is tedious. In order to investigate the influence of airflow resistivity on sound absorption performance in a simple way, the correlation between them has been illustrated in Figure 4.8. It is found that below 6000 Pa•s/m² with the increase of airflow resistivity the sound absorption ability increases as well. The highest value of both average value of SAC

and NRC appeared at the range between 5000 and 7000 Pa•s/m² of airflow resistivity. After that, the sound absorption ability shows a decrease trend with the increasing of airflow resistivity. This phenomenon is completely compatible to Zent and Long's research.[41]

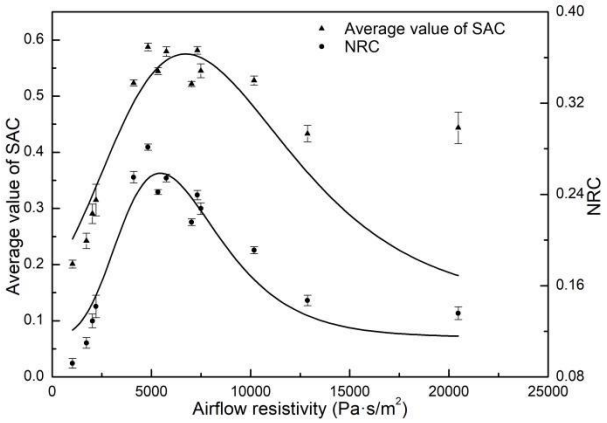

Figure 4.8 Effect of airflow resistivity on sound absorption performance

Table Statistical characteristics of regression

	Equation **y = y0+A*exp(-exp(-z)-z+1)** **z = (x-xc)/w**	**Value**	**t-test Significance "Yes" or "No"**	**Adj. R-Square**	**F-test Significance "Yes" or "No"**
Average value of SAC	y0	0.12862	Yes	0.79362	Yes
	xc	6722.1163	Yes		
	w	4422.3725	Yes		
	A	0.44647	Yes		
NRC	y0	0.11483	Yes	0.82725	Yes
	xc	5452.544	Yes		
	w	2494.0218	Yes		
	A	0.14384	Yes		

4.2 Sound absorption properties of aerogel based nonwovens

The sound absorption coefficient (SAC) of single layer aerogel based nonwoven fabrics is shown in Figure 4.9. By examining the curve of all samples, the SAC of the test samples lies in the range of 0.0003-0.832. It is observed that the SAC of samples A, B and C increase with the increase of frequency. In addition, the SAC of all samples A, B and C exhibit a steady increase at the whole measurable frequency bands (50-6400 Hz). Single layer of sample C shows the best sound absorption ability in whole test band. SAC of samples A, B and C attain peak values at 6400 Hz, the maximum values are 0.385, 0.766 and 0.832, respectively.

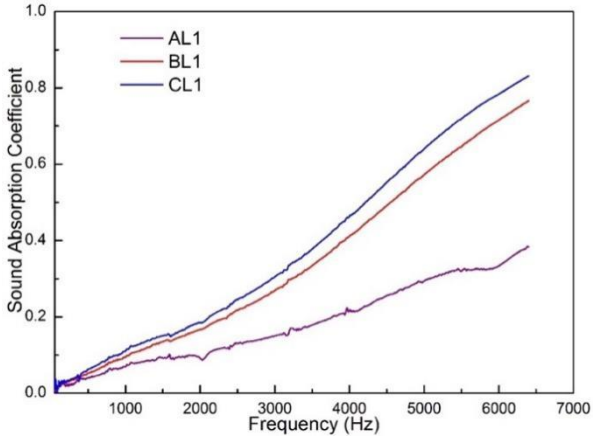

Figure 4.9 Sound absorption coefficients of single layer aerogel based nonwoven fabrics

For numerical analysis, the noise reduction coefficient (NRC) of all single layer aerogel based nonwoven fabrics was calculated. The NRC of aerogel based nonwoven fabrics was calculated using the equation 4.1. The NRC for single layer aerogel based nonwovens are listed in Table 4.2. The NRC is a dimensionless number. The NRC values of single layer aerogel based nonwoven fabrics are found to lie in the range of 0.0556-0.0858, indicating that single layer aerogel based nonwoven fabrics are not effective absorbers for low-frequency sound absorption. It is also observed that sample C exhibits higher sound absorption ability, superior to samples A and B although sample C has lowest aerogel content. It indicates that aerogel content is not a crucial factor in determining the sound absorption ability compared to the thickness and density.

Table 4.2 Noise reduction coefficient (NRC) of single layer aerogel based nonwoven fabrics

Samples	Sample codes	Mean value	95% confidence interval
AP-A	AL1	0.0556	0.0556 ± 0.000789
AP-B	BL1	0.0862	0.0862 ± 0.00263
AP-C	CL1	0.0977	0.0862 ± 0.00263

To further understand the effect of aerogel content on sound absorption performance of aerogel based nonwoven fabric, the comparable absorption index was developed by dividing the average value of sound absorption coefficient and air permeability under 200 Pa pressure drop by corresponding areal density and thickness. The absorption index of single layer aerogel based nonwoven fabrics was calculated by the following equation.

$$Absorption\ index = \frac{\bar{\alpha} \cdot q}{GSM \cdot L} \times 10\ , \tag{4.4}$$

where, $\bar{\alpha}$ the average value of sound absorption coefficient calculated according to equation 4.3, q is the air permeability (mm/s), GSM (areal density) is the gram per square meter (g/m^2), L is thickness (mm).

Figure 4.10 exhibits the single layer samples' aerogel content and corresponding absorption index. It can be seen that samples with higher aerogel content have lower absorption index, while the lowest aerogel content sample exhibits the highest absorption index. This dramatic phenomenon could be explained by following reasons. First, the acoustic properties of silica aerogel are sensitive to geometry and boundary condition[52], the aerogel-fiber structure and irregular aerogel particles can cause adverse effect on sound absorption ability of aerogel based nonwoven fabrics. Moreover, the sound absorption performance of fibrous materials is strongly depending on specific airflow resistance which is inversely proportional to fabric porosity.[92] Aerogel has very high air-saturated porosity. Generally, increase of aerogel content leads an increase in the porosity of aerogel based nonwoven fabrics. Consequently, the sound absorption performance of samples will decline due to the decrease of specific airflow resistance.

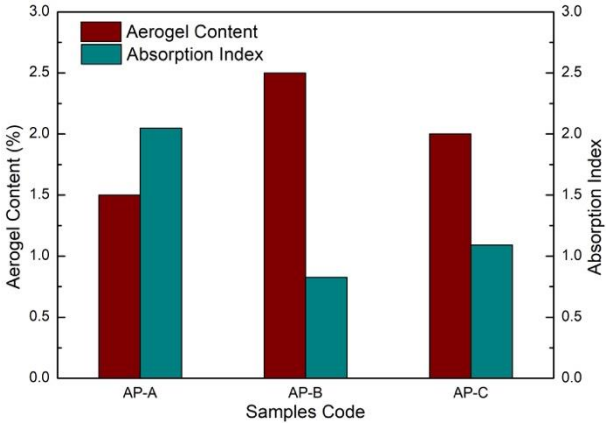

Figure 4.10 Absorption index of single layer aerogel based fabrics

The multilayer sound-absorbing materials, with the increased thickness, are the most commonly used method to improve the sound absorption ability at low frequencies. In this section, the SAC and NRC of the sound-absorbing materials multilayered with the same kind of aerogel based nonwoven fabric are presented.

The sound absorption performance of sound-absorbing materials is depending on a series of physical parameters, such as material thickness, fiber size, material density, bonding method,

airflow resistance and so on.[2] Generally, material thickness is a very important factor determining the sound absorption ability of porous structures. The thickness of the sound-absorbing materials has a direct relationship with the sound absorption ability. As the material gets thicker, the sound absorption at low frequency increases as well.[98] But the effect of increasing of thickness on SAC at low frequencies is limited, since the SAC no longer increase after the thickness reaches a critical value.

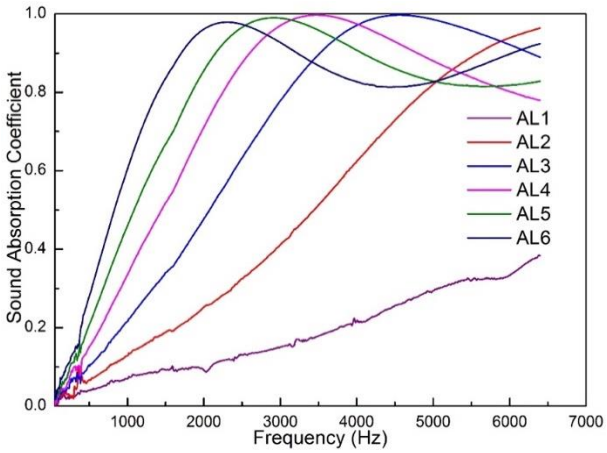

Figure 4.11 SAC of multilayered aerogel based nonwoven fabric A

The SAC of multilayered sample A is shown in Figure 4.11. It is found that two layers of sample A have a significant improvement in the sound absorption ability in the whole measurable frequency bands. It is also observed that as the thickness increased, the SAC at low frequencies increased as well. However, the SAC decreased at high frequencies after two layers, and the peaks of SAC curves shift towards the lower frequency side.

Figure 4.12 shows the SAC of multilayered sample B. It can be found that the SAC significantly increase with the increase of blanket layers. In addition, after three layers, the SAC sharply increase at low frequencies. However, the SAC decrease when they increase up to peak values due to resonance. Moreover, the resonance phenomenon region shifts toward the lower frequencies side with an increase of the fabric layers. Because of the resonance, two peaks show on the SAC curves of four, five and six layers of sample B.

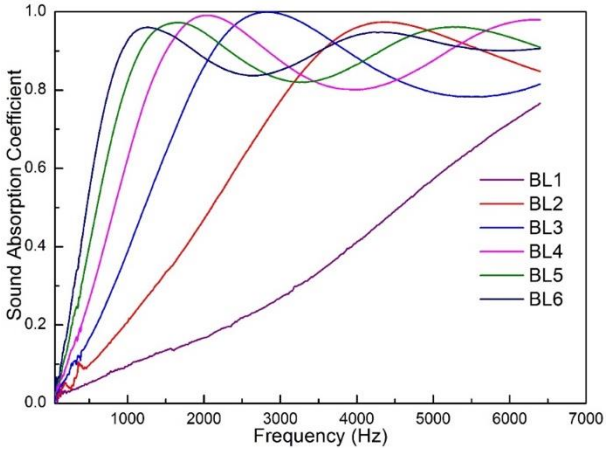

Figure 4.12 SAC of multilayered aerogel based nonwoven fabric B

The SAC of multilayered sample C are shown in Figure 4.13. It can be found that the two layers of sample C have a significant improvement, and the SAC of two layers attains its maximum value 0.9978 at 4136 Hz. However, after two layers, as the increase of fabric layers the maximum values of the SAC decrease. It is also observed that SAC of five and six layers have slight improvement compared with four layers. Besides, the resonance phenomenon also can be found, and the resonance regions shift towards the lower frequencies side with an increase of layers.

According to the SAC curves in Figure 4.11 to Figure 4.13, it can be predicted that the SAC will steadily increase with the increasing of the nonwoven fabrics layers. So, it is expected that the better sound absorption performance of aerogel based nonwoven fabrics can be obtained if enough layers are used.

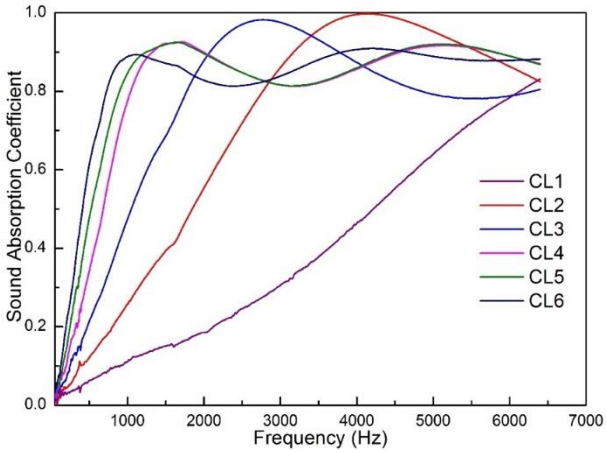

Figure 4.13 SAC of multilayered aerogel based nonwoven fabric C

In order to investigate the effect of multilayered structure on sound absorption performance of aerogel based nonwoven fabrics, the NRC of different layers were calculated. The NRC of

multilayered samples is shown in Table 4.3 and Figure 4.14. The NRC of multilayered samples A, B and C were found to lie in the range of 0.0556-0.4900, 0.0862-0.6465 and 0.0977-0.6491, respectively. It was observed that the NRC of all aerogel based nonwovens increase with the increase of fabric layers. The NRC of sample A exhibits a steady increase. However, for samples B and C, the improvement of NRC became slower after four layers. As described earlier, it could be predicted that the NRC of samples B and C may slightly increase with the increase of layers when the layers reach critical values.

Table 4.3 Noise reduction coefficient (NRC) of multilayered nonwoven fabrics

Samples	Sample codes	Layers	Mean value	95% Confidence Interval
AP-A	AL1	1	0.0556	0.0556 ± 0.000789
	AL2	2	0.1186	0.1186 ± 0.00263
	AL3	3	0.2145	0.2145 ± 0.00841
	AL4	4	0.3189	0.3189 ± 0.00438
	AL5	5	0.4057	0.4057 ± 0.0105
	AL6	6	0.4900	0.49 ± 0.00149
AP-B	BL1	1	0.0862	0.0862 ± 0.00263
	BL2	2	0.2038	0.2038 ± 0.00877
	BL3	3	0.3746	0.3746 ± 0.00666
	BL4	4	0.5015	0.5015 ± 0.00517
	BL5	5	0.5869	0.5869 ± 0.00456
	BL6	6	0.6465	0.6465 ± 0.00657
AP-C	CL1	1	0.0977	0.0977 ± 0.00123
	CL2	2	0.2462	0.2462 ± 0.00272
	CL3	3	0.4169	0.4169 ± 0.0028
	CL4	4	0.5422	0.5422 ± 0.00561
	CL5	5	0.6056	0.6056 ± 0.00412
	CL6	6	0.6491	0.6491 ± 0.00412

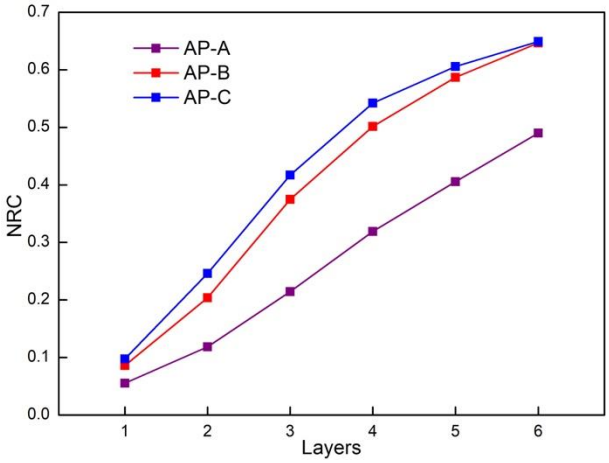

Figure 4.14 Effect of multilayered samples on NRC of aerogel based nonwoven fabrics

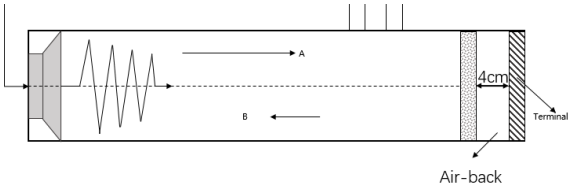

Figure 4.15 Effect of 4 cm air-back cavity on SAC impedance tube experiment schematic

In order to investigate the effect of the air-back cavity on SAC of aerogel based nonwoven, SAC of sample A with 4, 8 and 12 cm air-back cavities were measured by impedance tube. 4 cm air-back cavity impedance tube experiment was shown in Figure 4.15. As can be seen in Figure 4.16, all the sound absorption curves are in the form of frequency spectra, because the air-back cavity causes frequency-selected sound absorption due to the resonance. It is observed that the increasing of air-back thickness results in narrower absorption frequency ranges. It is also found that the air-back cavity obviously improves the SAC of sample A at low frequency range. In addition, as the thickness of air-back increase, the first peak of SAC curve moves toward to lower frequency side. However, an increase in thickness of air-back cavity does not significantly improve the SAC of aerogel based nonwoven fabric.

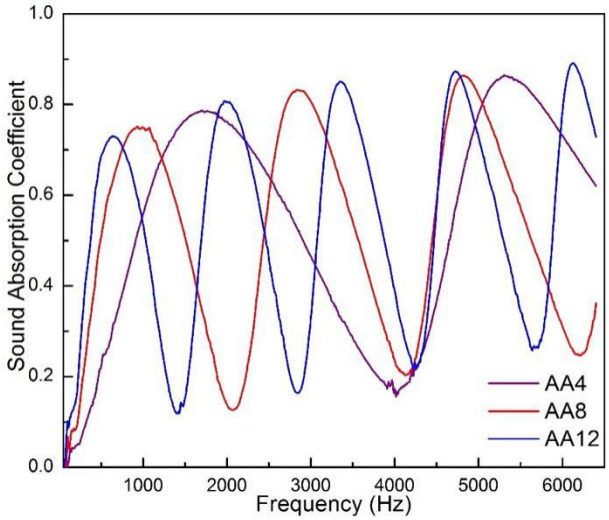

Figure 4.16 Effect of air-back cavity on SAC of aerogel based nonwoven fabric

4.3 Some airflow resistivity models for multi-component polyester fiber assembly

As described in Table 3.2, samples A, B and C are made by same fiber content which are 30% hollow PET, 45% staple PET and 25% bi-component PET while sample D, E, F and G are made by other fiber content. Thus, this section will only discuss the airflow resistivity of sample A, B, C and their compressed samples. The selected samples for airflow resistivity models study are listed in Table 4.5. The relative density is equal to 1 minus porosity.

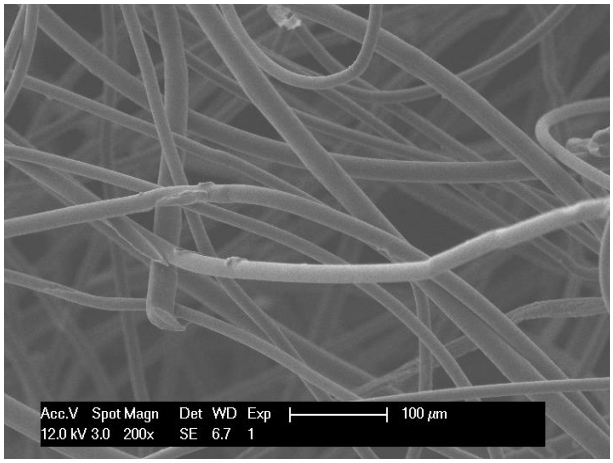

Figure 4.17 The scanning electron microscope (SEM) image of sample A

As shown in Table 2.2-2.4, it can be seen that the fiber diameter is one of the key parameters to predict the airflow resistivity with a theoretical model. In this section, the perpendicularly-laid nonwoven materials were made with three types of fiber. The fiber diameter has been determined by scanning electron microscope (SEM) images and ImageJ software. The ImageJ software based on the scanning electron microscope (SEM) images (see Figure 4.17) to measure the fiber diameter, so that the fiber diameter distribution for polyester nonwovens

were obtained. 2358 fiber diameters from 150 SEM images were measured in total to ensure reproducible statistics.

Table 4.4 Characteristics of polyester materials

Samples type	Samples code	Porosity (%)	Relative density (%)	Airflow resistivity (Pa·s/m²)	Fibrous layer orientation angle (º)
Original	A	98.15	1.85	5757 ± 589	56.07
Heat compressed	A1	97.86	2.14	7319 ± 243	45.65
	A2	97.66	2.34	8630 ± 408	40.88
	A3	97.59	2.41	10329 ± 376	39.41
	A4	96.89	3.11	14990 ± 285	29.44
	A5	96.86	3.14	15410 ± 167	29.17
	A6	96.01	3.99	22230 ± 433	22.56
Original	B	98.52	1.18	4011 ± 316	87.26
Heat compressed	B1	97.94	2.06	7498 ± 332	45.70
	B2	97.85	2.15	7412 ± 328	43.35
	B3	97.29	2.71	13400 ± 277	32.99
	B4	96.59	3.41	16750 ± 442	27.18
Original	C	98.15	1.85	4108 ± 199	79.09
Heat compressed	C1	97.86	2.14	5337 ± 217	58.53
	C2	97.66	2.34	7029 ± 356	47.67
	C3	97.59	2.41	10180 ± 259	37.02
	C4	96.89	3.11	13370 ± 199	28.40
	C5	96.86	3.14	20470 ± 687	21.88

The fiber diameter distribution is shown in Figure 3.6. Thus, samples have triple fiber components with rough diameter of 13, 19 and 22 μm. The mean fiber diameter of multi-component polyester materials was determined according to the following equation:

$$d = \frac{\sum_{i=1}^{n} d_i}{n} \ , \tag{4.5}$$

where n is the total fiber count, d_i is the diameter for each fiber.

The accuracy of the airflow resistivity prediction models presented in Tables 2.2-2.4 was

compared against the obtained experimental data. The accuracy of theoretical and empirical models was investigated by comparing the relative prediction errors. In this calculations the values of the material density and porosity were taken from Table 4.4. In order to investigate the accuracy of airflow resistivity models, the mean absolute values of relative error (MAVRE) was calculated according to the following equation:

$$\Delta = \frac{\sum_{n=1}^{N} \Delta_n}{N} = \frac{1}{N} \sum_{n=1}^{N} \frac{|\sigma_{p,n} - \sigma_{m,n}|}{\sigma_{m,n}} \quad , \tag{4.6}$$

where σ_p is the predicted airflow resistivity, σ_m is the measured airflow resistivity, and N is the total number of material specimens studied (N=18). A MAVRE of 0.2 means a difference of 20% from the measured value.

4.2.1 Prediction of airflow resistivity based on theoretical models

Due to the same fiber content in samples A, B and C the airflow resistivity was descried as a function of relative density which was determined as a ratio of the material density over the density of polyester. The predicted airflow resistivity values based on capillary channel theory (see the models listed in Table 2.2) are show in Figure 4.18 as a function of the relative density.

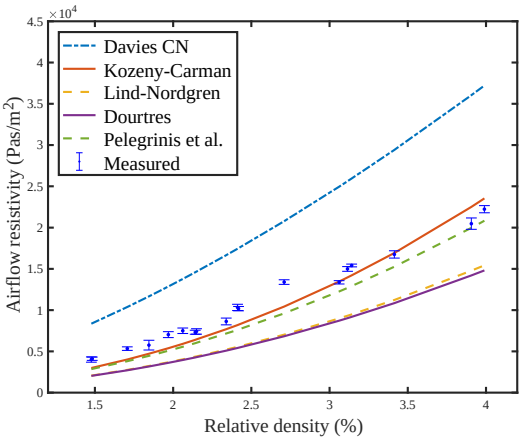

Figure 4.18 Predicted airflow resistivity based on capillary channel theory

The mean absolute values of relative error (MAVRE) of capillary channel theory models are compared in Figure 4.19. It can be seen that Doutres and Lind-Nordgren models predict similar values of the airflow resistivity. The Kozeny-Carman model agrees closely with that by Pelegrinis *et al*. This difference can be explained by the fact that the two sets of models make use of rather different coefficients in the flow resistivity equations: 180 for the Kozeny-Carman type models; and 128 for the Lind-Nordgren models. This difference in the predicted

airflow resistivity increases proportional to the material density. The Davies CN model shows the highest value of predicted airflow resistivity and a relatively high error. It is observed that the maximum MAVRE for this model is 83.8%. The MAVRE of Kozeny-Carman model, with a maximum value of 15% which is the lowest among the five models considered. The maximum error for the Pelegrinis *et al.* model is relatively low which is 19.7%. It was also found that the Kozeny-Carman model is more reliable when the material density is relatively low. However, it begins to overestimate the airflow resistivity as the relative less than 4%.

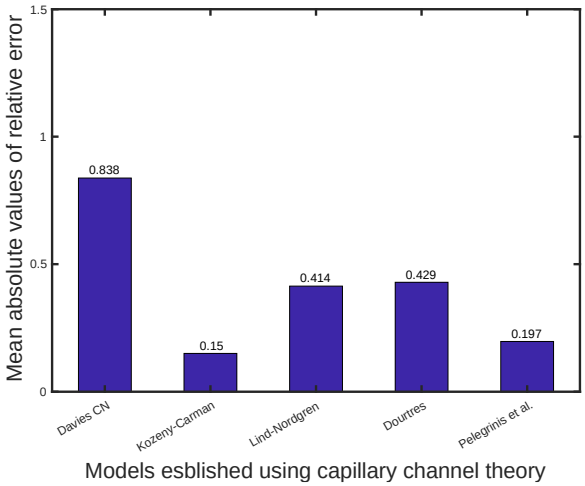

Figure 4.19 The MAVRE of airflow resistivity based on capillary channel theory

The calculated airflow resistivity of multi-component polyester materials based on the drag force theory is presented in Figure 4.20 as a function of the relative density. Figure 4.21 presents the mean absolute values of relative error (MAVRE). The keys to the model type can be found in Table 2. The results presented in Figure 4.21 suggest that the model by Happel (Happel B model) for the airflow perpendicular to fibers significantly overestimate the resistivity by over 390%. The predictions by Hasimoto, Kuwabara, Happel A (airflow parallel to the fibers) and Tarnow C (airflow perpendicular to fibers arranged in the form of lattice) are very similar and overestimate the measured airflow resistivity by 160-200%. The predictions by the Langmuir and Tarnow A (airflow parallel to the fibers arranged in square lattice) are almost identical but overestimate the airflow resistivity by approximately 31.1%. The predictions by Tarnow D model (airflow is perpendicular to the fibers arranged in random lattice) fall between the two latter groups. The most accurate model for the flow resistivity of this kind of fibers is the Tarnow B model (airflow is parallel to fibers arranged in random lattice). This model is accurate within 13%. In addition, it can be seen that the Tarnow B model is more accurate when the materials have relatively low density, however

this model exhibits higher variation comparing to measured values at high density range. This phenomenon can be explained by the decrease of fibrous layer orientation angle with increased density for high specimen compression as illustrated in Figure 4.20. When the fibrous layer orientation angle decreases, the airflow is no longer parallel to the fibers. When the orientation angle is close to 0 the airflow becomes perpendicular to the fibers. For these materials the measured flow resistivity (see Figure 4.20) is higher than that predicted with Tarnow B models which work better when the flow is parallel to the fibers.

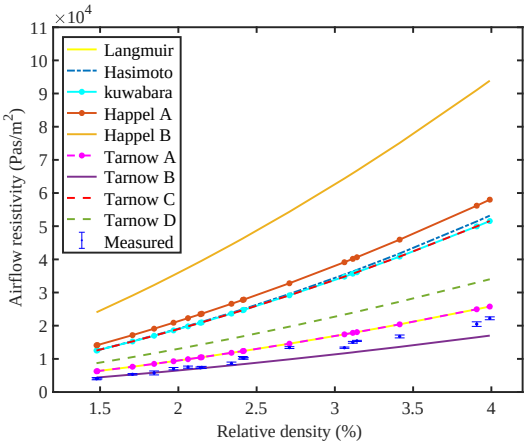

Figure 4.20 Predicted airflow resistivity based on drag force theory

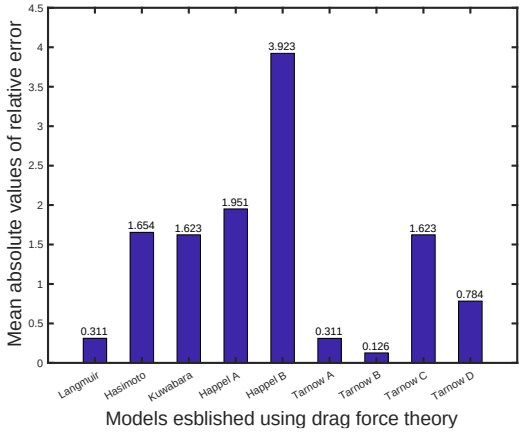

Figure 4.21 The MARVE of airflow resistivity based on drag force theory

4.3.2 Prediction of airflow resistivity using empirical models

The predicted airflow resistivity calculated from empirical models are presented in Figure 4.22. Figure 4.23 presents the prediction MARVE data. The Bies-Hansen and Manning RB models give significantly underestimated airflow resistivity of multi-component polyester materials in comparison with measured values. This can be explained by the different materials and bonding method in their studies in comparison with in the current study.[85, 87]

Garai, Manning MB and TB models exhibit similar results and relative good agreement by comparing the measured airflow resistivity. It is observed that the MARVE for these three models range from 15.8% to 41.2%. The predictions by Manning TB and Garai are very close, but Manning TB method shows better predictions. The MARVE for Manning RB/TB and Garai models increase with the increased value of the relative density. The relative error for these models is below 10% when the relative density of the fibrous material is below 3%.

Although one drag force theory model exhibits acceptable prediction for multi-component polyester nonwovens, the the empirical models are not reliable which overestimate the airflow resistivity by 16%. One same type simple empirical model was developed by power-fitting the values of measured resistivity, the model presented in equation 4.6. The fitted empirical model is show in Figure 4.22 - 4.23. The relative prediction error of the fitted empirical model is 5.1%.

$$\sigma = \frac{1.053\times10^{-8}\times\rho^{1.645}}{d^2} \tag{4.7}$$

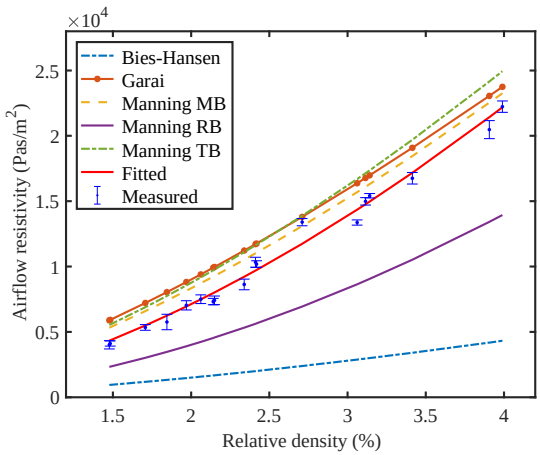

Figure 4.22 Predicted airflow resistivity based on empirical models

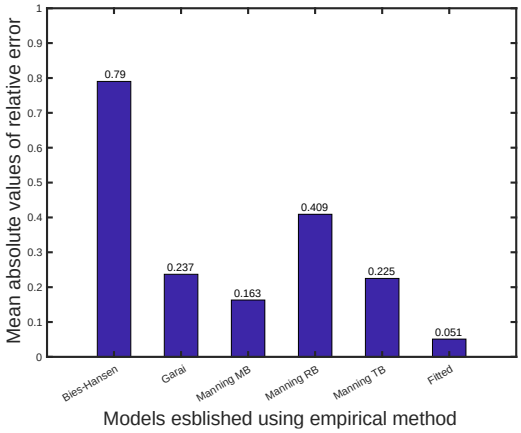

Figure 4.23 The MARVE of airflow resistivity based on empirical models

4.4 Numerical analysis of acoustic properties of perpendicularly-laid nonwovens

As presented in Chapter 2, the normal sound absorption coefficient surface impedance can be obtained form Zwikker and Kosten theory by applying material thickness and airflow resistivity.[18] This section discussed four commonly used impedance models, such as Delany-Bazley, Miki, Garai-Pompoli and Komatsu models. The accuracy between measured values these models will be presented. The impedance tube measurement has been detailed in Chapter 3. The 45 mm impedance tube manufactured by Materiacustica was applied to obtain the impedance. The measurement frequency range starts from 200 and goes up to 4200 Hz. The selected samples A, A1, A2, A3, A4, A5, A6, B1, B3, C, C1, C2, C3, C4 and C5 are listed in Table 3.2.

The effect of surface morphology on an acoustic wave can be characterized by four interrelated acoustic quantities: impedance, admittance, pressure reflection coefficient and absorption coefficient. The impedance, admittance and pressure reflection coefficient describe the magnitude and phase change on reflection. The absorption coefficient only gives information about the energy change on reflection.[3] The impedance models introduced in previous section were used to predict characteristic impedance and wavenumber. By applying characteristic impedance and wavenumber into equations 2.6 and 2.7, the surface impedance and sound absorption can be easily obtained. The surface impedance contains real part (resistance) and imaginary part (reactance). The real part of surface impedance is associated with energy changes, and the imaginary part with phase changes. Thus, the surface acoustic impedance gives more insight information about the absorbing properties of a material than the absorption coefficient. The predicted surface impedance and absorption coefficient will

be demonstrated in this section. In addition, the accuracy between predicted and measured absorption coefficient will be presented.

Delany and Bazley advised that their method is more accurate in the range of $10^{-2} \leq \frac{f}{\sigma} \leq 1$, where f is the frequency, σ is the airflow resistivity.[88] In order to verify the adaptability of Delany-Bazley model for predicting impedance and sound absorption of multi-component polyester nonwovens, the $\frac{f}{\sigma}$ against frequency has been plot in Figure 4.24 The slope of each line is equal to the reciprocal of airflow resistivity (σ). It can be seen that one sample with 4108 Pa·s/m² airflow resistivity demonstrates high value of $\frac{f}{\sigma}$ (i.e. > 1) from 4108 to 4200 Hz which means the sample with lowest airflow resistivity has 2.3% invalid prediction range in the whole measurement range (200 - 4200 Hz). Miki, Garai and Komatsu stated that their methods has wider confident prediction range compared with Delany-Bazley method.[86, 89-90] Thus, the predicted and measured impedance absorption coefficients will be compared at the frequency band of 200 - 4200 Hz in this section.

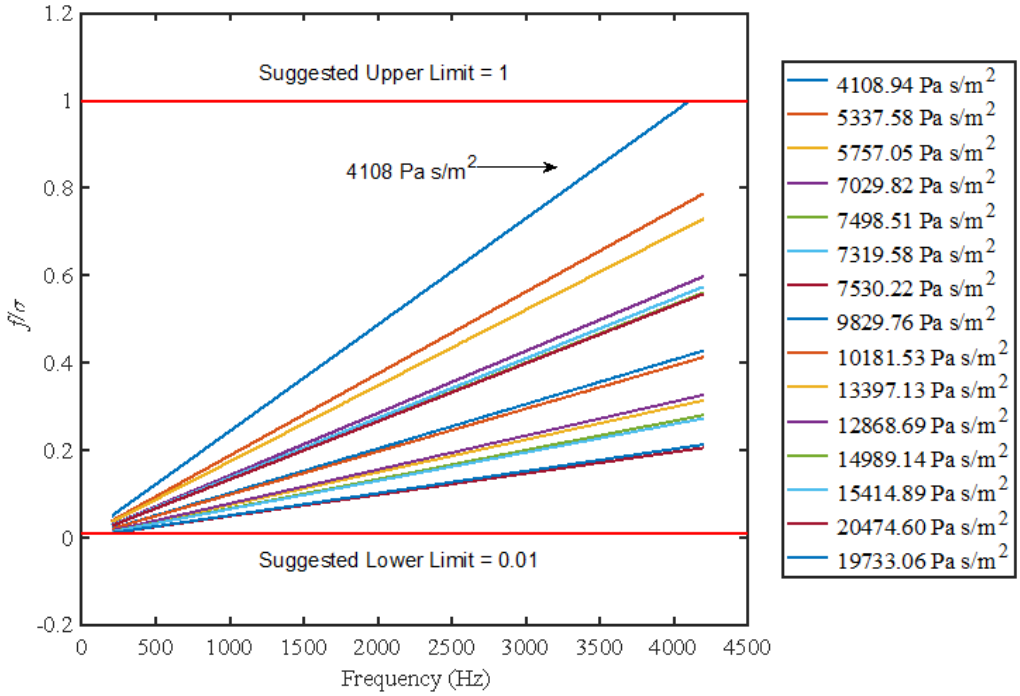

Figure 4.24 Range of the ratio of frequency to airflow resistivity of nonwoven samples

Sample A with 5757 Pa·s/m² airflow resistivity was chosen to figure out the most suitable model for impedance prediction of multi-component polyester nonwoven. Figure 4.25 demonstrates the comparisons of normalized impedance between the measured values and the values calculated using the Delany–Bazley model, the Miki model, the Garai-Pompoli and

the Komstsu model. The normalized surface impedance is the ratio of surface impedance to the characteristic impedance of air ($Z_s/\rho_0 c_0$). It can be seen that Delany-Bazley and Miki model have accurate predictions on normalized surface impedance, while Komatsu model exhibits significant difference compared to measured values especially at low to mid frequency range. The reason for the inaccuracy of Komatsu method can be attributed to the wider airflow resistivity range (i.e. 6000 - 72900 Pa·s/m²) used to derive the impedance prediction equations compared with the range from 4108 to 20474 Pa·s/m² in this study. It also can be found that Delany-Bazley model exhibits more acceptable predictions not only on real part of normalized surface impedance but also imaginary part by comparing with Miki and Garai-Pompoli models. The predictions of surface impedance for other types of nonwoven samples with varying airflow resistivity are presented in Figure 4.25 - 4.30.

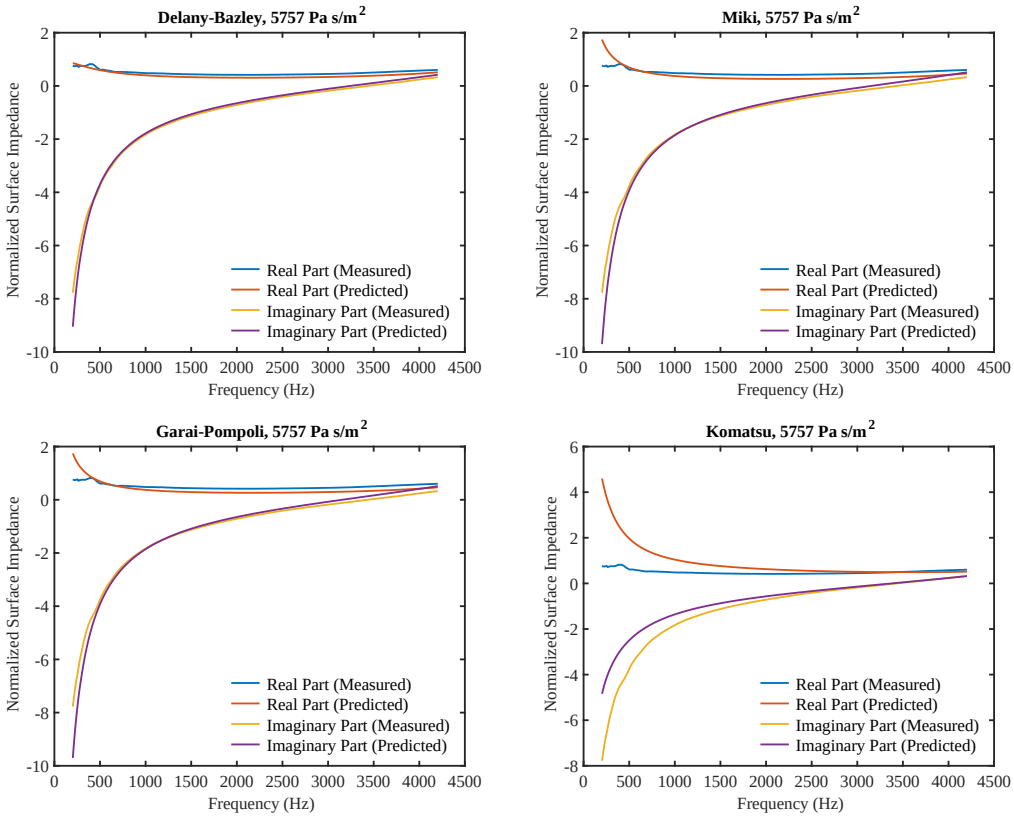

Figure 4.25 Measured and predicted impedance for the sample with airflow resistivity of 5757 Pa·s/m²

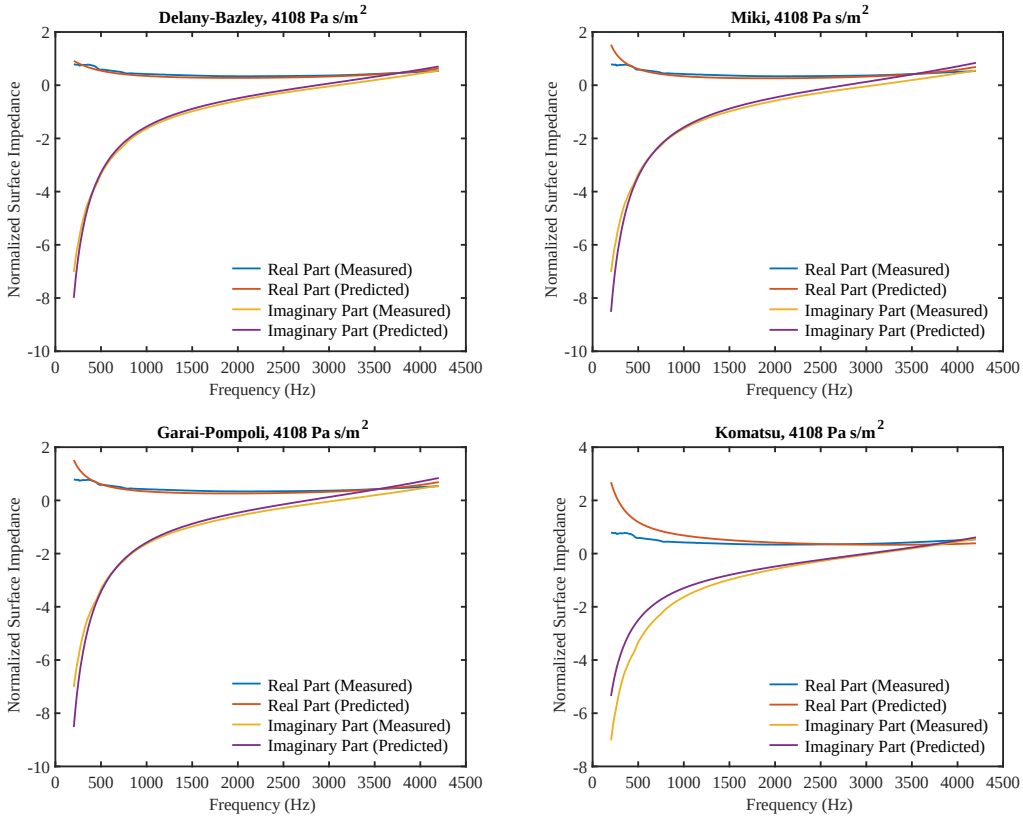

Figure 4.26 Measured and predicted impedance for the sample with airflow resistivity of 4108 Pa·s/m²

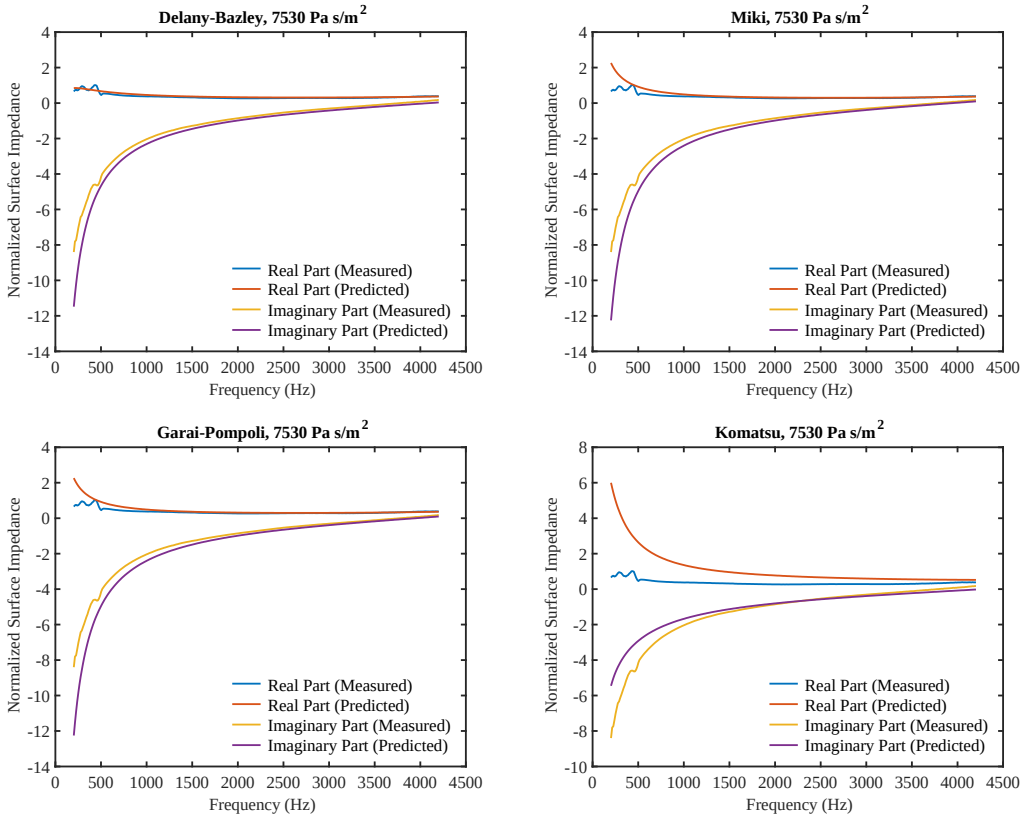

Figure 4.27 Measured and predicted impedance with airflow resistivity of 7530 Pa·s/m²

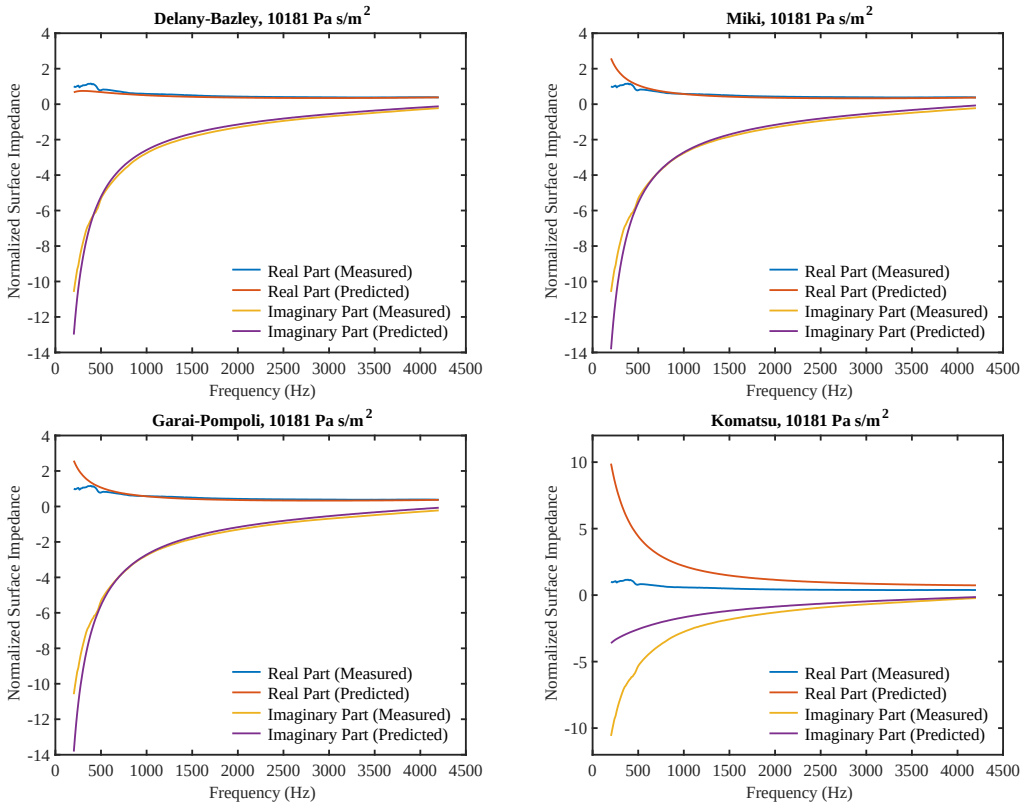

Figure 4.28 Measured and predicted impedance for the sample with airflow resistivity of 10181 Pa·s/m²

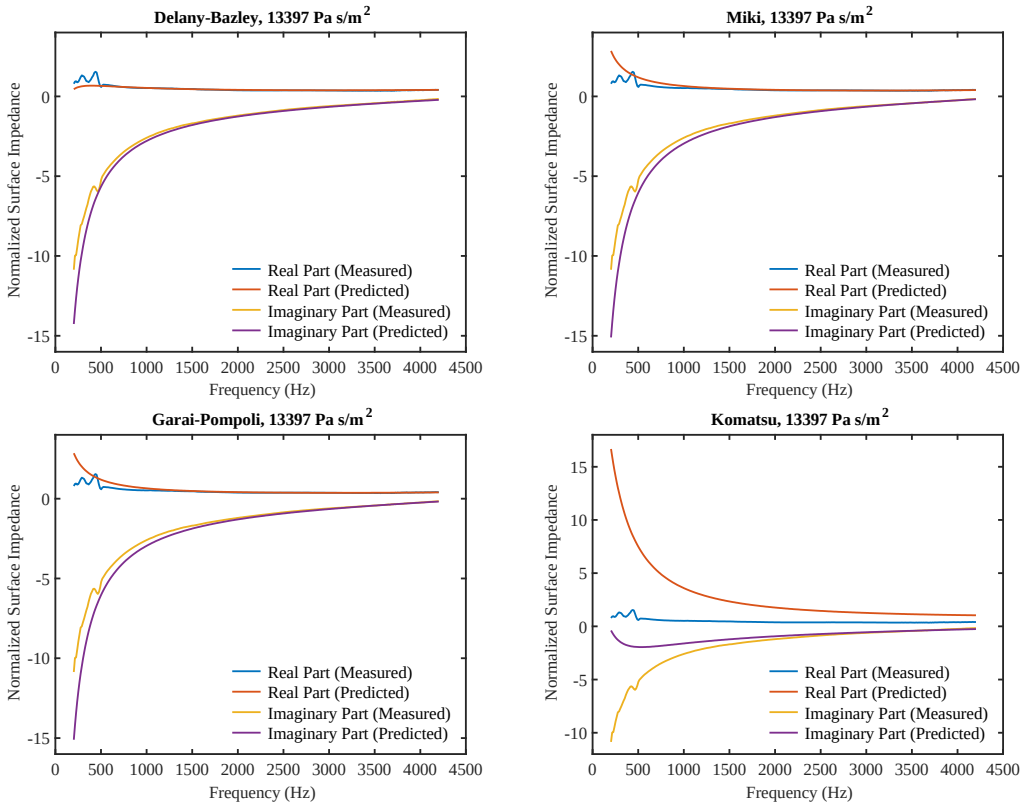

Figure 4.29 Measured and predicted impedance with airflow resistivity of 13397 Pa·s/m²

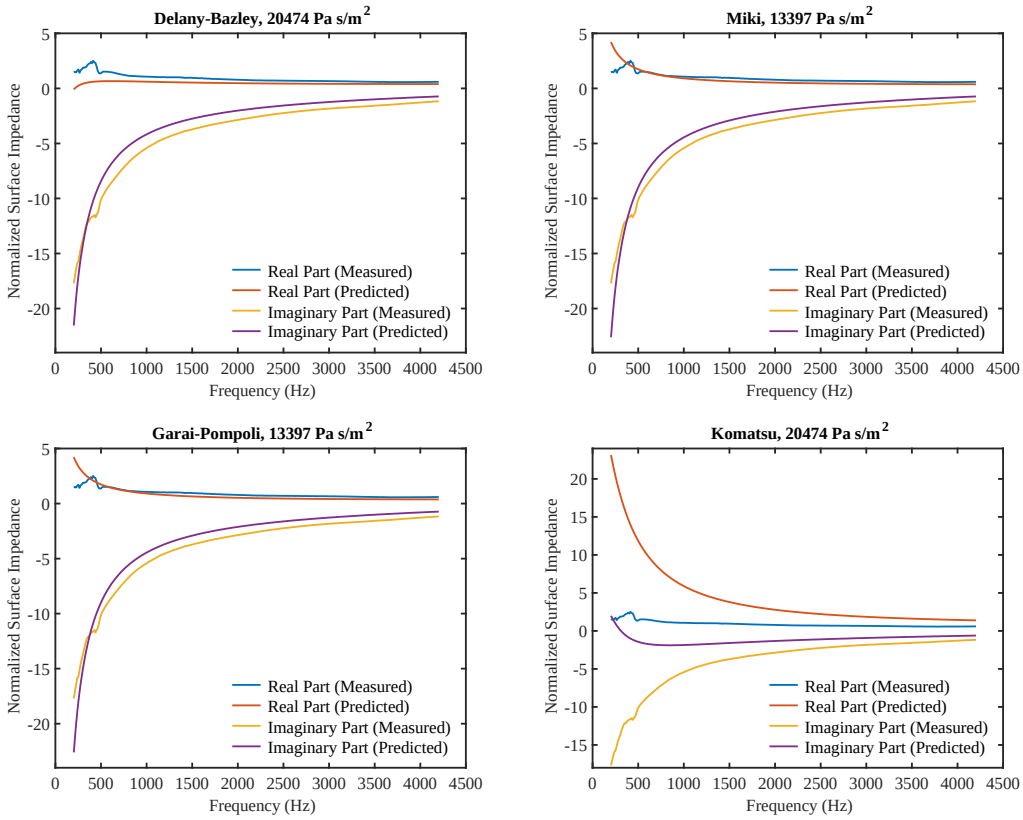

Figure 4.30 Measured and predicted impedance for the sample with airflow resistivity of 20474 Pa·s/m²

By applying predicted surface impedance into equation (2.7), the calculated absorption coefficient can be rapidly attained. A similar method for comparison between measured and predicted airflow resistivity was used to analyze the prediction errors of sound absorption coefficient among the four models. The MAVRE for sound absorption prediction were calculated according to the following equation:

$$error = \frac{|\sum \alpha_{meas} - \sum \alpha_{pred}|}{\sum \alpha_{meas}} \times 100\% \,, \tag{4.8}$$

where α_{meas} is the measured absorption coefficient, and α_{pred} is the predicted value.

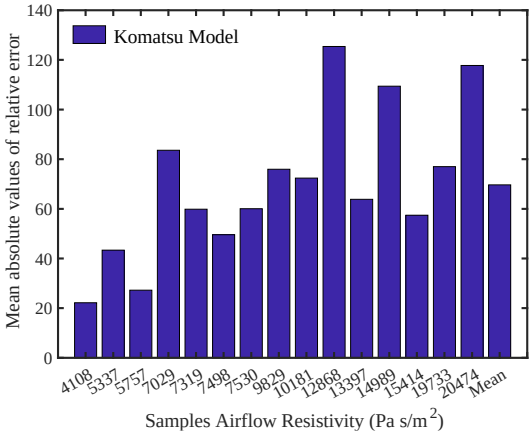

Figure 4.31 MAVRE based on Komatsu model. The airflow resistivity on horizontal axis represents corresponding samples

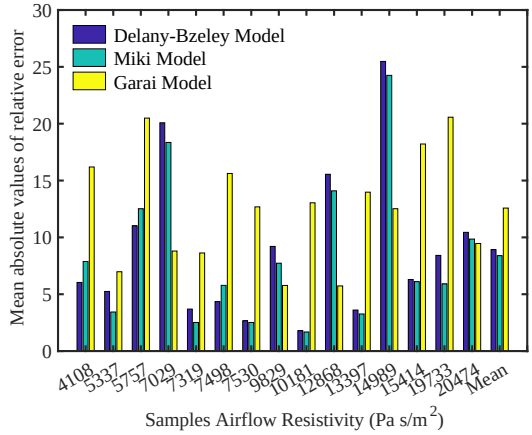

Figure 4.32 MAVRE based on Delany–Bazley model, Miki model and Garai-Pompoli model

As shown in Figure 4.25 - 4.30, the Komatsu model demonstrates unsuitable predictions on surface impedance. Consequently, the error of absorption coefficient based on Komatsu model can be very high compared with Delany-Bazley model and Miki model. In order to clearly show the adaptability of the models for multi-component polyester nonwovens, the MAVRE of Komatsu model was separately presented in Figure 4.31. The MAVRE based on Delany-Bazley model, Miki model and Garai-Pompoli model were shown in Figure 4.32. The Komatsu model exhibits the highest MAVRE of 125% for the sample with 12868 Pa·s/m² airflow resistivity. MAVRE is relatively low when the resistivity is small. The Komatsu method shows around 70% mean MAVRE, while the values from other three methods are less than 15%. From Figure 4.32, it is found that Delany–Bazley model and Miki model have similar results. The difference on their mean MAVRE is less than 0.6% which are 8.92% and 8.39%, respectively. However, it is obviously found that the absorption coefficient predicted by Miki model yields closer results for most of the samples than that from Delany-Bazley

model. The MAVRE between the Delany-Bazley and Miki methods and measured values of the absorption coefficient are smaller than those between the Garai-Pompoli method and measured values. The maximum MAVRE of 25.48% is found between the absorption coefficient predicted by the Delany-Bazley model and that measured for the sample with 14989 Pa·s/m² airflow resistivity. The maximum MAVRE of Garai-Pompoli model is 20.57% for the sample with 19733 Pa·s/m² airlow resistivity. The minimum values of MAVRE based on Delany-Bazley and Miki methods are 1.79% and 1.67%, respectively.

It is considered that the results with an error less than 10% are accurate for this kind of analysis, as the value of bulk density and thickness for a fibrous material can vary due to several uncertainties during measurements. Uncertainties such as fabric compression, fiber density and any inaccuracy or noise that is present during the acquisition of the acoustical data might have resulted in erroneous data.[67] Thus, it can be concluded that the Delany-Bazley and Miki models are superior in terms of the sound absorption coefficient by comparing Garai-Pompoli and Komatsu models. It can also be concluded that Miki model can be used to accurately predict sound absorption coefficient of multi-component polyester nonwovens.

4.5 Compression property of perpendicularly-laid nonwovens

The samples were chosen to carry out the compression property study are listed in Table 3.2. Cross-sectional microscopic images of samples are shown in Figure 4.33. The resultant compression for perpendicularly-laid nonwovens is compression of the nonwoven fabric structure constructed by change of fibers position.[48]

The compression properties of all the perpendicularly-laid nonwovens are given in Table 4.5 and shown in Figure 4.34. The absorbed energy was computed by multiplying load pressure and thickness reduction of samples. It can be found that sample C5 exhibits highest compressional resistance at 50 % and 90 % thickness reduction, while sample C3 absorbs the highest energy during the compression test. In addition, sample F shows lowest compressional resistance and energy absorption of compression.

Table 4.5 Compression properties of perpendicularly-laid nonwovens

Sample codes	50 % Thickness reduction	90 % Thickness reduction	90 % Thickness reduction
	Pressure (kPa)	Pressure (kPa)	Absorbed energy (10^{-3} J)
A	1.909	5.038	321.888
A1	2.693	11.199	432.159
B	2.124	7.614	451.673
B1	3.005	11.067	469.267
C	4.298	11.954	815.708
C1	5.816	17.268	988.175
C2	7.954	20.234	1111.066
C3	10.96	31.864	1277.924
C4	12.643	35.423	1129.402
C5	15.003	50.568	1132.771
D	3.279	6.075	413.628
E	2.685	4.905	331.906
F	0.889	2.605	130.661
G	1.413	3.574	208.086

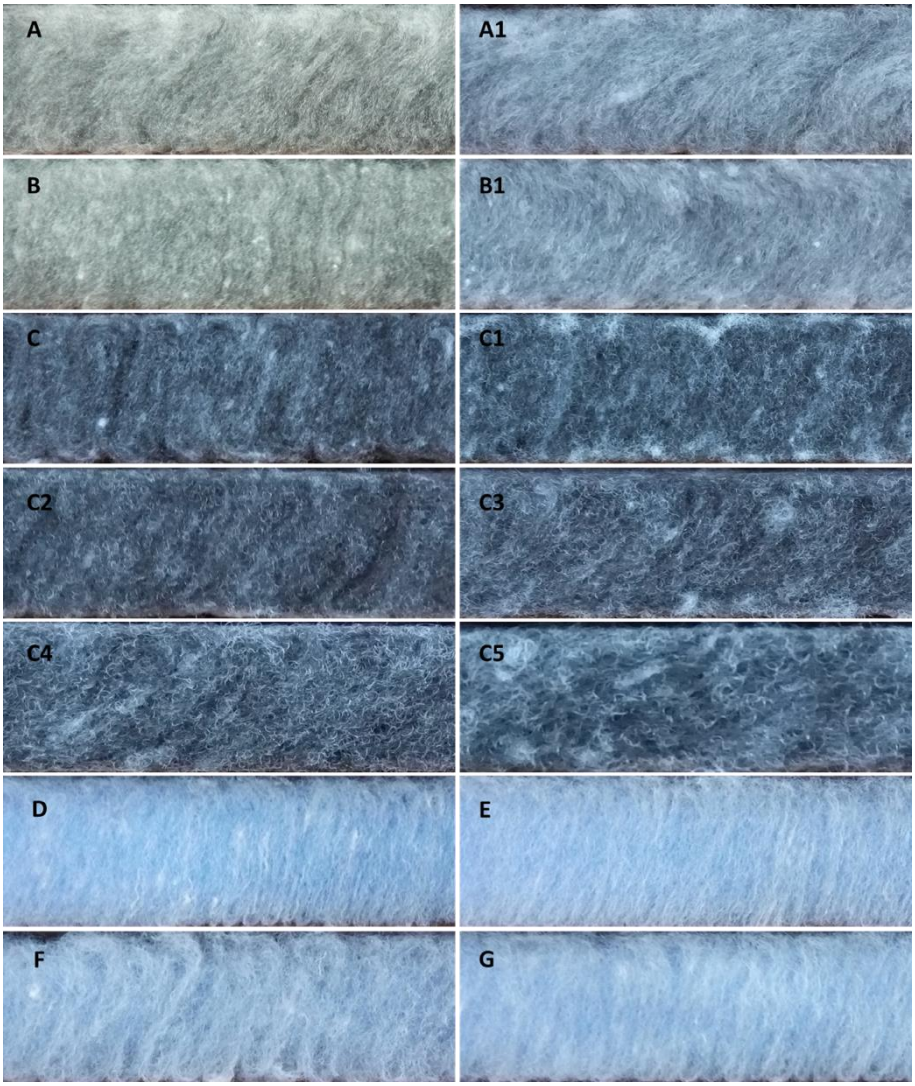

Figure 4.33 Cross-sectional microscopic pictures of perpendicularly-laid nonwovens before compression

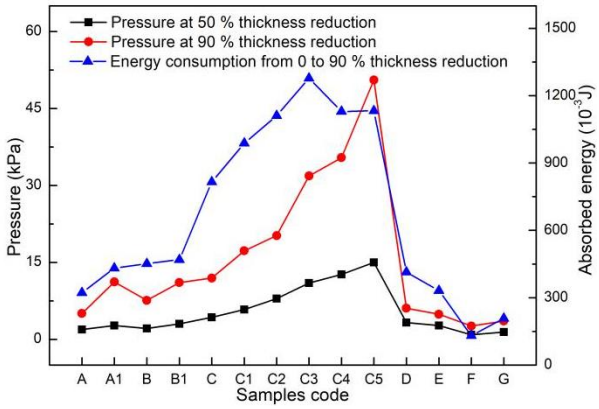

Figure 4.34 Compression properties of perpendicularly-laid nonwovens

The compression curves of samples prepared by vibrating and rotating perpendicular lappers are compared in Figure 4.35. It can be seen that nonwovens (samples B, B1) produced by

vibrating perpendicular lapper exhibit better compressional resistance compared to nonwovens (samples A, A1) prepared by rotating perpendicular lapper. From Table 4.7, it is also observed that samples B, B1 absorb more energy during compression measurement although samples A, A1 have higher density. The reason for this phenomenon can be explained by the different fibrous layer orientation in these samples. Obviously, sample B, B1 have higher fiber orientation angle compared to samples A, A1 in Figure 4.33. As stated earlier, the nonwoven structure compression is performed prior to the compression of fibers themselves. Samples with higher initial fibrous layer orientation angle require higher amount of energy at compression stage. Thus, it can be concluded that perpendicularly-laid nonwovens made by perpendicularly-laid have better compression properties than WAVEMAKER nonwovens.

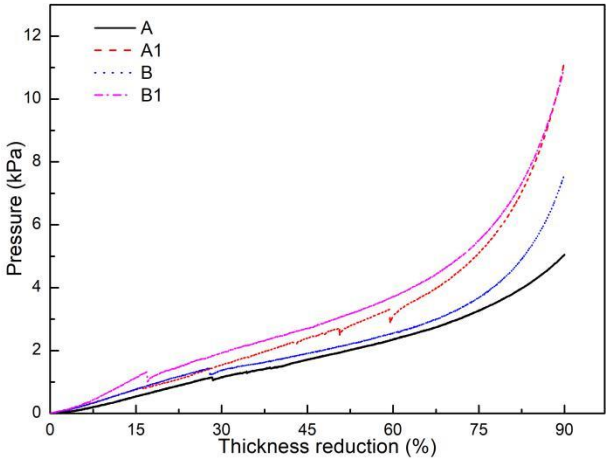

Figure 4.35 Compression pressure of samples produced by different manufacturing techniques

The compression properties of samples treated by heat-pressing method are shown in Figure 4.36. It is observed that sample C exhibits lowest compressional resistance. The compressional resistance increases with the decreasing thickness. It is also found that the pressure sharply rises with the increase of thickness reduction during compression measurement of samples C3, C4 and C5, while the compressional resistance curves of samples C, C1 and C2 remain relatively flat before 75 % thickness reduction.

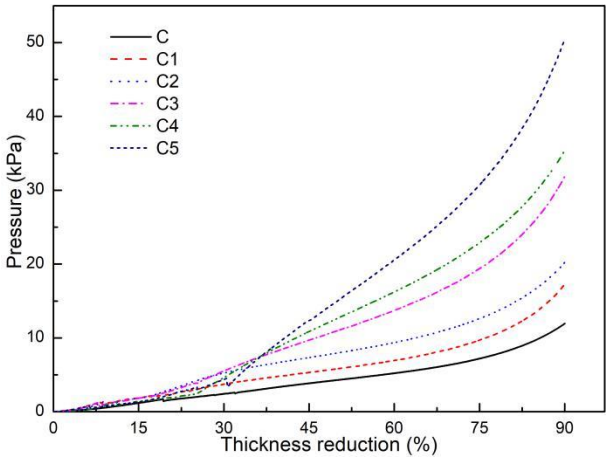

Figure 4.36 Compression curves of samples treated by heat-pressing

Samples B1, D, E, F and G, with similar thickness, were prepared by vibrating perpendicular lapper. These samples were chosen to investigate the effect of density on compression property. From Figure 4.37, it can be seen that compressional resistance decreases with the increase of density. The compressional resistance of perpendicularly-laid nonwovens has a strong correlation with density, with an adjusted coefficients of determination of 0.97185, which means the perpendicularly-laid nonwovens with higher density usually exhibit better compression property.

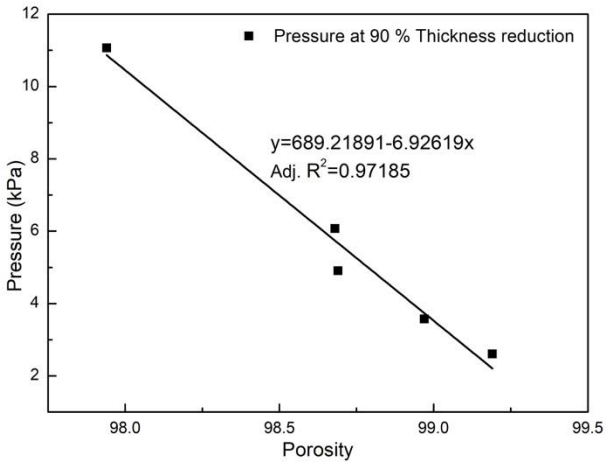

Figure 4.37 Effect of porosity on compression property

Table statistical characteristics of regression

	Equation y = y0 + b*x	**Value**	**t-test Significance "Yes" or "No"**	**Adj. R-Square**	**F-test Significance "Yes" or "No"**
Pressure	y0	689.21891	Yes	0.97185	Yes
	b	-6.92619	Yes		

The cross-sectional microscopic images of samples A, B and C at different compression state are shown in Figure 4.38. ImageJ software was used to obtain fiber orientation angle based on cross-sectional microscopic pictures of nonwovens, each average orientation angle was calculated from 10 measurements. Figure 4.39 describes the effect of thickness reduction on fibrous layers' angle. From these two graphs, it is found that the fibrous layers' angle decreases with the increase of thickness reduction. Also, samples B and C have higher initial fibrous layers' angle compared to sample A, the initial fibrous layers' angle of samples A, B and C are 56.07˚, 87.26˚ and 79.09˚, respectively. Apparently, the majority of fibrous layers are oriented towards same direction as the thickness reduction increases. The shearing deformation happens in compression process as can be seen in Figure 4.38. At the beginning, the compression is applied along the fiber axis for perpendicularly-laid nonwovens. Some fibers stay in stable equilibrium, and others fail by buckling because of the irregularity of fiber length and non-uniformity of fiber position in the nonwoven structure. With the increase of compression load, the fibers yield to higher stress by buckling.

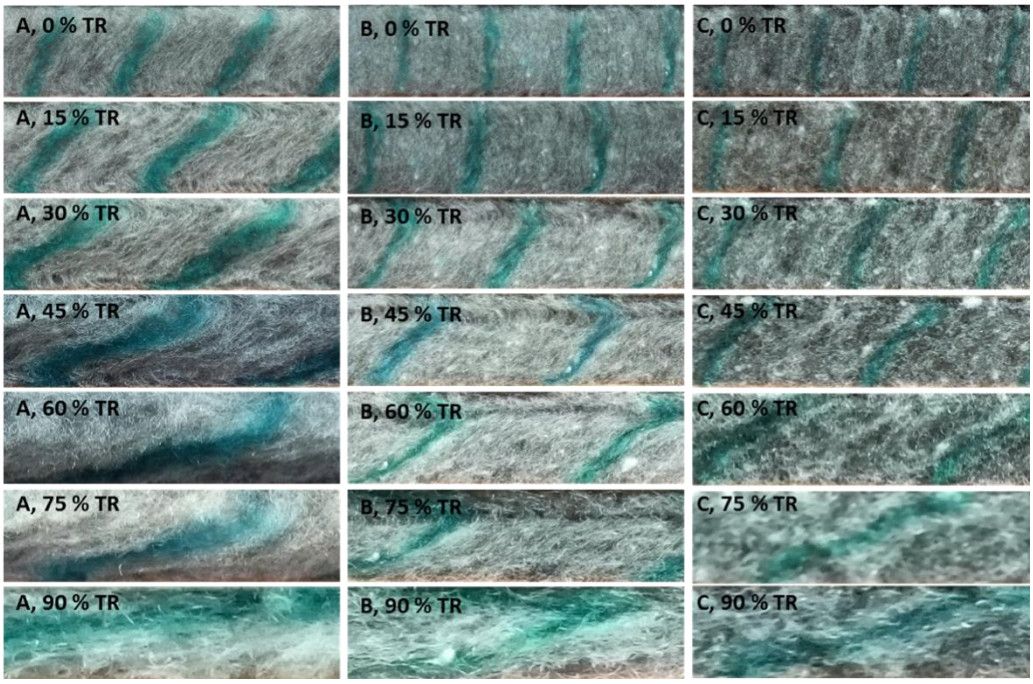

TR is the thickness reduction.

Figure 4.38 Fibrous layer orientation of perpendicularly-laid nonwovens under different compression state

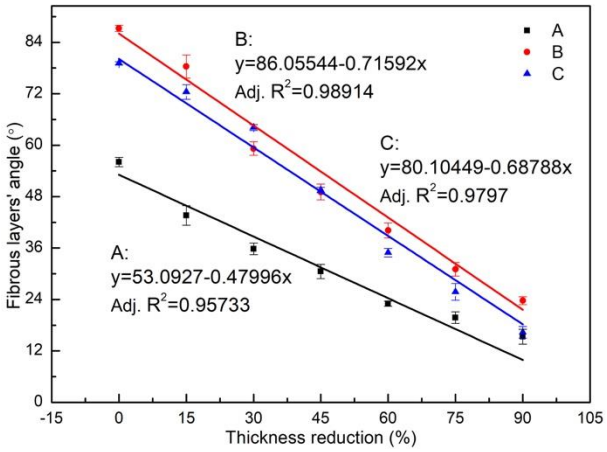

Figure 4.39 Effect of thickness reduction on fibrous layers' angle

Table statistical characteristics of regression

	Equation y = y0 + b*x	Value	t-test Significance "Yes" or "No"	Adj. R-Square	F-test Significance "Yes" or "No"
Fibrous layers' angle (A)	y0	53.0927	Yes	0.95733	Yes
	b	-0.95733	Yes		
Fibrous layers' angle (B)	y0	86.05544	Yes	0.98914	Yes
	b	-0.71592	Yes		
Fibrous layers' angle (C)	y0	80.10449	Yes	0.9797	Yes
	b	-0.68788	Yes		

The effect of compression load on fiber orientation angle is shown in Figure 4.40. It can be seen that the fiber orientation angle sharply decreases with the increase of compression load, but the slopes turn to be flat at the end of compression cycle. It is also observed that sample B and C have higher orientation angle compared to sample A under same compression load. This indicates that perpendicularly-laid nonwovens with higher fiber orientation angle exhibit better compression resistance.

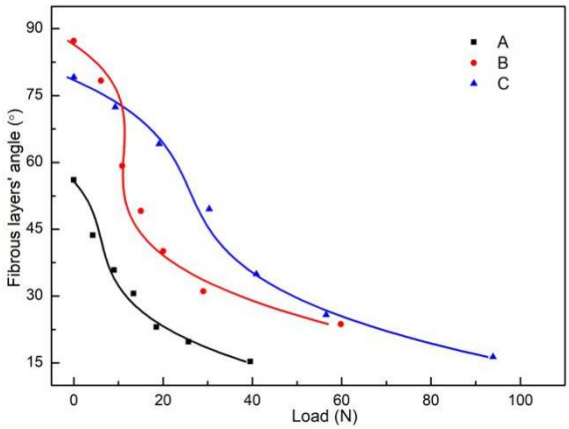

Figure 4.40 Effect of compression load on fibrous layers' angle

Table statistical characteristics of regression

	Equation $y = y0 + b1*x^1 + b2*x^2 + b3*x^3$	**Value**	**t-test Significance "Yes" or "No"**	**Adj. R-Square**	**F-test Significance "Yes" or "No"**
Fibrous layers' angle (A)	y0	114.24341	Yes	0.97542	Yes
	b1	-7.12911	Yes		
	b2	0.16174	Yes		
	b3	-0.00127	Yes		
Fibrous layers' angle (B)	y0	212.00302	Yes	0.95208	Yes
	b1	-9.84664	Yes		
	b2	0.15996	Yes		
	b3	$-8.60953*10^{-4}$	Yes		
Fibrous layers' angle (C)	y0	199.34783	Yes	0.99295	Yes
	b1	-8.82359	Yes		
	b2	0.15642	Yes		
	b3	$-9.72944*10^{-4}$	Yes		

4.6 Thermal properties of perpendicularly-laid nonwovens

4.6.1 Thermal conductivity and resistance

The original perpendicularly-laid nonwovens have been chosen to carry out the thermal properties measurements. Thermal conductivity and thermal resistance of perpendicularly-laid nonwovens are presented in Table 4.6 and Figure 4.41.

Table 4.6 Thermal properties of perpendicularly-laid nonwovens

Sample codes	Thermal conductivity			Thermal resistance		
	Mean value 10^{-3} W·m^{-1}·K^{-1}	SD	95 % confidence intervals	Mean value 10^{-3} K·m^2·W^{-1}	SD	95 % confidence intervals
A	55.84	1.86	55.84 ± 1.15	431.80	15.48	431.8 ± 9.59
B	61.70	3.28	61.7 ± 2.03	460.60	22.78	460.6 ± 14.1
C	60.04	1.95	60.04 ± 1.21	458.20	18.71	458.2 ± 11.6
D	63.30	1.35	63.3 ± 0.837	329.20	6.61	329.2 ± 4.1
E	63.42	0.59	63.42 ± 0.366	313.00	13.17	313 ± 8.16
F	71.10	0.70	71.1 ± 0.434	283.00	6.36	283 ± 3.94
G	67.00	1.49	67 ± 0.923	308.40	16.04	308.4 ± 9.94

For nonwovens with approximately the same thickness (samples D, E, F and G), thermal

resistance increases with the increasing of fabric areal density and thermal conductivity shows an adverse trend. This is because increase in areal density causes increase in fiber to fiber contact and packing density as well as tortuosity, so less heat flows through the channels in nonwoven, and thermal resistance therefore increases correspondingly. Moreover, for samples A, B and C, since they have slightly different areal density and varying thickness, the increase of thermal resistance with the increase in sample thickness indicated that fabric thickness plays a major role in deciding thermal resistance of perpendicularly-laid nonwovens.

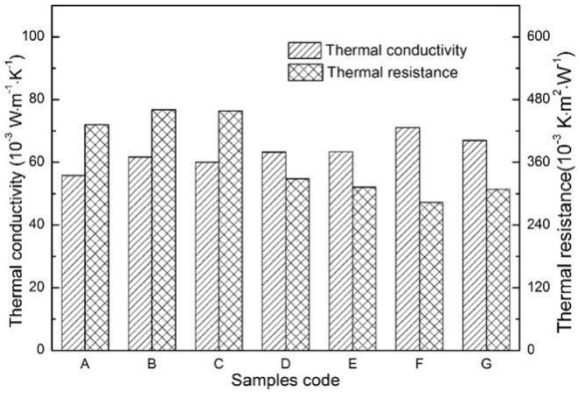

Figure 4.41 Thermal properties of perpendicularly-laid nonwovens

Nonwoven fabrics possess a large amount of void space, which can entrap large volumes of stagnant air. Resulted from the much lower conductivity of still air in comparison to textile fibres, the thermal insulation performance of nonwoven textiles is determined by the trapped air in the inter-fibre spaces. The effect of porosity on thermal properties of perpendicularly-laid nonwovens is illustrated in Figure 4.42. Results showed that the thermal properties of high-porous nonwovens have strong correlation with porosity. Especially, the thermal resistance is directly proportional to fabric porosity, with adjusted coefficients of determination 0.891, indicating that nonwovens with higher porosity usually exhibit better thermal insulation performance since they can preserve more still air.

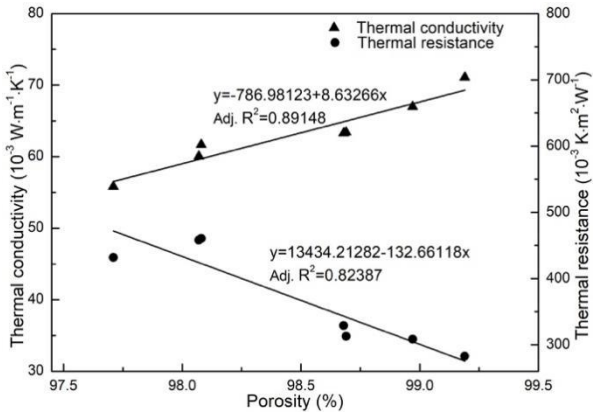

Figure 4.42 Effect of porosity on thermal properties

Table statistical characteristics of regression

	Equation y = y0 + b*x	**Value**	**t-test Significance "Yes" or "No"**	**Adj. R-Square**	**F-test Significance "Yes" or "No"**
Thermal conductivity	y0	-786.981	Yes	0.89148	Yes
	b	8.63266	Yes		
Thermal resistivity	y0	13434.21	Yes	0.82387	Yes
	b	-132.662	Yes		

4.6.2 The relationship between acoustic and thermal properties

Since the fabric thickness, fiber fineness and fabric areal density are very important factors in determining both acoustic and thermal properties of perpendicularly-laid nonwovens, there appears a great interest to investigate the relationship between these two properties for perpendicularly-laid nonwovens.

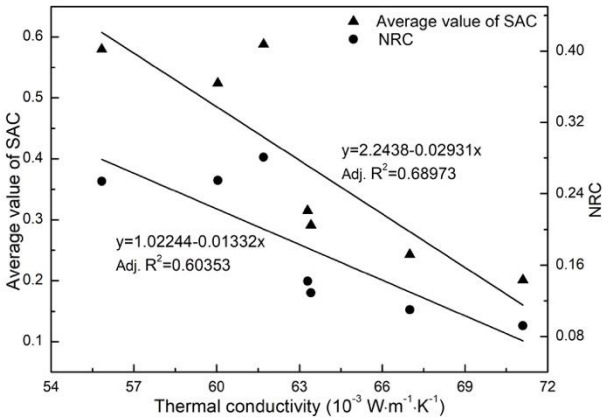

Figure 4.43 Estimation of correlation between thermal conductivity and sound absorption (NRC and average value of SAC)

Table statistical characteristics of regression

	Equation y = y0 + b*x	Value	t-test Significance "Yes" or "No"	Adj. R-Square	F-test Significance "Yes" or "No"
Average value of SAC	y0	2.2438	Yes	0.68973	Yes
	b	-0.02913	Yes		
NRC	y0	1.02244	Yes	0.60353	Yes
	b	-0.01332	Yes		

Figure 4.43 illustrates the estimation of correlation between thermal conductivity of perpendicularly-laid nonwovens and sound absorption, NRC and average value of SAC ($\bar{\alpha}$). It is observed that both NRC and $\bar{\alpha}$ have insignificant correlation with thermal conductivity, the adjusted coefficients of determinations are 0.60353 and 0.68973, respectively. The reason could be that thermal conductivity is not dependent on fabric thickness while fabric thickness is a determining factor for sound absorption.

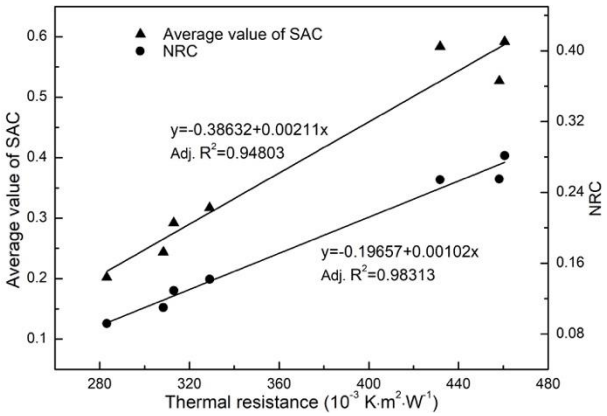

Figure 4.44 Estimation of correlation between thermal resistance and sound absorption (NRC and average value of SAC)

Table statistical characteristics of regression

	Equation y = y0 + b*x	Value	t-test Significance "Yes" or "No"	Adj. R-Square	F-test Significance "Yes" or "No"
Average value of SAC	y0	-0.38632	Yes	0.94803	Yes
	b	0.00211	Yes		
NRC	y0	-0.19578	Yes	0.98313	Yes
	b	0.00102	Yes		

Estimation of correlation between thermal resistance and sound absorption, NRC and $\bar{\alpha}$, are

presented in Figure 4.44. The adjusted coefficients of determination between NRC and thermal resistance is 0.98313, and this value is 0.94803 for SAC and thermal resistance, indicating that the sound absorption performance of perpendicularly-laid nonwovens has a very strong correlation with thermal resistance. It can be concluded that NRC and SAC are directly proportional to thermal resistance of perpendicularly-laid nonwovens. That means for different perpendicularly-laid nonwovens, a higher thermal resistance suggests a better sound absorption performance.

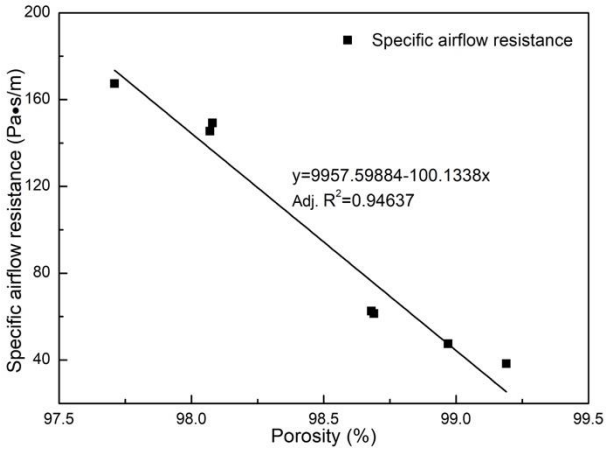

Figure 4.45 Effect of porosity on specific airflow resistance

Table statistical characteristics of regression

	Equation y = y0 + b*x	**Value**	**t-test Significance "Yes" or "No"**	**Adj. R-Square**	**F-test Significance "Yes" or "No"**
Porosity	y0	9957.599	Yes	0.94637	Yes
	b	-100.134	Yes		

The relationship between sound absorption performance and thermal resistance could be explained by the strong dependence of sound absorption and thermal insulation on pore characteristics of nonwoven fabrics. The thermal resistance of perpendicularly-laid nonwoven is directly proportional to fabric porosity. Moreover, the sound absorption performance of perpendicularly-laid nonwoven strongly depends on its specific airflow resistance, and this specific airflow resistance is also observed to be proportional to fabric porosity, with adjusted coefficients of determination 0.94637 as shown in Figure 4.45. Generally, for high porous perpendicularly-laid nonwovens, when the pressure wave penetrates into the material through the open pores of the surface and gets scattered by a high number of internal reflections before being lost to the environment, these reflections transfer energy to the solid structure through frictional losses and efficiently absorb sound. As the

porosity decreases, less energy is transferred into the solid structure and more is reflected from the surface, making the material less useful as an acoustic absorber. Thus, the sound absorption performance of perpendicularly-laid nonwoven is indirectly correlated to its thermal resistance.

4.7 Air permeability of perpendicularly-laid nonwovens

4.7.1 Air permeability

It is believed that fibers will be deformed by the airflow under a given air pressure during the measurement of air permeability of a fabric due to flexibility of textile fibers. It is reported that most fabrics are easily deformed under pressure load especially below 200 Pa with an evident deformation and this would significantly affect the air permeability.[54] In order to examine the effect of fiber deformation on the measured air permeability of perpendicularly-laid nonwovens, different pressure gradients 50 Pa, 100 Pa, 150 Pa and 200 Pa were chosen to carry out air permeability testing. The measured air permeability is listed in Table 4.7. Each value is the average of five test results.

Table 4.7 Measured air permeability of samples

Samples Code	Air Permeability (mm/s)							
	ΔP =50Pa	95% Confidence Interval	ΔP =100Pa	95% Confidence Interval	ΔP= 150Pa	95% Confidence Interval	ΔP= 200Pa	95% Confidence Interval
A	320.1	320.1 ± 11.4	597.6	597.6 ± 20.9	848.7	848.7 ± 29.7	1070.5	1070.5 ± 39.2
B	320.1	320.1 ± 36.3	652.1	652.1 ± 46.5	923.3	923.3 ± 63.5	1177.6	1177.6 ± 84.4
C	370.6	370.6 ± 9.55	687.3	687.3 ± 17.2	968.3	968.3 ± 22.3	1227	1227 ± 28.8
D	908.8	908.6 ± 20.7	1598	1598 ± 36	2166	2166 ± 45.9	2712	2712 ± 59
E	929.8	929.8 ± 37	1628	1628 ± 59.7	2220	2220 ± 80.7	2760	2760 ± 99.1
F	1548	1548 ± 26.1	2608	2608 ± 59	3508	3508 ± 104	4336	4336 ± 191
G	1234	1234 ± 18.9	2104	2104 ± 26.5	2824	2824 ± 36.6	3468	3468 ± 25.3

Note: Samples were held by clamping arm under the load 50N

Since perpendicularly-laid nonwoven is loose fabric, the large spacing between fibers enables the majority of air to flow through these gaps. Obviously, samples A, B and C exhibit much lower air permeability while F and G show the highest air permeability. Similar to the sound absorption performance, this is also attributed to their difference in areal density and fabric thickness. For s perpendicularly-laid nonwovens with higher areal density and fabric

thickness, there is less pores and air space in textile structure to allow air flow go through.

Air permeability increases with the increasing of pressure gradient. Usually, with the increasing of pressure gradient, the airflow velocity increases as well. If the airflow velocity exceeds a limit, turbulence flow may occur and the air permeability value will sharply decrease in that case. In this study, assuming flow in a circular channel, the calculated Reynolds numbers are all less than the critical value (2300). That means no turbulent flow occurs during the measurement.

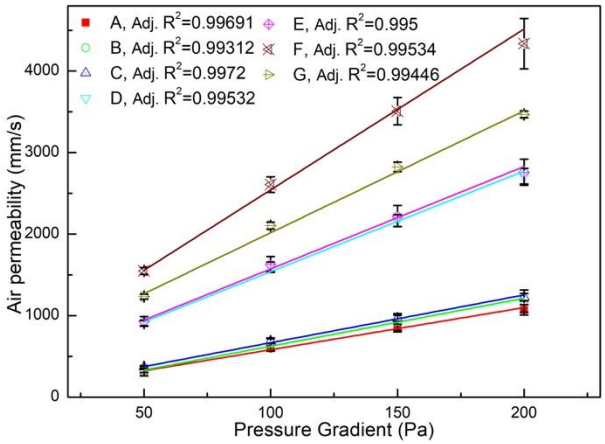

Figure 4.46 Effect of pressure gradient on air permeability

Table statistical characteristics of regression

	Equation y = y0 + b*x	**Value**	**t-test Significance "Yes" or "No"**	**Adj. R-Square**	**F-test Significance "Yes" or "No"**
Air permeability (A)	y0	65.30485	Yes	0.99691	Yes
	b	5.16632	Yes		
Air permeability (B)	y0	37.90913	Yes	0.99312	Yes
	b	5.87269	Yes		
Air permeability (C)	y0	82.22684	Yes	0.9972	Yes
	b	5.85668	Yes		
Air permeability (D)	y0	304.96928	Yes	0.99532	Yes
	b	12.34672	Yes		
Air permeability (E)	y0	317.12012	Yes	0.995	Yes
	b	12.56062	Yes		
Air permeability (F)	y0	569.41397	Yes	0.99534	Yes
	b	19.73267	Yes		
Air permeability (G)	y0	520.54964	Yes	0.99446	Yes
	b	14.96385	Yes		

The effect of pressure gradient on air permeability is illustrated in Figure 4.46. Air permeability is strongly correlated to pressure gradient, the adjusted coefficients of determination between pressure gradient and air permeability are all above 0.99 for seven samples, indicating there is linear relationship between pressure gradient and air permeability. This is completely compatible to Darcy's law. Results also reveal that the fiber deformation of perpendicularly-laid nonwoven has insignificant effect on the measured air permeability. This is because the samples are firmly clamped by the arm and the loose nonwoven structures are partly compressed during the measurement, so the fibers are not easily deformed by the high speed airflow. Moreover, the fibers are oriented approximately in parallel with the airflow direction, which will significantly reduce the airflow force suffered by fibers.

The interaction effect of fabric areal density and thickness on air permeability is shown in Figure 4.47. It is observed that air permeability of perpendicularly-laid nonwovens tends to decrease with the increasing of areal density and fabric thickness, which is similar to conventional textile fabrics.

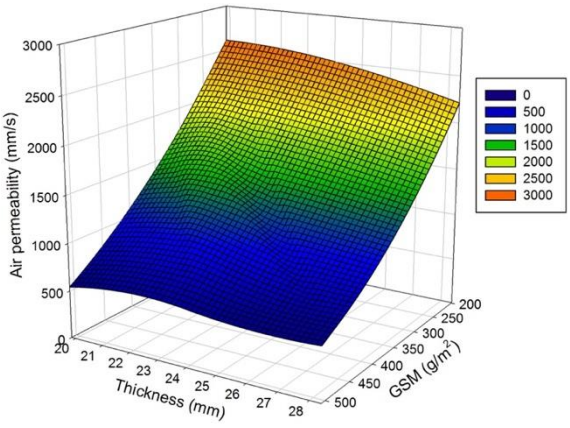

Figure 4.47 Effect of areal density and thickness on air permeability

As shown in Figure 4.48, the porosity of the material has a strong influence on the air permeability of the material. It is obvious that the increase in porosity leads to increase in air permeability. The quadratic correlations dependences between porosity and air permeability were also calculated and mentioned in Figure 4.48. It is found that porosity has a quadratic relation with air permeability with adjusted coefficients of determination 0.99261.

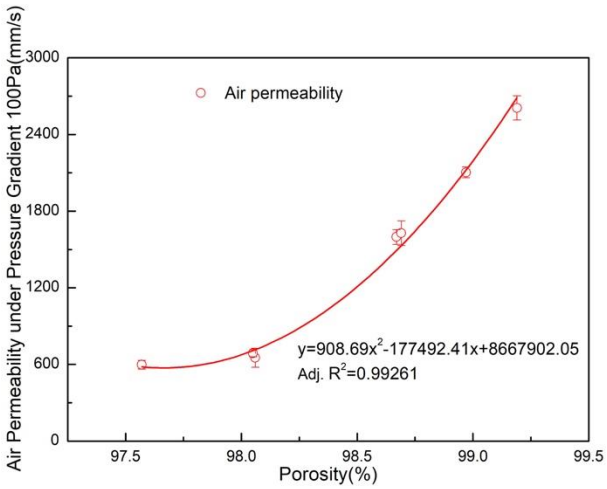

Figure 4.48 Effect of porosity on air permeability

Table statistical characteristics of regression

	Equation y = A*x^2+B*x+C	**Value**	**t-test Significance "Yes" or "No"**	**Adj. R-Square**	**F-test Significance "Yes" or "No"**
Air permeability	A	908.68695	Yes	0.99261	Yes
	B	-177492.41183	Yes		
	C	$8.6679*10^6$	Yes		

4.7.2 The relationship between sound absorption properties and air permeability

From the above analysis, it can be seen that the fundamental structural parameters such as porosity and fabric thickness have profound effect on acoustic performance and air permeability of perpendicularly-laid nonwoven. Remarkably, they show completely inverse effect on acoustic performance and air permeability. Thus, there should be some indirect relation between air permeability and acoustic performance of perpendicularly-laid nonwovens.

Estimated correlation between air permeability and sound absorption is presented in Figure 4.49. It is observed that $\bar{\alpha}$ has significant correlation with air permeability, the adjusted coefficients of determination is about 0.98, indicating the existence of an inverse relation between air permeability and sound absorption of perpendicularly-laid nonwovens. That means perpendicularly-laid nonwoven with lower air permeability usually exhibits better sound absorption performance. This may provide a new method to evaluate the sound absorption property of perpendicularly-laid nonwovens by means of air permeability testing.

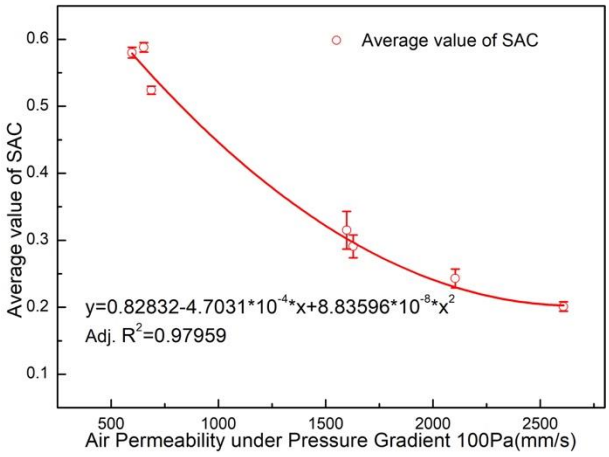

Figure 4.49 Estimated correlation between air permeability and sound absorption

Table statistical characteristics of regression

	Equation y = y0 + b1*x^1 + b2*x^2	**Value**	**t-test Significance "Yes" or "No"**	**Adj. R-Square**	**F-test Significance "Yes" or "No"**
Average value of SAC	y0	0.82832	Yes	0.97959	Yes
	b1	$-4.70315*10^{-4}$	Yes		
	b2	$8.83596*10^{-8}$	Yes		

Chapter 5 Conclusions

In this study, the acoustic properties, airflow resistivity, compressibility, thermal properties and air permeability of perpendicularly-laid nonwovens were investigated. Besides, the sound absorption properties of aerogel based nonwovens have been analyzed.

Sound absorption property of perpendicularly-laid nonwovens were tested by Brüel and Kjær measuring instrument. The effect of manufacturing techniques on sound absorption performance was investigated. The effect of porosity and airflow resistivity on sound absorption ability was studied. It is found that there is no significant influence of two manufacturing techniques on sound absorption performance. The increase of areal density results in improvement of sound absorption ability. The increase of thickness can improve sound absorption coefficient at low-frequency range, but decrease of the coefficient occurred at high-frequency range. A quadratic relationship between porosity and sound absorption ability has been found.

An investigation on sound absorption performance of aerogel based nonwoven fabrics was carried in this study. Polyester/polyethylene nonwovens embedded with hydrophobic amorphous silica aerogel were chosen for sound absorption measurements. The sound absorption coefficient (SAC) of single and multilayered of aerogel nonwovens blankets was tested by Brüel and Kjær impedance tube. The effect of air-back cavities on SAC of single layer aerogel based nonwoven fabrics was investigated. The results show that there is a decrease in SAC with the increase of aerogel content. It is observed that the noise reduction coefficient (NRC) linearly increased with the increase of layers for all the samples. It was also found that the air-back cavities result in resonance phenomenon, as the increase in thickness of air-back cavities the peak values of SAC shift towards lower frequencies.

The airflow resistivity is a key parameter to predict accurately the acoustical properties of fibrous media. There is a large number of theoretical and empirical models which can be used to predict the airflow resistivity of this type of porous media. However, there is a lack of experimental data on the accuracy of these models in the case of multi-component fibrous media. This study presents a detailed analysis of the accuracy of several existing models to predict airflow resistivity which make use of the porosity, bulk density and mean fiber diameter information. The AFD300 AcoustiFlow device was employed to measure airflow resistivity. It is shown that some existing models largely under- or overestimate the airflow

resistivity when compared with the measured values. A novel feature of this work is that it studies the relative performance of airflow resistivity prediction models that are based on the capillary channel theory and drag force theory. These two groups of models are then compared to some purely empirical models. It is found that the mean absolute values of relative error (MAVRE) by some models is unacceptably high (e.g. >20-30%). The results suggest that there are existing models which can predict the airflow resistivity of multi-component fibrous media with 12.6% accuracy. A simple empirical model based on fiber diameter and fabric bulk density has been obtained through power-type model. This model exhibits very small error which is 5.1%.

15 types of perpendicularly-laid nonwoven samples were chosen to study their acoustic properties. The surface impedance and sound absorption coefficient were determined by using 45mm Materiacustica impedance tube. The widely used impedance models such as Delany-Bazley, Miki, Garai-Pompoli and Komatsu models were used to predict acoustical properties. Comparison between measured and predicted values has been performed to get the most acceptable model for perpendicularly-laid nonwovens. It is shown that Delany-Bazley and Miki models can accurately predict surface impedance of multi-component polyester nonwovens, but Komatsu model has inaccuracy in prediction especially at low-frequency band. The results indicate that Miki model is the most acceptable method to predict the sound absorption coefficient with mean error 8.39% from all the samples. The values are 8.92%, 12.58% and 69.67% for Delany-Bazley, Garai-Pompoli and Komatsu models, respectively.

Perpendicularly-laid nonwovens with varying thickness and areal density were prepared by heat-pressing method to investigate the effect of structural parameters such as thickness and areal density on compressibility. The effect of laying techniques on compression properties was investigated. The influence of density and fibrous layers' orientation angle on compression properties was analyzed. The results show that samples prepared by vibrating perpendicular lapper exhibit better compression properties. The results also show that the compressional resistance has a strong relation with porosity, the adjusted coefficients of determination is 0.97, indicating that the compressional resistance is directly proportional to the density of perpendicularly-laid nonwovens. The results indicate that the perpendicularly-laid nonwovens with higher initial fibrous layer orientation angle have better compression properties.

An experimental investigation on the thermal properties of perpendicularly-laid nonwovens was carried for establishing relationship between thermal and acoustic properties. Seven perpendicularly-laid nonwoven fabrics were selected to examine thermal properties including thermal conductivity and thermal resistance. Alambeta was used for evaluation thermal properties. The influence of structural parameters on thermal properties were investigated and analyzed. The effect of porosity on specific airflow resistance and thermal properties was studied in detail. The result indicated that porosity has a strong correlation with specific airflow resistance and thermal properties. It was also observed that sound absorption, the NRC and mean value of sound absorption coefficient ($\bar{\alpha}$), have insignificant correlation with thermal conductivity, while they are strongly correlated with thermal resistance. The adjusted coefficients of determination of NRC with thermal resistance is 0.98, indicating that NRC is directly proportional to thermal resistance of perpendicularly-laid nonwovens.

This study also investigated the air permeability of perpendicularly-laid nonwovens and their relation to acoustic performance. Air permeability of perpendicularly-laid nonwovens was examined by using FX3300 Textech Air Permeability Tester. Perpendicularly-laid nonwovens with high areal density and fabric thickness showed lower air permeability. It was observed that $\bar{\alpha}$ were inversely proportional to air permeability, with adjusted coefficients of determination 0.98. It was concluded that air permeability can be used as a criterion of sound absorption behavior of perpendicularly-laid nonwovens, a lower air permeability suggested a better sound absorption performance for perpendicularly-laid nonwoven fabric.

5.1 Scope for future work

The ideas, experiments and data generated as part of this research, have added to the knowledge base that could be useful to define the future direction and provide insightful references to researchers. The potential of this research can be realized by pursuing further studies into areas given below:

- Applying semi-phenomenological and empirical models, such as Johnson-Champoux-Allard-Lafarge model, on the acoustical investigation of perpendicularly-laid nonwovens to further study their acoustic behaviour.
- To develop a suitable inverse method to obtain porosity, fibre diameter and density of polyester sound-absorbing materials.
- Optimizing sound absorption of fibrous material under set frequency bands using numerical method based on existing models.

- Investigate the acoustic behaviour of waste natural fibers (e.g. wool, cotton, ramie, hemp, flax and jute waste) through practical and numerical method, and figure out the most suitable models for each type of natural fiber.

References:

1. What are the effects of noise pollution? http://eschooltoday.com/pollution/noise-pollution/effects-of-noise-pollution.html. Accessed July 10, 2018.

2. Küçük M, Korkmaz Y. The effect of physical parameters on sound absorption properties of natural fiber mixed nonwoven composites. *Text Res J* 2012; 82(20):2043-2053.

3. Cox TJ and D'Antonio P. Acoustic Absorbers and Diffusers: Theory, Design and Application. 2nd ed. London; New York: Taylor & Francis, 2009, p. 156-157.

4. Albrecht W, Fuchs H and Kittelmann W. *Nonwoven fabrics*. Weinheim: Wiley-VCH, 2003, p.748.

5. Struto International Inc., Struto® Nonwoven, http://www.struto.com. Accessed July 26, 2018.

6. Parikh DV, Calamari TA, Goynes WR, Chen Y and Jirsak O. Compressibility of cotton blend perpendicularly-laid nonwovens. *Text Res J* 2004; 74: 7–12.

7. Vasile S and Van-Langenhove L. Automotive industry a high potential market for nonwovens sound insulation. *J Text Appl Tech Mgmt* 2004; 3: 1–5.

8. Kalinova K. Theoretical assessment of sound absorption coefficient for anisotropic nonwovens. *QScience Connect* 2013; 3: 3-10

9. Jirsak O, Burian T and Sasková P. Improvements in Compressional Properties of Highlofts. *Fibred Text East Eur* 2003; 11(3): 80–83.

10. Parikh DV, Calamari TA, Sawhney APS, Robert K Q, Kimmel L, Glynn E, Jisak O, Mackova I and Saunders T. Compressional behavior of perpendicularly-laid nonwovens containing cotton. *Text Res J* 2002; 72(6): 550–554.

11. Crocker MJ and Arenas JP, "Use of Sound-Absorbing Materials," Chapter 57 in Handbook of Noise and Vibration Control (M.J. Crocker, Ed.), John Wiley and Sons, New York, 2007.

12. Arenas JP, Crocker MJ. Recent Trends in Porous Sound-Absorbing Materials. *Sound Vib* 2010; 12-17.

13. Rouquerol J, Avnir D, Fairbridge CW, Everett DH, Haynes JM, Pernicone N, Ramsay JDF, Sing KSW and Unger KK. Recommendations for the Characterization of Porous Solids. *Pure Appl Chem* 1994; 66(8): 1739-1758.

14. Kazragis A, Gailius A and Jukneviciute A. Thermal and Acoustical Insulating Materials Containing Mineral and Polymeric Binders with Celluloses Fillers. *Mater Sci* 2002; 8(2): 193-195.

15. Magrini U and Ricciardi P. Surface Sound Acoustical Absorption and Application of Panels Composed of Granular Porous Materials. Proceedings of Inter-Noise 2000, pp. 27-30, Nice, France, 2000.

16. Asdrubali F and Horoshenkov KV. The Acoustic Properties of Expanded Clay Granulates. *Building Acoustics* 2002; 9(2): 85-98.

17. Attenborough K and Umnova O. "Acoustics of Rigid-Porous Materi- als," in Lecture Notes on the Mathematics of Acoustics (M.CM. Wright, Ed.), Imperial College Press, London, pp. 157-176, 2005.

18. Zwikker C and Kosten CW. Sound Absorbing Materials, Elsevier, New York, 1949.

19. Zulkifli R, Mohd Nor MJ, Mat Tahir MF, Ismail AR and Nuawi MZ. Acoustic Properties of Multi-Layer Coir Fibres Sound Absorption Panel. *Journal of Applied Sciences* 2008; 8(20): 3709-3714.

20. Koizumi T. The Development of Sound Absorbing Materials Using Natural Bamboo Fibers and their Acoustic Properties. Proceedings of Inter-Noise 2002, Dearborn, MI, 2002.

21. Del Rey R, Alba J and Sanchiz V. Proposal of an Empirical Model for Absorbent Acoustical Materials Based in Kenaf. Proceedings of the 19th International Congress on Acoustics, Madrid, Spain, 2007.

22. Tascan M and Vaughn E A. Effects of Fiber Denier, Fiber Cross- Sectional Shape and Fabric Density on Acoustical Behavior of Vertically Lapped Nonwoven Fabrics. *J Eng Fiber Fabr 2008*; 3(2): 32-38.

23. Vaughn EA and Tascan M. Effects of Total Surface Area and Fabric Density on the Acoustical Behavior of Needle punched Nonwoven Fabrics. *Text Res J* 2008; 78(4): 289-296.

24. Arenas JP. Applications of Acoustic Textiles in Automotive/Transportation. Chapter 7 in Acoustic Textile (Padhye R and Nayak R, Ed.), Springer, Singapore, 2016.

25. Crocker MJ. Introduction to interior transportation noise and vibration sources. In: Crocker MJ (ed) Handbook of noise and vibration control. Wiley, New York, pp 1149–1158, 2007.

26. Fung W and Hardcastle M. Textiles in automotive engineering. Woodhead Publishing Limited, Cambridge, 2001.

27. Shishoo R (ed). Textile advances in the automotive industry. Woodhead Publishing Limited, Cambridge, 2009.

28. Matsuo T. Automotive applications. In: Deopura BL, Alagirusamy R, Joshi M and Gupta M (eds) Polyesters and polyamides. Woodhead Publishing Limited, Cambridge, pp 525–541, 2008

29. Wang CN and Torng JH. Experimental Study of the Absorption Characteristics of Some Porous Fibrous Materials. *Appl Acoust* 2001; 4: 447–459.

30. Chen Y and Jiang N. Carbonized and Activated Non-Wovens as High-Performance Acoustic Materials: Part I Noise Absorption. *Text Res J* 2007; 77: 785–791.

31. European Council Directive 67/548/EEC of 27 June 1967, On the approximation of laws, regulations and administrative provisions relating to the classification, packaging and labelling of dangerous substances, Official Journal of the European Union 1967; 196: 1-98.

32. Mamtaz H, Fouladi MH, Al-Atabi M and Namasivayam SN. Acoustic Absorption of Natural Fiber Composites. *J Eng* 2016; 2016: 1-11.

33. Tang X and Yan X. Acoustic energy absorption properties of fibrous materials: A review. *Compos Part A-Appl S* 2017; 101: 360-380.

34. Thilagavathi G, Pradeep E, Kannaian T and Sasikala L. Development of Natural Fiber Nonwovens for Application as Car Interiors for Noise Control. *J Ind Text* 2010; 39: 267–278.

35. Oldham DJ, Egan CA and Cookson RD. Sustainable Acoustic Absorbers from the Biomass. *Appl Acoust* 2011; 72: 350–363.

36. Pelegrinis MT, Horoshenkov KV and Burnett A. An Application of Kozeny–Carman Flow Resistivity Model to Predict the Acoustical Properties of Polyester Fibre. *Appl Acoust* 2016; 101: 1–4.

37. Koizumi T, Tsujiuchi N and Adachi A. The Development of Sound Absorbing Materials Using Natural Bamboo Fibers, High Performance. WIT Press, 2002.

38. Sun F, Banks-Lee P and Peng H. Sound Absorption in An Anisotropic Periodically Layered Fluid-Saturated Porous Medium. *Appl Acoust* 1993; 39: 65-76.

39. Lee Y and Joo C. Sound Absorption Properties of Recycled Polyester Fibrous Assembly Absorbers. AUTEX Res J 2003; 3(2): 2003.

40. Na Y, Lancaster J, Casali J and Cho G. Sound absorption coefficients of micro-fiber fabrics by reverberation room method. *Text Res J* 2007; 77: 330–335.

41. Zent A and Long JT. Automotive sound absorbing material survey results. *SAE International* 2007; 2007-01-2186.

42. Suvari F, Ulcay Y and Pourdeyhimi B. Sound absorption analysis of thermally bonded high-loft nonwovens. *Text Res J* 2016; 86: 837–847.

43. Ingard U. Notes on Sound Absorption Technology, Noise Control Foundation, New York, 1994.

44. Yilmaz ND, Banks-Lee P, Powell NB and Michielsen S. Effects of porosity, fiber size, and layering sequence on sound absorption performance of needle-punched nonwovens. *J Appl Polym Sci* 2011;121(5): 3056-3069.

45. Riffat SB and Qiu G. A review of state-of-the-art aerogel applications in buildings. *International Journal of Low-Carbon Technologies* 2013; 8(1): 1–6.

46. Gross J, Fricke J and Hrubesh LW. Sound propagation in SiO2 aerogels. *J Acoust Soc Am* 1992; 91(4): 2004–2006.

47. Forest L, Gibiat V and Woignier T. Biot's theory of acoustic propagation in porous media applied to aerogels and alcogels. *J Non-Cryst Solids* 1998; 225: 287–292.

48. Forest L, Gibiat V and Woignier T. Evolution of the acoustical properties of silica alcogels during their formation. *Ultrasonics* 1998; 36(1): 477–481.

49. Hrubesh LW. Aerogel applications. *J Non-Cryst Solids* 1998; 225: 335–342.

50. Schmidt M and Schwertfeger F (1998). Applications for silica aerogel products. *J Non-Cryst Solids* 1998; 225: 364–368.

51. Akimov YK. Fields of application of aerogels (review). *Instrum Exp Tech*+ 2003; 46(3): 287–299.

52. Gibiat V, Lefeuvre O, Woignier T, Pelous J and Phalippou J. Acoustic properties and potential applications of silica aerogels. *J Non-Cryst Solids 1995;* 186: 244–255.

53. Oh KW, Kim DK and Kim SH. Ultra-porous flexible PET/Aerogel blanket for sound absorption and thermal insulation. *Fiber Polym* 2009; 10(5): 731–737.

54. Xiong X, Yang T, Huang J, Mishra R, Kotresh TM and Militky J. Heat transfer through thermal insulation materials Part I- nonwoven fabrics. Recent developments in fibrous material science, VOL.II, 85-104 (2015).

55. Arambakam R, Vahedi Tafreshi H and Pourdeyhimi B. A simple simulation method for designing fibrous insulation materials. *Mater Design* 2013; 44: 99–106.

56. Behera BK, Mishra R. Artificial neural network-based prediction of aesthetic and functional properties of worsted suiting fabrics. *Int J Cloth Sci Tech* 2007; 19: 259-276

57. Vallabh R, Banks-Lee P and Mohammadi M. Determination of radiative thermal conductivity in needle punched nonwovens. *J Eng Fiber Fabr* 2008; 3: 46–52.

58. Kang KY, Lee KY, Jo KJ, et al. Anisotropy in structure and mechanical properties of perpendicularly-laid nonwovens. *J Mater Sci* 2008; 43: 2754–2760.

59. Parikh DV, Calamari TA, Goynes WR, et al. Compressibility of cotton blend perpendicularly-laid nonwovens. *Text Res J* 2004; 74: 7–12.

60. Parikh DV, Calamari TA, Sawhney APS, et al. Compressional behavior of perpendicularly-laid nonwovens containing cotton. *Text Res J* 2002; 72: 550–554.

61. Piekaar HW and Clarenburg LA. Aerosol filters - the tortuosity factor in fibrous filters. *Chem Eng Sci* 1967; 22(12): 1817–1827.

62. Xiao X, Zeng X, Bandara P and Long A. Experimental study of dynamic air permeability for woven fabrics. *Text Res J* 2012; 82(9): 920–930.

63. Soltani P and Zarrebini M. Acoustic performance of woven fabrics in relation to structural parameters and air permeability. *J Text I* 2013; 104(9): 1011–1016.

64. Yang S and Yu W. Air permeability and acoustic absorbing behaviour of nonwovens. *J Fiber Bioeng Infor* 2011; 3: 203-207.

65. ISO 9053-1991: Acoustics -- Materials for acoustical applications -- Determination of airflow resistance.

66. Xue Y, Bolton JS, Gerdes R, Lee S and Herdtle T. Prediction of Airflow Resistivity of Fibrous Acoustical Media Having Two Fiber Components and a Distribution of Fiber Radii. *Appl Acoust* 2018; 134: 145–153.

67. Hurrell AI, Horoshenkov KV and Pelegrinis MT. The Accuracy of Some Models for the Airflow Resistivity of Nonwoven Materials. *Appl Acoust* 2018; 130: 230-237.

68. Zwikker C and Kosten CW. Sound Absorbing Materials. New York: Elsevier: 1949.

69. Luu HT, Perrot C, Monchiet V, Panneton R. Three-dimensional reconstruction of a random fibrous medium: Geometry, transport, and sound absorbing properties. *J Acoust Soc Am* 2017; 141: 4768-4780.

70. Xue Y, Bolton JS. Prediction of Airflow Resistivity of Fibrous Acoustical Materials Having Double Fiber Components and a Distribution of Fiber Radii. Proceedings of International Congress on Noise Control Engineering 2017, Hong Kong.

71. Sutera SP, Richard S. The History of Poiseuille's Law. *Annu Rev Fluid Mech* 1993; 25: 1–20.

72. Carman PC. Flow of Gases through Porous Media. New York: Academic Press, 1956.

73. Davies CN. The Separation of Airborne Dust and Particles. Proceedings of the Institution of Mechanical Engineers, Part B: Management and Engineering Manufacture 1953; 1: 185–213.

74. Carman PC. Fluid Flow through Granular Beds. *Chem Eng Res Des* 1997; 75: 32–48.

75. Chen X. Modelling and Predicting Textile Behaviour. Woodhead Publishing Series in Textiles, no. 94. Cambridge: Boca Raton, Fla: Woodhead Publishing: In association with the Textile Institute; CRC Press, 2010.

76. Lind-Nordgren E and Göransson P. Optimising Open Porous Foam for Acoustical and Vibrational Performance. *J Sound Vib* 2010; 329: 753–67.

77. Doutres O Atalla N and Dong K. Effect of the Microstructure Closed Pore Content on the

Acoustic Behavior of Polyurethane Foams. *J Appl Phys* 2011; 110: 064901.

78. Scheidegger AE. THE PHYSICS OF FLOW THROUGH POROUS MEDIA, Adrian E.: University of Toronto Press, Toronto Hardcover, 2nd Edition, 1963.

79. Langmuir I. Report of Smokes and Filters, Part IV of a report for the Office of Scientific Research and Development, OSRD No. 865, Ser. No. 353, Filtration of Aerosols and the Development of Filter Materials, by Rodebush, W. H. et al., September 4, 1942.

80. Tarnow V. Airflow Resistivity of Models of Fibrous Acoustic Materials. *J Acoust Soc Am* 1996; 100: 3706–3713.

81. Hasimoto H. On the Periodic Fundamental Solutions of the Stokes Equations and Their Application to Viscous Flow Past a Cubic Array of Spheres. *J Fluid Mech* 1959; 5: 317-328.

82. Kuwabara S. The Forces Experienced by Randomly Distributed Parallel Circular Cylinders or Spheres in a Viscous Flow at Small Reynolds Numbers. *J Phys Soc Jpn* 1959; 14: 527-532.

83. Happel J. Viscous Flow Relative to Arrays of Cylinders. *AIChE J* 1959; 5: 174-177.

84. Nichols RH. Flow-Resistance Characteristics of Fibrous Acoustical Materials. *J Acoust Soc Am* 1947; 19: 866–71.

85. Bies DA, C Ho Hansen. Flow Resistance Information for Acoustical Design. *Appl Acoust* 1980; 13: 357–391.

86. Garai M, Pompoli F. A Simple Empirical Model of Polyester Fibre Materials for Acoustical Applications. *Appl Acoust* 2005; 66: 1383–1398.

87. Manning J, Panneton R. Acoustical Model for Shoddy-Based Fiber Sound Absorbers. *Text Res J* 2013; 83: 1356–70.

88. Delany ME and Bazley EN. Acoustical Properties of Fibrous Absorbent Materials. *Appl Acoust* 1970; 3: 105–116.

89. Miki Y. Acoustical Properties of Porous Materials-Modifications of Delany-Bazley Models. *Journal of the Acoustical Society of Japan* 1990; 11: 19–24.

90. Komatsu T. Improvement of the Delany-Bazley and Miki Models for Fibrous Sound-Absorbing Materials. *Acoust Sci & Tech* 2008; 29: 121-129.

91. Jirsak O and Wadsworth L. Nonwoven Textiles. Durham, NC: Carolina Academic Pr, 1998, p. 57-58.

92. Yang T, Xiong X, Mishra R, Novak J and Militky J. Acoustic evaluation of Struto nonwovens and their relationship with thermal properties. *Text Res J* 2018; 88: 426–437.

93. ASTM C830-00: 2000. Standard test methods for apparent porosity, liquid absorption, apparent specific gravity, and bulk density of refractory shapes by vacuum pressure.

94. McRae JD, Naguib HE and Atalla N. Mechanical and Acoustic Performance of Compression-Molded Open-Cell Polypropylene Foams. *J Appl Polym Sci* 2010; 116: 1106–1115.

95. ISO 9073-1:1989. Textiles -- Test methods for nonwovens -- Part 1: Determination of mass per unit area.

96. Venkataraman M, Mishra R, Wiener J, Militky J, Kotresh TM and Vaclavik M. Novel techniques to analyse thermal performance of aerogel-treated blankets under extreme temperatures. *J Text I* 2015; 106(7): 736–747.

97. Venkataraman M, Mishra R, Subramaniam V, Gnanaman A, Kotresh KM and Militky J. Dynamic heat flux measurement for advanced insulation materials. *Fiber Polym* 2016; 17(6): 925–931.

98. Yang T, Xiong X, Venkataraman M, Mishra R, Novák J, Militký J. Investigation on sound absorption properties of aerogel based nonwovens. *J Text I.* 2018. doi: 10.1080/00405000.2018.1472540

99. ISO10534-2:1998. Determination of sound absorption coefficient and impedance in impedance tubes, Part 2: Transfer-function method international organization for standardization.

100. Jiang N, Chen JY and Parikh DV. Acoustical evaluation of carbonized and activated cotton nonwovens. *Bioresource Technol* 2009; 100: 6533–6536.

101. Hes L and Dolezal I. New method and equipment for measuring thermal properties of textiles. Sen'i Kikai Gakkaishi (Journal of the Textile Machinery Society of Japan) 1989; 42: T124–T128.

102. Gun AD. Dimensional, physical and thermal comfort properties of plain knitted fabrics made from modal viscose yarns having microfibers and conventional fibers. *Fiber Polym* 2011; 12: 258–267.

103. Xiao X, Hu J, Hua T, Zeng X and Long A. Through-thickness air permeability of woven fabric under low pressure compression. *Text Res J* 2015; 85(16): 1732–1742.

104. Coates M and Kierzkowski M. Acoustic textiles: lighter, thinner and more sound absorbent. *Tech Text Int* 2002; 11: 15–18.

105. Ibrahim MA and Melik RW, Physical Parameters Affecting Acoustic Absorption Characteristics of Fibrous Materials, *Proc Math Phys Soc Egypt* 1978; 46: 4610-4617.

106. Yanping L, Hong H. Sound Absorption Behavior of Knitted Spacer Fabrics. *Text Res J* 2010; 80: 1949–1957.

107. Seddeq HS. Factors influencing acoustic performance of sound absorptive materials. *Aus J Basic Appl Sci* 2009; 3: 4610–4617.

Research Outputs

Journal Publications

[1] **Tao Yang**, Xiaoman Xiong, Rajesh Mishra, Jan Novák, and Jiří Militký. "Acoustic Evaluation of Struto Nonwovens and Their Relationship with Thermal Properties." *Textile Research Journal* 88, no. 4 (February 1, 2018): 426–437 (***Impact factor: 1.540***).

[2] **Tao Yang**, Xiaoman Xiong, Rajesh Mishra, Jan Novák, Jiří Chaloupek, Filip Sanetrnik, and Jiří Militký. "Investigation on Acoustic Behavior and Air Permeability of Struto Nonwovens." *Fibers and Polymers* 17, no. 12 (December 2016): 2078–2084 (***Impact factor: 1.353***).

[3] **Tao Yang**, Xiaoman Xiong, Rajesh Mishra, Jan Novák, and Jiří Militký. "Sound Absorption and Compression Properties of Perpendicularly-laid Nonwovens." *Textile Research Journal*, January 18, 2018, doi: 10.1177/004051751775363(***Impact factor: 1.540***).

[4] **Tao Yang**, Xiaoman Xiong, Mohanapriya Venkataraman, Rajesh Mishra, Jan Novák and Jiří Militký. "Investigation on sound absorption properties of aerogel nonwoven blankets." *The Journal of the Textile Institute,* Accepted (***Impact factor: 1.174***).

[5] **Tao Yang**, Kirill V Horoshenkov, Rajesh Mishra, Alistair Hurrell and Ferina Saati. "A study of some airflow resistivity models for multi-component polyester fiber assembly." *Applied Acoustics* 139, 2018: 75-81 (***Impact factor: 1.721***).

[6] **Tao Yang**, Xiaoman Xiong, Ferina Saati, Kai Yang, Rajesh Mishra, Kirill V Horoshenkov, Rajesh Mishra, Steffen Marburg and Jiří Militký. "Study on sound absorption behavior of multi-component polyester nonwovens: Practical and numerical methods." *Textile Research Journal* (Under review).

[7] Xiaoman Xiong, **Tao Yang**, Rajesh Mishra, Hiroyuki Kanai, Jiri Militky, Thermal and Compression Characteristics of Aerogel-encapsulated Textiles, *Journal of Industrial Textiles*, Vol.47, 1998-2013, 2017 (***Impact factor: 1.283***).

[8] Xiaoman Xiong, **Tao Yang**, Rajesh Mishra, Jiri Militky and Jakub Wiener, Investigation on Laser Engraving based Application of Silica Aerogel into Nonwovens, *Fibers and Polymers*, Vol.18, No. 12, 2469-2475, 2017 (***Impact factor: 1.353***).

[9] Xiaoman Xiong, **Tao Yang**, Rajesh Mishra, Jiri Militky, Transport Properties of Aerogel-based Nanofibrous Nonwoven Fabric, *Fibers and Polymers*, Vol.17, No.10, 1709-1714, 2016 2084 (***Impact factor: 1.353***).

[10] Xiaoman Xiong, Mohanapriya Venkataraman, Darina Jašíková, **Tao Yang**, Rajesh Mishra and Jiří Militký, Experimental investigation of convective heat transfer in aerogel-embedded nonwovens, *Journal of Industrial Textiles*, under review.

[11] Xiaoman Xiong, Mohanapriya Venkataraman, Darina Jašíková, **Tao Yang**, Rajesh Mishra and Jiří Militký, Thermal performance of aerogel-encapsulated fibrous materials by convection, under preparation.

Book Chapters

[1] **Tao Yang**, Xiaoman Xiong, Rajesh Mishra, Jan Novak and Jiří Militký, Comparative Analysis on Acoustic Properties of Different Struto-type Nonwovens, Advances in fibrous material science, ISBN 978-80-87269-48-0, 2016.

[2] **Tao Yang**, Xiaoman Xiong, Rajesh Mishra, Jan Novák, Filip Sanetrník and Jiří Militký, A Review of Acoustic Properties Measurements and Wave Propagation Models of Porous Materials, Recent developments in fibrous material science, ISBN 978-80-87269-45-9, 2015.

[3] Xiaoman Xiong, **Tao Yang**, Rajesh Mishra, Juan Huang and Jiří Militký, A Review on Nanofibrous Membranes and Their Applications, Advances in fibrous material science, ISBN 978-80-87269-48-0, 2016.

[4] Xiaoman Xiong, **Tao Yang**, Rajesh Mishra, Juan Huang, T M Kotresh and Jiří Militký, Heat Transfer through Thermal Insulation Materials Part I – Nonwoven Fabrics, Recent developments in fibrous material science, ISBN 978-80-87269-45-9, 2015.

[5] Xiaoman Xiong, **Tao Yang**, Rajesh Mishra, Juan Huang, T M Kotresh and Jiří Militký, Heat Transfer through Thermal Insulation Materials Part II – Nano-porous Aerogel, Recent developments in fibrous material science, ISBN 978-80-87269-45-9, 2015.

Conference Publications

[1] **Tao Yang**, Xiaoman Xiong, Rajesh Mishra and Jiri Militky. Relationship Between Sound Absorption Property and Transmission Behavior of Struto Nonwoven, Textile Bioengineering and Informatics Symposium, TBIS-2017, Wuhan, China, 18-20 May, 2017.

[2] **Tao Yang**, Xiaoman Xiong, Rajesh Mishra and Jiri Militky. Acoustic and thermophysiological properties of Struto nonwovens, 44th Textile Research Symposium, IIT Delhi, December 14-16, 2016.

[3] **Tao Yang**, Xiaoman Xiong, R Mishra, V. Arumugam, Mohanapriya Venkataraman and Jiri Militky. Study on Acoustic and Thermal Performance of Struto Nonwovens, 21st Strutex, december 1-2, p. 345-350, ISBN:9788074942693, Liberec, 2016.

[4] **Tao Yang**, Xiaoman Xiong and R. Mishra. 3D orthognal fabric composites from carbon fiber, 8th TBIS-APCC International conference, Zadar, 14-17 June, 2015.

[5] **Tao Yang,** Xiaoman Xiong, R Mishra, Jan Novák and Jiri Militký. Sound absorption behaviour of perpendicular-laid nonwovens, 46th Textile Research Symposium, Teijin Academy Fuji, Japan, September 3-5, 2018.

[6] Xiaoman Xiong, **Tao Yang**, Rajesh Mishra, Jiri Militky, Transport Properties of Nonwovens with Aerogel, CLOTECH 2017, Lodz, Poland, October 11-14, 2017.

[7] Xiaoman Xiong, **Tao Yang**, Rajesh Mishra, Jiri Militky, Laser Engraving based Application of Silica Aerogel into Nonwovens for Thermal Insulation, 45th Textile Research Symposium, KIT Kyoto, September 14-16, 2017.

[8] Xiaoman Xiong, **Tao Yang**, Rajesh Mishra, Jiri Militky, Investigation on Thermal and Compression Performance of Aerogel Incorporated Textiles, Textile Bioengineering and Informatics Symposium, TBIS-2017, Wuhan, China, May 18-20, 2017.

[9] Xiaoman Xiong, **Tao Yang**, Rajesh Mishra, and Jiri Militky, Thermophysiological Performance of Aerogel Embedded Electrospun Nonwoven Layers, 44th Textile Research Symposium, IIT Delhi, December 14-16, 2016.

[10] Xiaoman Xiong, **Tao Yang**, Rajesh Mishra, Effect of weaving friction on yarn hairiness and mechanical properties, 8th TBIS-APCC International conference, Zadar, June 14-17, 2015.